WAVE GENERATED BEDFORMS IN THE NEAR-SHORE SAND ENVIRONMENT

By

CHRISTOPHER D. JETTÉ

A DISSERTATION PRESENTED TO THE GRADUATE SCHOOL
OF THE UNIVERSITY OF FLORIDA IN PARTIAL FULFILLMENT
OF THE REQUIREMENTS FOR THE DEGREE OF
DOCTOR OF PHILOSOPHY

UNIVERSITY OF FLORIDA

1997

ACKNOWLEDGMENTS

I wish to express a great deal of thanks to my advisor and supervisory committee chairman, Dr. Daniel M. Hanes, for his support and guidance during my graduate research. I would also like to thank the members of my supervisory committee, Dr. Robert G. Dean, Dr. Joann Mossa, Dr. Donald M. Sheppard, and Dr. Robert J. Thieke. I would also like to thank the ONR Coastal Sciences Program for funding this research.

I would like to thank my parents, Sandie and Bill Kline and Don Jetté, for their love and support over the years. I would also like to recognize my grandparents, Alma and Leon Jetté, for their unending encouragement. Thanks to my wife, Monica, for her support and for making my life wonderful. Thanks to Pierre and Helene for their support. Thanks to Eric Thosteson for help in data collection and reduction, and for being a great friend. Thanks to Mike and Craig for their aid in the collection of field data.

Thanks to everyone at the Coastal Engineering Lab, without their help this research never would have been possible. Thanks to Chuck, Sidney, Vernon, Vic, Danny, and J.J.. Thanks also to the clerical staff, Becky, Sandra, Cynthia, and Lucy, for having patience with my general failure to meet deadlines. Thanks to everyone at the Army Corps of Engineers Field Research Facility in Duck, North Carolina for allowing us to use their facility and for their assistance when it was needed.

Thanks also to my friends for the great times and sanity checks; thanks big Paul, little Paul, Phil, Pedro, Darwin, Kenny, Mark, Tim, Al, Mike, Rob, Cindy, Marc, Louis, and Christina. Thanks for entertainment go to Iron Wood Golf Course, Market Street Pub, Butler Beach, S. R. 441 bike rides, and 97X. I would like to thank God for my family, friends, and health, and also for giving us yeast. Much thanks to King Neptune for the awesome waves he has sent my way.

TABLE OF CONTENTS

page

ACKNOWLEDGMENTS ii

LIST OF TABLES v

LIST OF FIGURES vi

LIST OF SYMBOLS ix

ABSTRACT xi

INTRODUCTION 1

PREVIOUS WORK 4

Mechanics of Ripple Formation 4
Rolling Grain Ripples 5
Vortex Ripples 6
Classification Schemes 6
Bagnold (1946) 6
Dingler and Inman (1976) 7
Clifton (1976) 7
Nielsen (1981) 9
Osbourne and Vincent (1993) 9
Recent Bedform Observations 10
Hay and Wilson (1994) 10
Hay, Craig and Wilson (1996) 11

THE MULTIPLE TRANSDUCER ARRAY 13

Previous Measurement Techniques 13
The MTA 14
Testing of the MTA 17
A field test 20
Analysis of measurements 21
Conclusions 24

FIELD MEASUREMENTS OF BEDFORMS AND A COMPARISON OF PREDICTION TECHNIQUES 26

Introduction 26
Instrumentation and experimental setup 27
Data Analysis 30
Ripple Model Descriptions 35
Nielsen (1981) field model 35
Wiberg and Harris (1994) 36
Model Comparisons 38
Nielsen (1981) 38
Wiberg and Harris (1994) 39
Using near bottom hydrodynamics in predicting ripple geometries 42
New Model Development 48
Comparison of new model with previous field ripple measurements 50
Conclusions 53

OBSERVATIONS OF BEDFORM DYNAMICS 55

Introduction 55
Experimental Setup 56
Ripple Flattening and Reformation 59
Ripple migration 67
Large Scale Migration 67
Small Scale Migration 74
Model Comparisons 82
Conclusions 86

DISCUSSION AND CONCLUSIONS 89

APPENDIX A: SIS95 AND SIS96 DATA AND PLOTS 93

Key to terms in appendix A. 93
Table A1. SIS96 Hydrodynamic data 94
Table A2. SIS96 Ripple Data 95
Table A3. SIS95 Hydrodynamic Data 96
Table A4. SIS95 Ripple Data 97

APPENDIX B: SIS95 AND SIS96 PROGRAMS AND DATA FILE DESCIPTIONS ... 98

Description of files 98
Listing of programs 100

BIOGRAPHICAL SKETCH 132

LIST OF TABLES

Table page

1. Wiberg and Harris (1994) ripple classification 36

2. Relative error between measured and predicted ripple geometries. 41

3. Relative error between measured and predicted ripple geometries when significant near-bottom conditions are used as input. 48

4. Relative error between measured and predicted ripple geometries for all previous small scale field data. 52

5. Relative error between measured and predicted ripple geometries for all available small scale field data; including the SIS95 and SIS96 data sets. 53

LIST OF FIGURES

Figure page

1. Schematic of the multiple transducer array ripple measurement system 15

2. Laboratory test of MTA with sand covered corrugated fiberglass target. 17

3. MTA profiles measured in a laboratory wave tank 20

4. MTA profiles measured during a field experiment in Duck, NC..... 24

5. Cross-shore beach profiles measured during SIS95 and SIS96 experiments. 28

6. SeaTek 64 element MTA used in SIS96 experiment. 29

7. SIS96 Instrument setup as viewed from the offshore direction. 29

8. Time series of mobility number and ripple profiles from SIS96 run 14. 31

9. Time series of mobility number and ripple profiles from SIS96 run 8. 32

10. Time series of mobility number and ripple profiles from SIS96 run 26. 33

11. Measured nondimensional ripple height (η/A) and nondimensional ripple length (λ/A) versus Mobility Number, and (c) ripple steepness versus Shields Parameter for SIS95 and SIS96 data with Nielsen (1981) model curves. 38

12. Nielsen (1981) predicted versus measured SIS95 and SIS96 ripple height, length, and steepness. 39

13. Measured SIS95 and SIS96 ripple data with Wiberg and Harris (1994) model curves 40

14. Wiberg and Harris (1994) predicted versus measured SIS95 and SIS96 ripple height, length, and steepness..... 41

15. Power spectrums for corrected surface elevation and near-bottom orbital excursion for run 6 of the SIS95 data set. 43

16. Orbital diameter versus run number and mobility number versus run number for near-bottom significant values and H_{mo} derived values for the SIS95 and SIS96 data sets. 45

17. Measured nondimensional ripple height (η/A), nondimensional ripple length (λ/A), and ripple steepness for SIS95 and SIS96 data with Nielsen (1981) model curves 46

18. Measured SIS95 and SIS96 ripple data with Wiberg and Harris (1994) model curves 47

19. Measured nondimensional ripple height (η/A) and ripple steepness for SIS95 and SIS96 data with the new model curves. 50

20. Nondimensional ripple height/ orbital semi-excursion and ripple steepness versus Mobility Number with new model curves and all available field ripple data. 51

21. Time series of mobility number and ripple height for run 2. 60

22. Small scale bedform profiles for run 2. 61

23. Time series of mobility number and ripple height for run 14 63

24. Small scale bedform profiles for run 14. 63

25. Time series of mobility number and ripple height for run 20. 65

26. Small scale bedform profiles for run 20. 65

27. Under-water video images from Run20. 66

28. Time series of mobility number for runs 19, 20, and 21 68

29. Bedform profiles for runs 19, 20, and 21 69

30. Rotating scanning sonar (RSS) image from the beginning of run 19 70

31. Mobility number time-series for run 9, and bedform time-series showing megaripple migration. 73

32. Time series of mobility number and ripple height for run 15. 75

33. Small scale bedform profiles for run 15. 75

34. Time series of mobility number and ripple height for run 16. 76

35. Small scale bedform profiles for run 16. 77

36. Time series of mobility number and ripple height for run 3. 78

37. Small scale bedform profiles for run 3. 78

38. Small scale bedform profiles for run 19. 79

39. Underwater video image from the beginning of run 19 showing brick-pattern ripples. 80

40. Measured SIS96 small scale and large scale ripple data versus nondimensional orbital diameter for nondimensional ripple height, length, and steepness. 84

41. Megaripple steepness versus nondimensional orbital diameter, d_o/d_{50}, mobility number, and mean current for the SIS96 data set. 85

LIST OF SYMBOLS

A	[L]	orbital amplitude of fluid just above boundary layer
A_r	[L^2]	cross-sectional area of megaripple
c	[LT^{-1}]	megaripple migration rate
dh/dx	[-]	bedslope
d_{50}	[L]	median grain diameter
d_o	[L]	wave orbital diameter
f	[T^{-1}]	wave frequency
f_p	[L]	diameter of acoustic foot print
$f_{2.5}$	[-]	grain roughness friction factor
g	[LT^{-2}]	acceleration due to gravity
h	[L]	water depth
H_{mo}	[L]	wave height determined from surface elevation spectrum
k	[L^{-1}]	wave number, $2\pi/L$
$Q_b(t)$	[L^2T^{-1}]	bedload transport rate
Q_s	[$MT^{-1}L^{-1}$]	sediment transport rate
s	[-]	sediment relative density
T_p	[T]	peak wave period from surface elevation spectrum
u	[LT^{-1}]	cross-shore velocity
u_m	[LT^{-1}]	maximum near bottom orbital velocity
z	[L]	vertical distance above bed
Δ	[-]	relative error
δ_ω	[L]	wave boundary layer thickness

ϕ	[-]	sediment porosity
$\Phi(t)$	[-]	non-dimensional bedload transport rate
η	[L]	ripple height
η_{ano}	[L]	anorbital ripple height
η_{orb}	[L]	orbital ripple height
η_{sub}	[L]	suborbital ripple height
λ	[L]	ripple length
λ_{ano}	[L]	anorbital ripple length
λ_{orb}	[L]	orbital ripple length
λ_{sub}	[L]	suborbital ripple length
$\theta_{2.5}$	[-]	grain roughness Shield's parameter
ρ	$[ML^{-3}]$	fluid density
ω	$[T^{-1}]$	radian frequency, $2\pi/T$
ψ	[-]	mobility number
$\frac{\partial h}{\partial x}$	[-]	local bed slope

Abstract of Dissertation Presented to the Graduate School
of the University of Florida in Partial Fulfillment of the
Requirements for the Degree of Doctor of Philosophy

WAVE GENERATED BEDFORMS IN THE NEAR-SHORE SAND ENVIRONMENT

By

Christopher D. Jetté

December 1997

Chairman: Daniel M. Hanes
Major Department: Coastal and Oceanographic Engineering

To measure bedform geometry, a high-resolution sea-bed profiling system has been developed. The multiple transducer array (MTA) consists of an array of ultra-sonic (5MHz) transducers. The first prototype MTA described herein measures two-dimensional bedform profiles over a length of 45 cm. Under ideal conditions, the instrument is capable of 1 mm vertical resolution and 2 cm horizontal resolution. Laboratory and field tests of the MTA show the system's capability to accurately measure bedforms of known geometry and the ability to work under conditions with relatively high suspended sediment concentrations. Previous high-resolution profiling systems have either had moving parts, or have been unable to obtain the resolution of the system described herein.

A multiple transducer array (MTA) was used to measure seabed geometry in a near-shore wave dominated environment in Duck, NC. The instruments were deployed using a sensor insertion system (SIS) installed on the research pier. Bedforms were measured under a variety of wave conditions and at several cross-shore locations. Two existing empirical ripple prediction models are compared to the measured field data. A new model

is also empirically determined from these measurements. This new model describes vortex ripple geometry strictly in terms of sediment and flow conditions and does not require the calculation of shear stress. When all available field measurements of small scale ripples are compared to these predictive models, the new model has lower errors in predicting ripple height, steepness, and length than any of the other models.

Both small scale ripples, with lengths of less than 40 cm, and large scale megaripples were measured during this experiment. Observations indicate that ripple flattening and reformation is a function of wave mobility number. Ripple reformation was commonly observed to occur in less than one minute after flattening, and under certain conditions reformation was observed to occur within a few wave periods. Observations of megaripple migration indicate that cross-shore sediment transport due to ripple migration may be a significant process. Estimated cross-shore bedload transport rates are a good indicator of small scale ripple migration direction. Measurements indicate that megaripple lengths are proportional to near-bed orbital diameter, and that these types of bedforms can exist at small and large values of mobility number and orbital diameter.

CHAPTER 1
INTRODUCTION

In the coastal environment the seabed is rarely flat. In contrast, it is usually covered with bedforms such as bars, dunes, sand ripples, and biological matter. In modeling sediment transport it is very important to be able to predict the geometry of the bedforms. The geometry of bedforms provides a bed roughness that influences the shear stress at the bed and the profile of the eddy viscosity or diffusion coefficient. Thus the bedform geometry is required to determine the concentration profile or the rate of sediment transport (Vongvisessomjai, 1987).

The modeling capability of bathymetric change is also dependent on the modeling of bedform geometry. Vincent and Osbourne (1992) found that under similar wave conditions the suspended sediment over a flat bed was restricted to the lowest 5 to 10 centimeters above the bed, whereas when bedforms were present suspensions to 30 and 40 centimeters were common. They also found bedform migration to be a significant part of the total cross-shore transport when the bedforms present had low steepness. Thus the ability to model sediment transport and bathymetric change is dependent on the ability to model bedform geometry and bedform migration.

Most ripple models currently in use are empirically based. Nielsen (1981) developed separate models for bedform geometry based on the type of waves present, i.e., one model for laboratory (regular wave) and a different model for field (irregular wave) conditions. These models are functions of the mobility number and the grain roughness Shield's parameter and can be applied to sediments of different densities. Wiberg (1994) developed a set of empirical models that are meant to work in both laboratory and field wave

conditions. These models use the wave orbital diameter and sediment size to predict the geometry of bedforms under oscillatory flows for a quartz sand bed.

One of the major problems in modeling bedform geometries under waves has been the lack of reliable field data. Nielsen's (1981) field ripple models were based on 126 data points, of which 54 were measured by scuba divers and 72 were measured using acoustic instrumentation. When Wiberg and Harris (1994) developed their models they took all of the data used by Nielsen plus 59 points recorded after 1981. All reliable existing field data sets were used to construct this model. Thus there were no data with which to check the model.

In the past, the most common method for measuring bedforms was for scuba divers to use some sort of manual measurement device. With the use of a meter stick, divers can accurately determine ripple lengths. Ripple heights, however, tend to be more difficult to measure. When measuring ripple heights, the weight of the meter stick tends to flatten the crests of the ripples. In addition, the water motion due to the waves tends to complicate matters (Dingler and Inman, 1972). In the past divers have also used a piece of clear plastic and a grease pencil to try to measure sand ripples in the field (Inman, 1957). Also divers have tried to use a large "comb" covered with grease so that once it is pushed down into the bed the sand sticks to the grease and thus the bed profile is recorded (Kawata et al., 1992).

More recently underwater video has been used to measure ripples. When water visibility allows, videography can be used to accurately measure ripple length. However, even using available image processing techniques, ripple height is still very difficult to determine in the field using underwater video.

The latest trend in measuring bedform dimensions is with the use of ultra-sonics. Dingler and Inman (1974) were one of the first groups to measure bedforms with ultrasound. They had a movable frame with a manually translated transducer which the divers moved back and forth over the rippled seabed recording the ripple profile. Today

there are similar automated systems such as the HRRTS (High Resolution Remote Tracking Sonar). With the use of a stepper motor, the HRRTS tracks an ultrasonic transducer back and forth across a stationary frame recording the bottom profile (Greenwood et al.(1993)). Also transducers have been used in side-scan mode to measure ripple lengths in conjunction with downward aimed transducers to measure ripple heights as ripples migrate underneath (Vincent and Osbourne, 1992). Because there have been inherent problems involved in all of these methods, a new approach to measuring bedform geometries has been developed. This technique involves no moving parts and is capable of remotely measuring bedform profiles with millimeter vertical resolution.

CHAPTER 2
PREVIOUS WORK

Mechanics of Ripple Formation

Once the wave shear stress acting on a movable sand bed reaches a strength strong enough for incipient sediment motion, the sediment begins to be carried as bed load. As the bed shear stress increases, the amount of suspended sediment increases and the flow becomes more vigorous. Then, once another critical value of shear stress is surpassed, the sediment begins to be carried as sheet flow. Bedforms may be active anytime the bed shear stress is above that required for incipient motion.

One non-dimensional parameter used to classify these different regimes is the grain roughness Shield's parameter ($\theta_{2.5}$),

$$\theta_{2.5} = 0.5\, f_{2.5}\, \psi \qquad \text{equation 2.1}$$

where "$f_{2.5}$" is the wave friction factor, given by Swart (1974) as:

$$f_{2.5} = \exp\left(5.213\left(2.5\, d_{50}/A\right)\right)^{0.194} - 5.977 \qquad \text{equation 2.2}$$

and Ψ is the mobility number, defined as:

$$\psi = \frac{(A\,\omega)^2}{(s-1)\,g\,d_{50}} \qquad \text{equation 2.3}$$

Where "d_{50}" is the median grain diameter, "A" is the water semi-excursion determined from the H_{mo} wave height and peak period, and "ω" is the peak angular frequency of the

waves as determined from the surface elevation spectrum. The mobility number is a non-dimensional term representing essentially the ratio between the water velocity amplitude and the settling velocity of the sediment for typical wave conditions (A of the order 0.1m-2m) and sand sizes (Nielsen, 1981).

Values of the grain roughness Shield's parameter are given to classify the different regimes of flow. For $\theta_{2.5}$ less than or equal to 0.05, the flow is considered to be too weak for sediment motion. For a $\theta_{2.5}$ greater than 0.05 and less than or equal to 1.0 the bed will be active and covered with bedforms that will be approximately in equilibrium with the flow conditions. When $\theta_{2.5}$ is greater than 1.0, the ripples are flattened and sheet flow occurs (Dingler, 1974).

Rolling Grain Ripples

Bedforms produced by the action of progressive waves on a horizontal bed were first classified into two groups by Bagnold (1946). Bedforms with a large enough height to length ratio to allow vortex formation in the lee of the crest he called "vortex ripples," and bedforms with too small of a height to length ratio to allow vortex formation he called "rolling-grain" ripples. On an initially flat bed without obstructions capable of forming vortices, rolling-grain ripples are the first bedforms to appear.

Sleath (1984) investigated rolling-grain ripple formation on a flat bed with a small disturbance present; the required disturbance could even be as small as a single grain of sediment projecting from the bed. He modeled the streamlines around this disturbance and found that the steady drifts, which form in the vicinity of the bed, tend to be directed toward the disturbance. This would carry sediment from the trough of the ripple to the crest. Such flow would promote ripple growth. Gravity acts as an opposing force to ripple formation, therefore limiting the maximum height attainable of the ripples under given wave conditions.

Vortex Ripples

If the flow is strong enough, once the height to length ratio of the rolling grain ripples reaches a critical value, vortex formation will occur in the lee of the ripple crests twice every wave period. Vortex ripples are commonly found at low to moderate transport rates (Sleath, 1984). Once separation occurs in the lee of the ripple crest both the mainstream flow on the upstream face, and the reverse flow on the lee side face of the crest tend to carry sediment from the trough to the crest of the ripple. The forces acting in opposition to vortex ripple formation are gravity and the erosional effects on the ripple crest by the main stream flow. Thus for given sediment and wave conditions, an equilibrium bedform geometry will exist where there is no net transport across any cross-section of the bedform profile.

Classification Schemes

Several previous investigators have classified bedforms in different ways. Most of the classifications used in sediment transport are based on the genesis of the bedforms. This section divides classification schemes up by authors and lists them in chronological order.

Bagnold (1946)

As mentioned in the above section, Bagnold (1946) was the first to develop a classification scheme for bedform ripples. He called ripples with a height to length ratio large enough for vortex formation in the lee of the ripple crest "vortex ripples," and ripples without this separation "rolling grain ripples." Bagnold's classification system is still widely used today. Rolling grain ripples appear to be stable at velocities smaller than twice that required for incipient motion (Bagnold, 1946). Because of this, rolling grain ripples are present when sediment transport is low; thus, most of the bedform research has been done in the vortex ripple regime where sediment transport rates are greater. The vortices formed by the flow over vortex ripples are strong; Tunsdall and Inman (1975) found that

the velocities within the vortices are of the same magnitude as that of the main stream flow.

Dingler and Inman (1976)

Dingler and Inman (1976) found that three distinct ripple types occur on fine sand beds in coastal areas. These are relict ripples, vortex ripples, and transition ripples. Relict ripples are found when wave parameters are not sufficient to initiate sediment motion on the bed. Relict ripples are the remains of ripples that were formed under a previous event when flow conditions were strong enough for sediment motion. Vortex ripples are defined as ripples that have a relatively constant steepness; even though the ripple heights and lengths change as the wave intensity becomes larger. Once the steepness of the ripples begins to decrease due to increased flow intensity, the ripples are called transition ripples. Transition ripples are found when the flow intensity is too large to maintain the relatively constant vortex ripple steepness of 0.15, but not large enough for sheet flow. Dingler and Inman (1976) used mobility number to classify flow intensity.

Values of mobility numbers (ψ) were determined for each of the ripple classes. When ψ was less than 40 but great enough for sediment motion, the bedforms were found to be in the vortex ripple class. When the flow intensity increased and ψ was greater than 40 but less than 240 the bedforms were found to be in the transition ripple class. When the flow intensity was greater yet (ψ greater than 240) no bedforms were present and sheet flow was observed (Inman and Dingler, 1976).

Clifton (1976)

Clifton (1976) found that when vortex ripple lengths were compared to the ratio of orbital diameter to median grain diameter (d_o/d_{50}) the ripples could be classified into three categories. First, when d_o/d_{50} is relatively small, less than 2000, the ripple length (λ) is proportional to orbital diameter, Clifton (1976) classified these ripples as orbital ripples. For large values of d_o/d_{50}, greater than 5000, the ripple length appears to be a function of

grain diameter and nearly independent of orbital diameter. Clifton (1976) refers to these ripples as anorbital ripples. There exists a transition range for intermediate values of d_o/d_{50} where both orbital and anorbital ripple formations appear possible, as well as ripples with intermediate lengths. Clifton (1976) called ripples in this transition range suborbital ripples.

Wiberg and Harris (1994) used the above ripple classification system, however they quantified values of flow parameters and bedform geometry for each of the different classes. Wiberg and Harris (1994) found orbital ripples to dominate in laboratory environments because of the limits on the maximum wave orbital diameter that can be generated in the laboratory with most wave flumes. Wiberg and Harris (1994) defined orbital ripples as ripples with heights twice as large as the thickness of the wave boundary layer, or $\delta_\omega/\eta < 0.5$. Since for this flow the thickness of the wave boundary layer (δ_ω) is roughly proportional to the wave orbital diameter (d_o), and d_o is more readily attainable in most instances, Wiberg and Harris (1994) defined orbital ripples as ripples with the ratio $d_o/\eta<10$. The Wiberg and Harris (1994) ripple model classifies the ripple regimes according to the ratio of d_o/η_{ano}, where η_{ano} is the predicted anorbital ripple height. When predicted anorbital ripple height is used, the definition of the orbital ripple regime becomes $d_o/\eta_{ano}<20$, which was determined empirically. Wiberg and Harris (1994) classify anorbital ripples as ripples with heights several times smaller than the wave boundary layer. By definition anorbital ripples have heights less than one quarter of the wave boundary layer thickness, or $\delta_\omega/\eta_{ano} > 4.0$. For ease of calculation, this value was also put in terms of orbital diameter; giving $d_o/\eta_{ano} > 100$.

Wiberg and Harris (1994) then classify the transitional suborbital regime for conditions where the ratio δ_ω/η_{ano} is greater than 0.5 and less than 4.0, or in terms of the wave orbital diameter, $20 < d_o/\eta_{ano} < 100$. When laboratory and field data are compared for a given value of d_o/d_{50} in the suborbital regime, the ripple wavelengths can differ by more than a factor of three. Anorbital ripples dominate on the continental shelf, and on

medium to coarse sand beds suborbital ripples can also be present. Under limited conditions on coarse sand beds orbital ripples can also be present on the continental shelf, however it is not common (Wiberg and Harris, 1994).

Nielsen (1981)

Nielsen (1981) studied vortex ripples and classified them by the type of waves present as either laboratory (regular wave) or field (irregular wave) ripples. He found that under field conditions, where the waves are often irregular and far from being sinusoidal, the steepness of the ripples tend to be less than those formed under laboratory conditions. In the past, laboratory studies could not generate prototype field wave conditions. However, with new large wave flumes operating under spectral conditions, prototype field wave conditions can be generated in the laboratory. This makes using the field and laboratory classification system obsolete since it is difficult to draw a fine line between the two conditions. Wiberg and Harris (1994) suggest that the differences Nielsen (1981) found between lab and field data are probably due to most of the data falling into the orbital ripple regime for the laboratory data, and into the suborbital and anorbital regime for the field data.

Osbourne and Vincent (1993)

Upon completion of a field study that included diver observations of bedforms, Osbourne and Vincent (1993) classified observed bedforms into two major categories, small-scale bedforms (η<4 cm, λ<20 cm) and large scale bedforms (η>4 cm, λ>20 cm). These bed types were then divided into subtypes depending on the number of crest dimensions, type of vortex shedding/suspension, and symmetry. The number of crest dimensions were defined as two dimensional if the bifurcation density was low (> 10 cm between bifurcations) and as three dimensional if the bifurcation density was high (<10 cm between bifurcations). The vortex shedding/suspension classification named pre-vortex ripples as ripples with no vortex shedding and no suspension. These types of ripples have

previously been referred to as rolling grain ripples. Vortex ripples were the same as defined previously, with sediment suspension and vortex shedding from crests at regular intervals under large waves. Post-vortex ripples were classified as ripples where sediment suspension and vortex shedding occurs at irregular bursts. The ripples were then characterized as being either symmetric or asymmetric in profile.

Osbourne and Vincent (1993) found that under non-breaking wave conditions small-scale bedforms dominated, while under breaking wave conditions large-scale bedforms dominated over the sea-bed. These large-scale bedforms were generally crescentic in planform and migrated on-shore, they have been called lunate-shaped megaripples by Clifton (1976). In their field study Osbourne and Vincent (1993) found that two dimensional small-scale bedforms (η=0.5 to 3 cm, λ=8 to 20 cm) had migration rates of up to 5 cm./min., and for well defined lunate megaripples (η=3 - 8 cm, λ=20 - 80 cm) migration rates of up to 3 cm/min were documented.

Recent Bedform Observations

Hay and Wilson (1994)

A rotating sidescan sonar (RSS) was used to measure bedforms within a 10 meter diameter field on the crest of a nearshore bar. Hay and Wilson (1994) documented planform images of three-dimensional bedforms present throughout a storm on Lake Huron in Burley Beach, Ontario. Such a sonar system proved capable of measuring the orientation and length of small and large-scale bedforms under certain conditions. Their measurements of bedforms indicate that the seabed can be highly three-dimensional.

Transitions of bedform types were observed during the progression of a storm. Clifton (1976) discussed such transitions in a cross-shore sense; however, Hay and Wilson (1994) observed such transitions in a single location as the wave and current conditions changed. The progression was observed during decay in the wave velocities. The

progression was from a 'flat' bed with no vortex ripples, to a bed populated with long-crested shore-parallel ripples with occasional megaripples. The seabed was then populated with oblique cross ripples combined with patchy shore-parallel ripples and occasional megaripples. Finally, the bed was covered with irregular short crested ripples. The time for this progression was approximately six hours. During the onset of the storm, a similar progression was observed, but in reverse sequence, and over the course of only 2 hours.

Hay and Wilson (1994) demonstrate that planform images of the seabed can be recorded with a rotating side-scan sonar under certain wave and current conditions. They also indicate that information on bedform amplitudes is contained in the images as shadow length, however it is not as readily accessible as bedform patterns. The major finding of this paper is that the local evolution of the bed involves transformations among two-dimensional and three-dimensional bedform fields, and that this transformation can occur on time scales of a few hours or less.

Hay, Craig and Wilson (1996)

Bedform measurements from Duck, NC are presented. A rotating side-scan sonar and a rotating pencil beam sonar were used to measure bedforms. The rotating pencil beam sonar consisted of a 2.25 MHz sonar with a 2 degree farfield beam-width that rotated about a horizontal axis. Vertical slice images recorded with this instrument were used to measure bedform height. The main focus of this investigation was to measure megaripple dynamics.

These observations were similar to the Hay and Wilson (1994) observations in the sequence of bedform patterns from megaripples, through cross-ripples, to irregular ripples as wave energy decreased. Also, in both circumstances the low energy end-state of the seabed was short-crested irregular ripples. They propose that such a progression suggests the existence of general relationships between fluid forcing and bedform patterns.

Their observations indicate that lunate megaripples migrate in the direction of their horns, and that megaripple migration rates appear to be a function of the bedform length scale. Both long-shore and cross-shore megaripple migrations were observed. These measurements indicate that the direction of migration depends on the strength of the longshore current. Migration rates reached 50-160 cm/hr longshore, and 20 cm/hr onshore during this experiment. The sediment transport rate resulting from the onshore migration of megaripples was in agreement with a cross-shore bedload transport formula based on laboratory experiments. This supports the suggestion of Hay and Bowen (1993) that the cross-shore sediment transport due to the migration of meter-scale bedforms during a storm could be predicted with laboratory-based bedload transport formula.

CHAPTER 3
THE MULTIPLE TRANSDUCER ARRAY

Previous Measurement Techniques

During the past forty years bedform measurement techniques in the field have evolved from scuba divers using meter sticks to remotely operated acoustic profilers (e.g. Inman 1957; Dingler and Inman, 1976; Osbourne and Vincent, 1993; Greenwood et al., 1993). Most of the previous acoustic systems used a single element sonar head, which was either translated over a track near the bed or was oriented in a side-scan mode. There are problems that exist with both of these arrangements.

Several systems have been developed using a single downward aimed transducer that is translated across a track supported by a frame near the sea bed (Dingler and Inman, 1976; Greenwood et al., 1993). These systems are able to measure bedform profiles, but there are some short-comings with such arrangements. The most difficult problem to overcome when using mechanical parts in the nearshore ocean environment is vibration of the sonar head during travel across the track. Also, the size of the complete system makes deployment difficult and could possibly influence the local hydrodynamics. An advantage to this system is that the measured profile length can span several meters.

In side-scan mode the sonar head is oriented slightly downward from horizontal in order to receive returns from the upslope portion of the bedforms. It is the authors' experience with such instruments that under times of relatively high flow intensity it is difficult, if not impossible, to separate the returns from the upslopes of the bedforms from the returns due to suspended sediment. Also, with this type of instrument only ripple

lengths can be measured. There are unacceptable errors when estimating small scale ripple heights from a single sonar with such orientation.

Recently, rotating side-scan sonars that can be used in sea-floor imaging have become commercially available. These systems operate similar to the side-scan system described above except that the transducer rotates about its vertical axis in order to give a 360 degree image of the sea-floor. These systems can be used to measure small-scale ripple lengths, however they have some of the same shortcomings as the stationary side-scan sonar described above. It is difficult under intense flows to separate suspended sediment returns from actual returns from the sea-floor. Also, small scale ripple heights have yet to be accurately measured with such a system. An advantage to this system is that under certain conditions ripple orientation and length can be recorded (Hay and Wilson, 1994).

The MTA

In this chapter an acoustic multiple transducer array (MTA) is described, which is capable of measuring bedform geometries with one millimeter vertical resolution and two centimeter horizontal resolution. This system uses an array of stationary downward aimed transducers, thus eliminating any moving parts and the necessity for a large support frame and track. The transducers are fired sequentially across the linear array. The bottom locations are recorded for each transducer, thus recording a two-dimensional sea-bed profile.

The first prototype multiple transducer array consists of 37 transducers. The center to center spacing of the 10 mm disk shaped transducers is 1.2 cm, which gives a profile length of 45 cm. The operating frequency of these transducers is 5 MHz, resulting in a wave length of 0.3 mm. The -3 dB half beam angle is 0.9 degrees and the mechanical quality factor (Q_m) for the transducers is 500. The length, width, and height of the array are 50 cm, 8.5 cm, and 5 cm respectively.

The transducer array is connected to a dedicated under-water electronics package. This package contains the driver and receiver circuitry, a multiplexer board, a data-logger, and the timing circuitry necessary to run the transducers. A multiplexer is used so that a single driver and receiver can be used for all of the transducers.

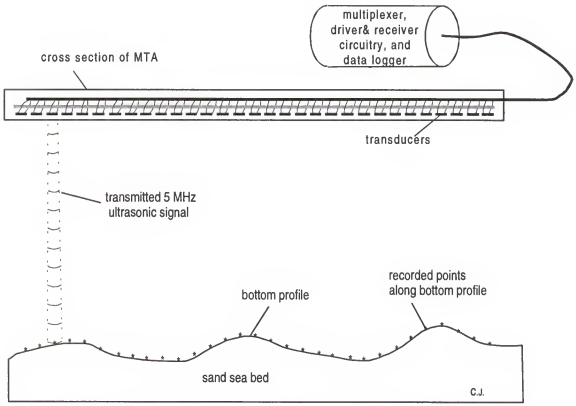

Figure 1. Schematic of the multiple transducer array ripple measurement system

A threshold method is used for bottom detection. Once the transmitted pulse is sent from the transducer a counter is started. When the amplitude of the 5 MHz return signal exceeds a certain threshold voltage the counter is stopped and the value on the counter is stored in memory. This value represents the amount of time taken for the sound to travel from the transducer to the target and back. Once this time is found, with knowledge of the speed of sound, the distance from the transducer to the target is determined.

Because the system is microprocessor controlled, many settings can be changed from a remote computer connected to the data logger. The hardware settings that are controllable remotely include blanking, threshold voltage, pulse width, and amplifier gain. Blanking refers to a delay between the time that the counter begins and the time that the voltage comparator begins to monitor the return signal. This blanking enables the comparator to only look for a return from the distance where the target should be, thus reducing the number of false returns from sediment in suspension. The threshold used by the comparator can also be controlled remotely. The pulse width, which is generally set at 12 micro-seconds, and the amplifier gain on the return signal are other settings that can be changed to optimize functionality under various environmental conditions.

Many software settings can also be changed remotely. These include the number of scans to record, the time between the beginning of scans, a value for the speed of sound, and any desired averaging technique. This system allows the user to take a few profiles, send them back to a computer where they can be analyzed, and then change the settings in order to reduce the amount of false returns and missed returns. Once the system settings are acceptable, the MTA can then start to collect data. With extended RAM on the data-logger, the MTA can run for over 30 uninterrupted hours while taking one 37 point scan every 6 seconds.

Each scan consists of a time stamp and the distances to the target in millimeters. The files are saved in a format that allows the data to be displayed within seconds of its retrieval on a remote computer.

Testing of the MTA

Laboratory tests were conducted at the University of Florida Coastal and Oceanographic Engineering Laboratory. For one of the tests a corrugated fiberglass sheet was coated with sand to represent a rippled bed. The cross-sectional profile of the

corrugated piece could roughly be represented by a sinusoidal curve with a height of 11 mm and a length of 67 mm. Five scans were recorded using the MTA. The measurements from these scans are plotted in figure 2. The measured distance between the transducer and the target has been subtracted from the average distance between the transducer and the target in order to invert the profile to its correct orientation (crests at higher elevation than troughs). Also plotted is a representative profile curve for the target that was found using the MTA data with analysis techniques which will be described in detail later. The methods used to determine ripple height and length from MTA data found a ripple height of 9 mm and a ripple length of 67 mm for the sand covered corrugated fiberglass target.

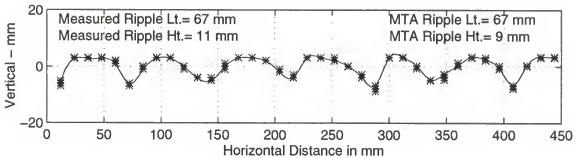

Figure 2. Laboratory test of MTA with sand covered corrugated fiberglass target.

The MTA was able to determine the wavelength of the corrugated target to within one millimeter. However, in determining the simulated ripple height of the target, the MTA data showed an average ripple height 2 mm less than the measured height of 11 mm between the crests and troughs of the target. This problem is due to the narrowness of the troughs. Since all of the elevations of the ripple crests are constant, it appears that the elevation of the crests has been captured correctly. However the measured elevations of the ripple troughs vary over the profile. This is due to the size of the acoustic footprint (~2 cm) compared to the length of the ripple trough (~1 to 2 cm).

Since this instrument uses a comparator to find the return echo, the first large return after the blanking period is used to determine the range to the target. If a significant portion of the footprint were to cover an area higher in elevation than the area that the majority of the footprint covered, it is possible that the echo from the area higher in elevation would be recorded as the echo from the target. Most likely the first strong acoustic return from the target, for the transducers above the troughs, came from the sloped area of the target on either side of the troughs. This would tend to vary the measured elevation of the troughs, which was observed.

The average distance to the target for this test was 48.5 cm, which would give a footprint on the order of 2 cm in diameter. Even if a transducer was perfectly lined up over a trough the elevation change of the target over the 2 cm footprint area would be 4 mm. Returns from the sides of the trough would decrease the measured range to the trough, which is what was observed.

Laboratory tests were also conducted in a large wave tank to determine the instrument's capability to measure actual bedforms composed of fine sand in an environment where other methods of bedform measurements were possible. The wave tank had a sloped bed composed of 0.09 mm sand. The measurements were taken after an experiment was run involving spectral waves. Measurements were taken at different stations along the profile in order to cover a variety of size and types of ripples.

The sides of the wave tank were glass so that the ripple profiles at the side of the tank could be measured visually using an incremented measuring device. Figure 3 contains five scans of raw data taken at each station as well as representative profiles for the four separate stations. Again each profile was analyzed using methods that will be described later to find a representative ripple height and length for each profile. These measurements along with visual measurements are also included as text in the plots.

In figure 3, plot (a), the observed ripples at this station could be classified as two dimensional ripples, indicating that the ripple heights and lengths were similar over the

area, and that the ripple crest lengths were long. For plots (b) and (c) the observed ripples were less regular than in the first plot, and in plot (d) the ripples were very irregular, or brick-patterned ripples.

For each of the profiles, the ripple heights and lengths were similar to what was measured at the side of the tank. The differences might have been due to actual changes in ripple dimensions from the side of the tank to the middle of the tank. For the profiles in plots (a) and (b) the ripple heights measured with the MTA were actually greater than the ripple heights measured at the side of the tank. The measured ripple lengths varied slightly between the two methods. For the profile found in plot (c) measured ripple dimensions were virtually identical with the visual measurements. The profile in plot (d) showed an irregular profile, which was observed, and the measurements were similar to the visual observations taken from the side of the tank. The elevation of the MTA above the bed was 18.5 cm, 22 cm, 23.5 cm, and 39.0 cm for profiles a, b, c, and d respectively.

Under ideal conditions, the system is capable of 1 mm vertical resolution and accuracy. However, as described above, the footprint of the acoustic beam at the design elevation of 40 to 50 cm is approximately 2 cm. Thus the system's accuracy will decrease as the change in bottom elevation over the footprint area increases. The horizontal resolution and accuracy for each transducer are taken as the footprint area of 2 cm at the design elevation. As shown, if several bedforms lengths are recorded with the MTA, much better accuratcy in determining bedform lengths can be achieved.

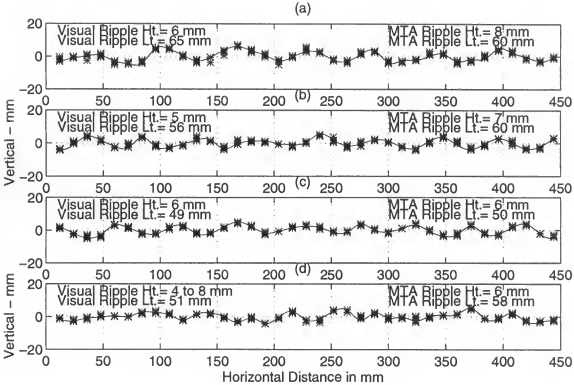
(a)
Visual Ripple Ht.= 6 mm
Visual Ripple Lt.= 65 mm
MTA Ripple Ht.= 8 mm
MTA Ripple Lt.= 60 mm
(b)
Visual Ripple Ht.= 5 mm
Visual Ripple Lt.= 56 mm
MTA Ripple Ht.= 7 mm
MTA Ripple Lt.= 60 mm
(c)
Visual Ripple Ht.= 6 mm
Visual Ripple Lt.= 49 mm
MTA Ripple Ht.= 6 mm
MTA Ripple Lt.= 50 mm
(d)
Visual Ripple Ht.= 4 to 8 mm
Visual Ripple Lt.= 51 mm
MTA Ripple Ht.= 6 mm
MTA Ripple Lt.= 58 mm
Vertical – mm
Horizontal Distance in mm

Figure 3. MTA profiles measured in a laboratory wave tank

A field test

A joint experiment was conducted with the University of Florida and the Army Corps of Engineer's Field Research Facility in Duck, NC during August 23-25, 1995. The sensor insertion system (SIS) located on the research pier was used to deploy the MTA along with many other sensors. The SIS allowed the instruments to be deployed at various locations along the near-shore profile.

During the three day experiment the MTA was deployed under a variety of wave and sediment conditions. Ripple profiles were recorded across the near-shore profile from off-shore of the bar, 225 m from shore, to the beach face, 30 m from shore. During the experiment the maximum H_{mo} wave height was 0.95 m with a 6 second peak period. The median sediment size varied from 0.18 mm to 1.66 mm over the area of measurements. The elevation of the MTA above the seabed was approximately 42 cm for all measurements.

The MTA proved capable of measuring bedform profiles under these wave and sediment conditions. As can be expected with all acoustic instruments, there were some false bottom returns from suspended sediment. However for every run the bedform profile was recorded sufficiently well to determine the geometry of the bedforms. In total there were 30, 13 minute, runs covering 9 locations along the near-shore profile.

Analysis of measurements

The prototype MTA system scans at a rate of one scan every six seconds. Several scans were combined in order to find a single representative bedform profile. For most of the analysis ten scans were compared to determine a profile representing the seabed for one minute of sampling.

Because of occasional false returns, an algorithm was developed to estimate the true bedform shape. For each of the 37 transducers a histogram was constructed of the measured bottom locations from the 10 scans. The bin size for this histogram was 1 mm. Only identical measurements were included in each bin. Then the histogram was analyzed to determine which bin had the highest number of occurrences in it. If two of the bins had the same number of occurrences, then the bin representing the farthest distance from the transducer was used. If the number of occurrences in this bin was three or greater, then this distance was recorded as the distance to the bed for the location being analyzed.

If the number of occurrences in this bin was less than three, another histogram was constructed. This second histogram had a bin size of 2 mm. If the number of occurrences in two of the bins were the same, then the bin farthest from the transducer was used. If the number of occurrences in this bin was 2 or greater, this bin was recorded as the distance to the bed. If the number of occurrences was less than 2, a third histogram was constructed with a bin size of 3 mm. Again the histogram was analyzed and the maximum bin farthest from the transducer was recorded as the distance to the bed. For the cases when the bin size was greater than one millimeter, the location of the bed within the appropriate bin was

set to the lower millimeter for the 2 mm bin size and to the second lowest millimeter within the bin for the 3 mm bin size.

This histogram method was carried out for each of the 37 locations along the profile in order to determine the bed location for each of the measured points. A cubic spline fit was then performed on the resultant 37 point profile in order to smooth the profile for further analysis. The smoothed profile had 109 points. This profile was then detrended to remove any linear trend, thus making the profile horizontal. Then the entire profile was subtracted from the mean bed location in order to invert the profile. This inverted profile is the variation of the bed about its mean value; where the positive elevation peaks represent bedform crests. Note that if the orientation of the MTA is known, then before detrending the data the local bottom slope can also be measured.

The smoothed representative profiles were then plotted with the original raw scan data to make sure that the correct bed-level locations were used. If there was ambiguity, scans taken previous to and after the profile in question were used to help determine the correct bed location. For profiles taken under waves sometimes a large suspension event can cause the MTA system to lose the bed. In these cases, profiles taken before and after the suspension event were used to determine the bed-level.

The smoothed and detrended ripple profiles were analyzed to determine representative ripple lengths and heights from each profile. All maximums and minimums in a profile were first located. A threshold of 3 mm was then set on the ripple height criterion. This was to eliminate the possibility of mistaking small fluctuations introduced during the smoothing process as ripples. The vertical distance between each adjacent maximum and minimum was then compared to this threshold value. If it was greater, this distance was recorded as a ripple height. If it was less than the threshold distance, and if the last point to exceed the threshold was a maximum, the routine continued to search for a minimum that met the threshold requirement. If during this search a larger maximum was found than the last one recorded, this larger maximum replaced the previously recorded

maximum. This process was continued until a minimum was found that met the threshold requirement. If the last recorded value was a minimum, then a similar process was executed to look for a maximum that met the threshold requirement.

Ripple heights were found by taking the average vertical distance between each adjacent maximum and minimum over the entire profile. Ripple lengths were found by taking the average horizontal distance between adjacent maximums and adjacent minimums. Ripple steepnesses were then found by dividing the average measured ripple height by the average measured ripple length for each profile.

The profiles were then analyzed again with a different threshold value for ripple height. Average ripple height, length, and steepness were then determined by this new set of threshold maximum and minimum values. The threshold value of one-half the average ripple height, which was the value found using a threshold of 3 mm, worked well to find a best fit ripple height and length for most of the ripple profiles in this data set.

An example of MTA data from the field experiment is shown in figure 4. The asterisks represent one minute of raw data (10 scans) with means subtracted. The solid curve is a representative bottom profile found using the data analysis method described above. Plot (a) is from offshore of a longshore bar, 225 m, from shore. Plot (b) is from inside the trough of a longshore bar, and plot (c) is from the beach face, 30 m from shore. The median sediment sizes for these runs are 0.28, 0.40, and 1.46 mm respectively. The water depths for these three runs were 6.2, 4.4, and 2.5 m and the H_{mo} wave heights were 0.7, 0.3, and 0.2 m respectively. The average measured ripple heights for the runs plotted in figure 4 are 13, 40, and 27 mm and the average measured ripple lengths are 103, 275, 197 mm respectively.

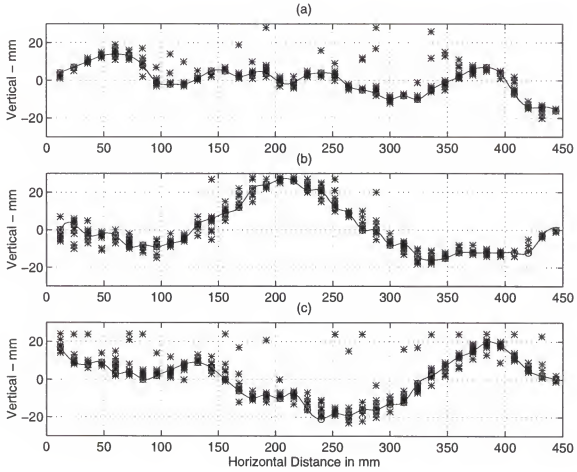

Figure 4. MTA profiles measured during a field experiment in Duck, NC

Several instances of false returns from suspended sediment can be seen in figure 4; these points are the asterisks well above the plotted curve. Since one minute of data is plotted in each plot, some of the scatter near the solid curve is most likely due to movement of the sensor frame and the seabed over this one minute period. Also, as mentioned earlier, near the bed there are a larger number of acoustic scatterers that can cause false bottom returns from the area just above the sea bed.

Conclusions

The Multiple Transducer Array (MTA) ripple measurement system can be used to measure small-scale, two-dimensional, bedform profiles. The MTA has several advantages

over its predecessors: (1) the system contains no moving parts, which in previous systems have caused vibration and have become fouled: (2) the system has the capability of taking complete profiles in less than 5 seconds, which allows the comparison of multiple scans to better eliminate false returns; (3) the system can be operated remotely even under severe sea-states, and the settings of the system can be changed remotely to better match the environment; (4) the size of the system is small compared to previous profilers which allows easier deployment and creates a lesser impact on flow patterns; (5) the system is capable of order millimeter vertical resolution and two centimeter horizontal resolution.

CHAPTER 4
FIELD MEASUREMENTS OF BEDFORMS AND A COMPARISON OF PREDICTION TECHNIQUES

Introduction

Field observations of the seabed indicate that bedforms are generally present on the inner shelf and near-shore regions. These bedforms can range from vortex ripples, 5 to 40 cm in length, to megaripples with lengths reaching over 1 meter. Small bedforms such as vortex ripples directly impact the structure of the wave boundary layer and thus influence sediment transport processes. Previous studies have observed that under similar flow conditions suspended sediment was limited to the lowest 5 to 10 cm when small scale ripples were not present, and suspensions of 30 to 40 cm were observed when ripples were present (Vincent et al., 1991).

Knowledge of bedforms is necessary to accurately describe the complete sediment transport process. Thus the prediction of bedform geometry is necessary for accurate sediment transport prediction. The major problem with ripple prediction has been the lack of quality field ripple measurements on which to base the models. Due to recent improvements in instrumentation, a large set of field ripple data has been recorded and is presented herein.

A new ultrasonic instrument, the SeaTek multiple transducer array (MTA), was used to measure bedform profiles in the field with millimeter vertical resolution. This instrument proved capable of measuring bedform profiles on temporal and spatial scales that previously were unobtainable. This chapter will present a comparison of existing

ripple predictive models to field data recorded with the MTA and to improve ripple prediction capabilities with a simple new model.

Instrumentation and experimental setup

The first data set to be presented herein was recorded from August 23 to 25, 1995 and will be referred to as the SIS95 data set. The second data set, SIS96, was recorded from October 29 to November 1, 1996. All of these measurements were recorded in Duck, North Carolina at the Army Corps of Engineers Field Research Facility. The Sensor Insertion System (SIS) was used to deploy the instruments off of the research pier in both cases.

The SIS95 bedform data set was recorded using a newly developed 37 element Multiple Transducer Array (MTA), as described in the previous chapter. Bedform profiles were recorded every six seconds during the 13 minute data runs. Other instruments deployed during the experiment include a pressure sensor, a bi-directional electro-magnetic current meter, an underwater video camera, and an acoustic concentration profiler. Sediment samples from the bed surface were also obtained with a clam-shell type sediment sampler. The data from all of the instruments was relayed back to a single data logger, which was cabled to a shore based computer system.

Due to the mobility of the Sensor Insertion System (SIS), measurements at many different cross-shore locations were possible. Measurements were made on the beach face, in the inner trough, near the inner bar, and offshore of the bar, as shown in figure 5a. Median sediment sizes ranged from 0.18 to 1.66 mm, water depths ranged from 2 to 7 meters, and H_{mo} wave heights ranged from 0.2 to 0.9 meters over the course of the experiment. The range in mobility number during this experiment was 2 to 71, with mobility number defined as in equation 2.3.

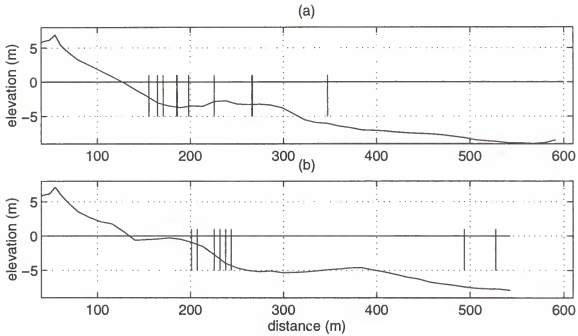

Figure 5. Cross-shore beach profiles taken during the SIS95 (a) and SIS96 (b) experiments. Vertical bars indicate locations of ripple measurements.

The SIS96 bedform measurements were made with a commercially available 64 element SeaTek MTA. This 2.5 meter long array was composed of three smaller arrays. The center MTA was 50 cm long and consisted of 32, 5 MHz transducers with a spacing of 1.5 cm. This center section was very similar to the single MTA used in the SIS95 experiment. The center MTA was flanked on both sides by 100 cm long arrays consisting of 16, 2 MHz, transducers with 6 cm spacing, as shown in figure 6. The SIS96 SeaTek MTA recorded one bedform profile every 2 seconds. This system allowed for the measurement of small scale bedforms with the center MTA and large scale bedforms with lengths reaching over 1 meter with the whole array.

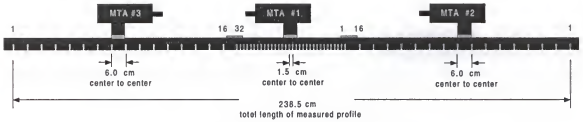

Figure 6. SeaTek 64 element MTA used in SIS96 experiment.

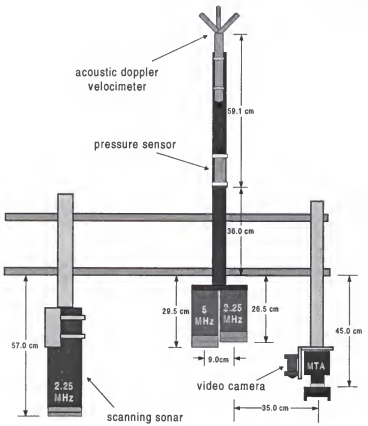

Figure 7. SIS96 Instrument setup as viewed from the offshore direction. The MTA range to the seabed for most runs was ~40 cm.

The SIS96 instrument suite consisted of the MTAs, two acoustic concentration profilers (5 and 2.25 MHz) Mesotech model 810 echo sounders, a rotating scanning sonar (2.25 MHz) manufactured by Mesotech, an under water video camera, a pressure sensor, and an Sontek acoustic doppler velocimeter (ADV). The length of data runs for the SIS96 data set ranged from 13 to 32 minutes. The instrument setup is shown in figure 7.

The SIS96 measurements were also made at several different cross-shore locations, as shown in figure 5b. Median sediment sizes ranged from 0.12 to 0.21 mm, depths ranged from 1.4 to 7 meters, and H_{mo} wave heights ranged from 0.32 to 1.2 meters. These conditions resulted in a range in mobility numbers from 26 to 256. The SIS96 experiment encountered much more energetic flows than the SIS95 experiment. See appendix for measured hydrodynamic and ripple data.

Data Analysis

The presence of suspended sediment can cause false returns and missed returns in the recorded MTA scans. Because of this, representative profiles were determined from several scans of data. Generally, 10 raw profiles were used to determine a single representative profile. For each transducer, the modal distance to the bed was found from the 10 scans. This distance was then recorded as the range to the bed for that transducer. Such analysis was carried out for every transducer in order to determine the whole representative profile for every 20 seconds of data.

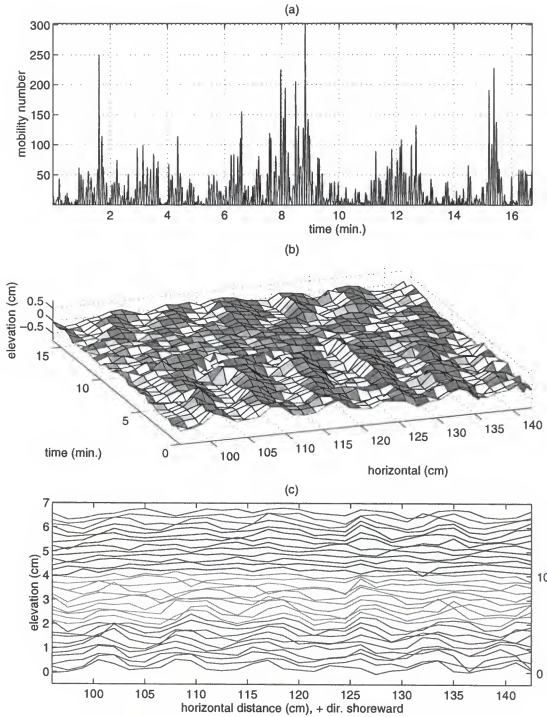

Figure 8. Time series of (a) mobility number and (b) and (c) ripple profiles from SIS96 run 14. Plot (b) has time on the y-axis and horizontal distance on the x-axis, with positive x in the onshore direction. Plot (c) has the first profile of the run plotted as the lower curve, subsequent profiles are offset by +0.2 cm. The time separation between profiles is 30 seconds. The right vertical axis indicates time in minutes for the profiles.

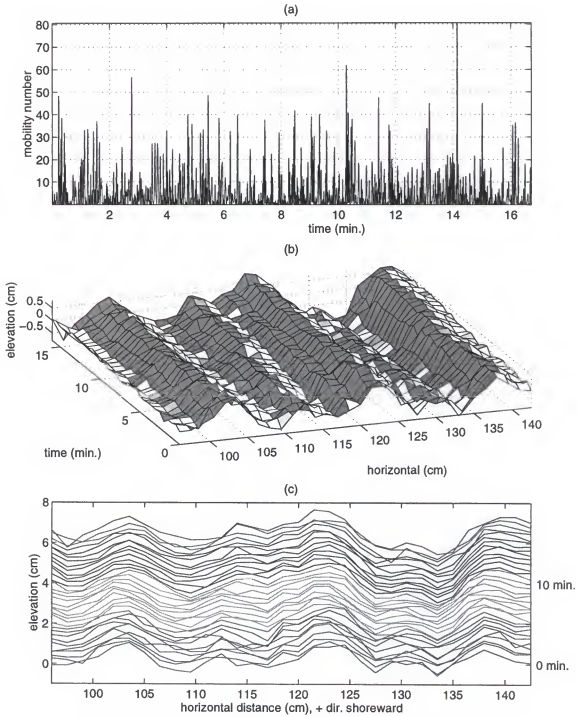

Figure 9. Corresponding time series of (a) mobility number and (b) and (c) ripple profiles from SIS96 run 8.

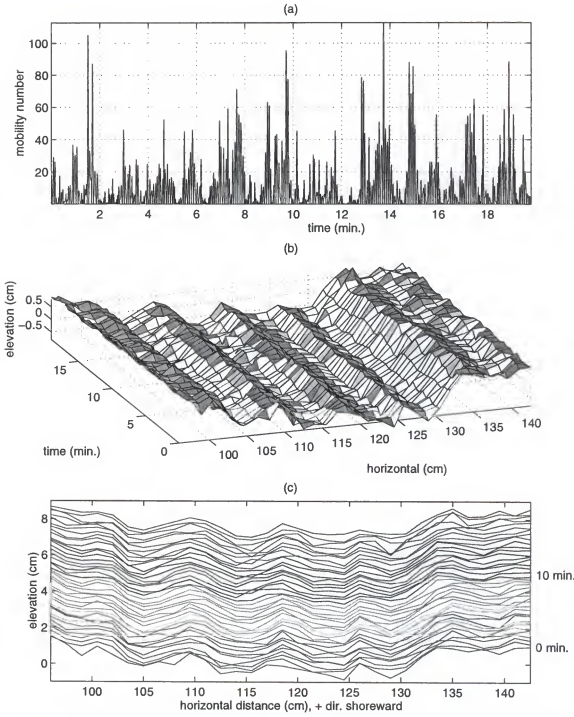

Figure 10. Corresponding Time series of (a) mobility number and (b) and (c) ripple profiles from the SIS96 experiment for run 26.

These representative profiles were then analyzed to find ripple height and length, using a threshold method. First, any linear trend present in the profiles was removed. The removal of the linear trend was to remove the beach slope from the profile data and any settling of the SIS during the run. Settling of the SIS was observed in several of the runs, especially during the first few minutes of the runs. All points of inflection in the profile were then found. The average distance between each minimum and maximum with a vertical separation of at least 3 mm was recorded. A threshold set to one half of this average value was then used to determine the ripple height. Only minimum and maximum range points separated by at least this threshold value were used. Ripple height was found by taking the average vertical separation of these minimum and maximum ranges over the entire profile. Ripple length was found by taking the average of the horizontal separations corresponding to the same maximum and minimum ranges.

For the model comparisons, each run was divided into four sections to show the range of ripple conditions observed during each run. For several of the SIS96 runs the ripple geometry changed over the course of the run. Ripple migration, flattening, and reformation were observed during several of the runs.

An example of ripple flattening and reformation is shown in figure 8. The mobility number time series is plotted in figure 8a. Ripple destruction is seen in figure 8b during periods of high flow intensity, minutes 8 through 9 in the time series. Ripple reformation is observed during periods of lower flow intensity, minutes 10 through 14 in the time series. Figures 9 and 10 are of data recorded under less intense flow conditions. For these runs the bedform profiles remained relatively constant.

It should be noted that many recorded bedform profiles contained both small scale and large scale bedforms. For the SIS96 experiment where large scale bedforms were measured with the 2.5 meter long array, 14 of the 28 runs had both small and large scale bedforms, 11 of the runs had only small scale ripples, and 3 runs had large scale bedforms exclusively because conditions were too energetic for the existence of small scale

bedforms. The ripple data presented herein is of small scale bedforms with lengths of less than 40 cm. This corresponds to ripples having lengths less than approximately $2000d_{50}$. For all of the SIS95 and SIS96 runs, ripples with lengths of less than 40 cm were observed except for a few very energetic flows when their existence was not expected. The large scale ripples measured during the SIS96 experiment with lengths of over 40 cm had rounded crests like megaripples (Clifton, 1976). Measurements and characteristics of these large scale ripples are addressed in chapter 5.

Ripple Model Descriptions

Nielsen (1981) field model

Two semi-empirical ripple prediction models are compared to the SIS95 and SIS96 ripple data sets. The Nielsen (1981) ripple prediction models for field conditions are shown. These models predict ripple height (η) and length (λ) using the near bottom semi-excursion (A) and the mobility number (ψ). Nondimensional ripple height is expressed as

$$\frac{\eta}{A} = 21\psi^{-1.85} \qquad \text{for } (\psi > 10) \qquad \text{equation 4.1}$$

$$\frac{\eta}{A} = 0.275 - 0.022\psi^{0.5} \qquad \text{for } (\psi < 10) \qquad \text{equation 4.2}$$

and nondimensional ripple length is expressed as

$$\frac{\lambda}{A} = \exp\left(\frac{693 - 0.37\ln^8\psi}{1000 + 0.75\ln^7\psi}\right) \qquad \text{equation 4.3}$$

where the mobility number (ψ) is as defined in equation 2.3. The near-bottom orbital velocity can be directly substituted for the ($A\omega$) term in the calculation of mobility number.

The Nielsen (1981) expression for ripple steepness

$$\frac{\eta}{\lambda} = 0.342 - 0.34\sqrt{\theta_{2.5}} \qquad \text{equation 4.4}$$

is in terms of the grain roughness Shields parameter ($\theta_{2.5}$). Which is defined in equation 2.1.

Wiberg and Harris (1994)

Wiberg and Harris (1994) classified bedforms according to the ratio of the near bed orbital diameter (d_o=2A) and anorbital ripple height (d_o /η_{ano}), which is an approximation of the ratio of wave boundary layer thickness to the ripple height (δ_w/η). From this ratio the ripples were classified as orbital, anorbital, or suborbital by the following criteria:

Table 1: Wiberg and Harris (1994) ripple classification

flow conditions	ripple classification
$d_o/\eta_{ano} < 20$	orbital ripples
$20 < d_o/\eta_{ano} < 100$	suborbital ripples
$d_o/\eta_{ano} > 100$	anorbital ripples

Clifton (1976) classified orbital ripples as ripples with lengths proportional to orbital diameter and anorbital ripples as ripples with lengths that are not proportional to orbital diameter. Wiberg and Harris (1994) found that orbital ripple length and height can be reasonably represented as a fraction of the near bed orbital diameter,

$$\lambda_{orb} = 0.62 d_o \qquad \text{equation 4.5}$$

and that orbital ripple steepness remains roughly constant at

$$(\eta/\lambda)_{orb} = 0.17 \qquad \text{equation 4.6}$$

From these two equations orbital ripple height can be found directly as the product of orbital ripple length and steepness.

Wiberg and Harris (1994) found anorbital ripple length to be a function of only grain size (d_{50}), giving;

$$\lambda_{ano} = 535\, d_{50} \qquad \text{equation 4.7}$$

Previous studies such as Nielsen (1981) and Grant and Madsen (1982), had found ripple steepness to be a function of non-dimensional bed shear stress; however, Wiberg and Harris (1994) found that anorbital ripple steepness can be defined in terms of (d_o/η). This allows the calculation of anorbital ripple height without the calculation of bed shear stress, which eliminates some of the complications and uncertainties that arise from the computation of bed shear stress. Wiberg and Harris (1994) found by comparing ripple steepness (η/λ) to non-dimensional orbital diameter (d_o/η) the relationship:

$$\frac{\eta}{\lambda} = \exp\left[-0.095\left(\ln\frac{d_o}{\eta}\right)^2 + 0.442\ln\frac{d_o}{\eta} - 2.28\right] \qquad \text{equation 4.8}$$

for $d_o/\eta > 10$; if $d_o/\eta \leq 10$, $\eta/\lambda = 0.17$.

Wiberg and Harris (1994) found that orbital ripple lengths are a function of orbital diameter and that anorbital ripple lengths are a function of grain diameter. By definition, suborbital ripples have ripple lengths that fall between these two limits. Thus a weighted geometric average of the bounding values of λ_{ano} and λ_{orb} was used to determine suborbital ripple length (λ_{sub}).

$$\lambda_{sub} = \exp\left[\left[\frac{\ln\left(d_o/\eta_{ano}\right) - \ln 100}{\ln 20 - \ln 100}\right]\left(\ln\lambda_{orb} - \ln\lambda_{orb}\right) + \ln\lambda_{orb}\right] \qquad \text{equation 4.9}$$

Model Comparisons

Nielsen (1981)

The Nielsen (1981) model curves for ripple height, length, and steepness are shown in figure 11 along with measured ripple dimensions from the SIS95 and SIS96 experiments. It is seen that the Nielsen (1981) ripple height model over-predicted heights at low mobility numbers ($\psi<30$) and performed better at higher mobility numbers. The model tended to under-predict ripple heights for $\psi>100$. It should be noted that only the data from the 5 MHz MTA is included. Thus only the small scale ripples are represented here.

The Nielsen (1981) ripple length model over-predicted ripple lengths at low mobility numbers ($\psi<15$), and tended to under-predict at high mobility numbers ($\psi>100$). This is shown in Figure 11b. Ripple steepness was over-estimated by the Nielsen (1981) irregular wave ripple steepness model for almost every run. The trend present in the steepness data was correctly captured with this model, however flattening of ripples was observed at lower than predicted Shields parameters, as shown in figure 11c.

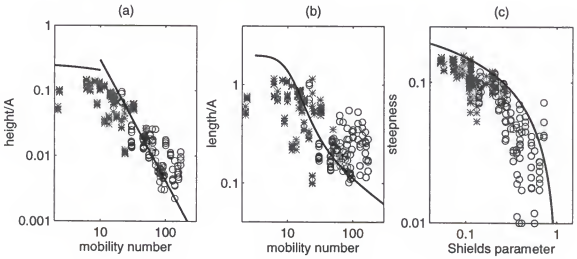

Figure 11. Measured (a) Nondimensional ripple height (η/A) and (b) nondimensional ripple length (λ/A) versus Mobility Number, and (c) ripple steepness versus Shields Parameter for SIS95 (*) and SIS96 (o) data with Nielsen (1981) model curves.

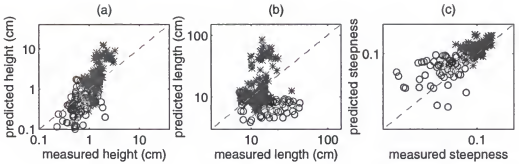

Figure 12. Nielsen (1981) predicted versus measured SIS95(*) and SIS96(o) ripple (a) height, (b) length, and (c) steepness.

Wiberg and Harris (1994)

The Wiberg and Harris (1994) ripple model curves are plotted with the measured SIS95 and SIS96 ripple data in figure 13. In figure 13a, ripple length data is compared to both the orbital and anorbital model curves. One problem encountered with the Wiberg and Harris (1994) model is the misclassification of ripples. Using the classification scheme outlined in Table 1, with calculated anorbital ripple height (η_{ano}), the 30 runs of SIS95 data were classified as 21 orbital, 1 anorbital, and 8 suborbital. When measured ripple heights were used the runs were classified as 6 orbital, 1 anorbital, and 23 suborbital. Thus for 15 of the 30 runs the ripples were incorrectly classified. For the SIS96 data set a more energetic environment was encountered. The SIS96 data set consists of 28 runs, 1 was classified as orbital, 25 as anorbital, and 2 as suborbital when calculated values for ripple height were used. When the measured values for ripple height were used, 0 were classified as orbital, 25 were classified as anorbital, and 3 were classified as suborbital. Thus only 1 of the 28 runs was misclassified for the SIS96 data set.

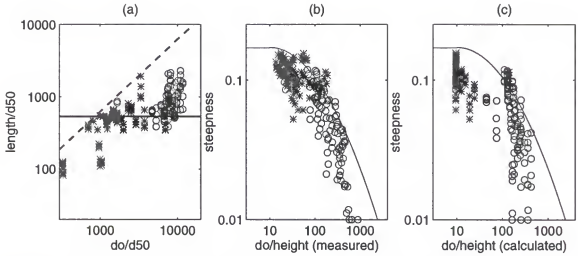

Figure 13. Measured SIS95 (*) and SIS96 (o) ripple data with Wiberg and Harris (1994) model curves, orbital (dashed) and anorbital (solid). (a) ripple length versus Orbital diameter, (b) and (c) steepness versus Orbital diameter / ripple height, (b) contains the measured ripple height where as (c) contains the predicted ripple height.

Figure 13a shows underprediction of ripple length for much of the anorbital ripple length data. It is also shown in figure 14b that the Wiberg and Harris (1994) model overpredicted ripple length for most of the SIS95 data. This was partly due to the misclassification of 15 of the 30 runs as orbital ripples, thus predicting large ripple lengths that are proportional to orbital diameter.

Measured ripple height is compared to predicted ripple height in figure 14a. It is shown that for most of the runs ripple height is overpredicted. The Wiberg and Harris (1994) ripple height model was more accurate in predicting ripple height for the SIS96 data set than for the SIS95 data set. This was mainly due to the ability of the model to correctly classify most of the more energetic SIS96 environment as conditions for anorbital ripples.

The Wiberg and Harris (1994) ripple models overpredicted ripple steepness for the majority of the SIS95 and SIS96 measurements. This was due to the overprediction of ripple height for the SIS95 data set and the underprediction of ripple length for the SIS96 data set.

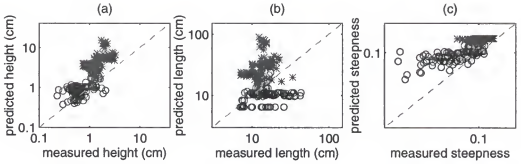

Figure 14. Wiberg and Harris (1994) predicted versus measured SIS95(*) and SIS96(o) ripple (a) height, (b) length, and (c) steepness.

The relative error (Δ) between measured and predicted values can be defined as;

$$\Delta = \exp\left\{\left[\frac{1}{n}\sum_{1}^{n}\left(\ln(u)-\ln(\hat{u})\right)^2\right]^{1/2}\right\} \qquad \text{equation 4.10}$$

where "u" is the measured value and "û" is the predicted value. This quantity is a multiplicative factor that indicates the variation about the predicted value. For example if Δ equals 1.34, the average error is equal to 34 percent.

Table 2. Relative error between measured and predicted ripple geometries.

	Nielsen (1981) field	Wiberg and Harris (1994)
ripple height	2.19	2.34
ripple length	2.02	1.93
ripple steepness	1.75	1.89

The Wiberg and Harris (1994) ripple model and the Nielsen (1981) irregular wave, or field, ripple model performed similarly for the SIS95 and SIS96 data sets. As shown in Table 2, the relative error for ripple height is 2.34 and 2.19 for the Wiberg and Harris

(1994) and Nielsen (1981) ripple models, respectively. Both models performed similarly at predicting ripple length and had relative errors of 1.93 and 2.02 for the Wiberg and Harris (1994) and the Nielsen (1981) models, respectively. The models did better at predicting ripple steepness than ripple height or ripple length independently. The Wiberg and Harris (1994) ripple model had a relative error of 1.89 whereas the Nielsen (1981) model had a relative error of 1.75 in predicting ripple steepness.

The Grant and Madsen (1982) ripple model was also compared to the SIS95 and SIS96 data set. This model was developed primarily from the Carstens et al. (1969) laboratory ripple measurements. The Grant and Madsen (1982) model produced large errors when compared to the new field data sets. The relative errors were 4.23, 3.23, and 1.63 for ripple height, length, and steepness respectively. Because of the large errors, this model was not included in the rest of this analysis.

Using near bottom hydrodynamics in predicting ripple geometries

For the model comparisons described earlier, H_{mo} and the peak wave period were determined from a surface elevation spectrum. A power spectrum was constructed from either the pressure time series or the cross-shore velocity time series. This spectrum was then transposed, using linear wave theory, into a surface elevation spectrum. H_{mo} was then calculated from the area under this spectrum, and the peak period was calculated from the peak frequency of this spectrum.

One problem with this method is that the transfer function from pressure at a given depth to surface elevation amplifies the higher frequency component more than the lower frequency component. If the surface elevation spectrum is then used to determine the peak frequency, which later is to be used to determine near-bottom orbital diameter, there is a potential to use a peak frequency that does not contain the most energy in the near-bottom flows. This can be shown by correcting a measured pressure time series for a

surface elevation spectrum and also for a near bottom orbital excursion spectrum. The lower frequencies are attenuated less than the higher frequencies in the transformation to near-bottom orbital excursion. Figure 15a is a surface elevation spectrum for a SIS95 run and figure 15b is a near-bottom orbital excursion spectrum from the same pressure time series. Clearly the peak frequencies are different for these two spectra. The transfer function used to determine the bottom orbital excursion spectrum from the surface elevation spectrum shown in figure 15 is the linear wave transformation of $1/\sinh^2(kh)$.

For much of the SIS95 data there was a low frequency swell from a hurricane located off-shore and a locally wind generated wave component. When the peak frequency was taken as the peak in the surface elevation spectrum for this data, the local wind generated wave frequency was recorded as the peak frequency for most of the runs. However, when the near-bottom orbital excursion spectrum was used, for most of the cases the peak frequency was from the lower frequency swell component. Because of this problem, another method was developed to determine the spatial and temporal scales of the near-bottom flow used in the prediction of bedform geometries.

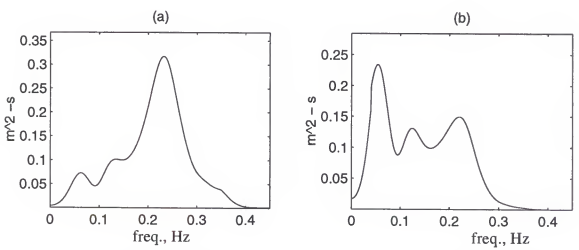

Figure 15. Power spectrums for (a) corrected surface elevation and (b) near-bottom orbital excursion for run 6 of the SIS95 data set.

First, a Fourier transform was performed on either the pressure or the cross-shore velocity time series. It is noted that for the SIS95 data the pressure time series was used, since problems with drift were evident in many of the current meter time series. For the SIS96 data analysis the current meter time series were used for all but three of the runs. During these three runs the current meter was exposed in the wave troughs. The resultant frequency spectrums were transposed to bottom velocity spectrums using linear wave theory. All energy at frequencies lower than $2\pi/25$, corresponding to a 25 second period, was removed. This was to remove all infragravity components, since the present models are based on gravity wave frequencies. An inverse Fourier transform was then performed on the spectrum, resulting in a time series of near bottom orbital velocity.

All zero upcrossings were then found for this near-bottom orbital velocity time series. The maximum absolute value of velocity was then recorded between each upcrossing. An average of the highest one-third of these maximum velocities was then recorded as the significant near-bottom orbital velocity.

In order to find the significant near-bottom orbital diameter, the near-bottom velocity time series was integrated over time. With the low frequency component removed from the near-bottom velocity time series, the near-bed orbital excursion is about a zero mean. Without filtering the low frequency component, the integrated near-bed velocity is dominated by low frequency oscillations with periods on the order of several minutes. A similar procedure was performed on this near-bottom excursion time series to determine significant values. All zero upcrossings were found, and the maximum (positive) and minimum (negative) excursions from the mean were recorded between each upcrossing. The differences between the maximum and minimum excursions for each upcrossing were recorded as near-bottom orbital diameters. The average of the largest one-third near-bottom orbital diameters was recorded as the significant near-bottom orbital diameter for the time series.

For many of the runs the hydrodynamics and the bedform geometry varied significantly over the course of a run, presumably due to the presence of wave groups. Because of this, each run was divided into four sections. Four values of significant near-bottom orbital diameter and significant near-bottom velocity were computed for each run. These correspond to the same time intervals that the four values for ripple height, length, and steepness were calculated. Figure 16a shows a comparison of orbital diameters calculated from H_{mo} and from the near bottom significant method for all of the SIS95 and SIS96 runs. Figure 16b is a similar plot showing a comparison of mobility numbers calculated from the two different methods.

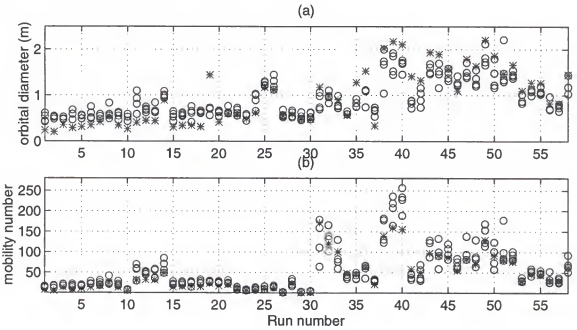

Figure 16. Orbital diameter versus run number (a) and mobility number versus run number (b) for near-bottom significant values (o) and H_{mo} derived values (*) for the SIS95 (run 1 to 30) and SIS96 (run 31 to 58) data sets.

The Wiberg and Harris (1994) and the Nielsen (1981) ripple models were then used with significant values for near-bottom velocity and orbital diameter to predict ripple geometry. In figure 17, the Nielsen (1981) model curves are compared to measured parameters with the hydrodynamics described as above. It is seen that for low values of

Mobility number, (ψ< 20) both nondimensional ripple height (η/A) and nondimensional ripple length (λ/A) are overpredicted by the Nielsen (1981) model. Whereas for large values of mobility number (ψ>100) both properties are underpredicted by this model.

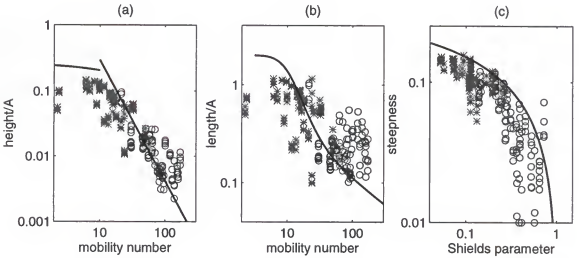

Figure 17. Measured (a) Nondimensional ripple height (η/A), (b) nondimensional ripple length (λ/A), and (c) ripple steepness for SIS95 (*) and SIS96 (o) data with Nielsen (1981) model curves with Mobility Number, Shields parameter, and semi-excursion calculated from significant near-bottom orbital velocity and orbital diameter.

Figure 18 shows the Wiberg and Harris (1994) model curves compared to the significant near-bottom conditions. The model results from the significant near-bottom conditions are very similar to those in the previous section. For most of the SIS95 data set, ripple heights and lengths are overpredicted, and for most of the SIS96 data ripple lengths are underpredicted. The primary reason for the consistent discrepancy in the SIS95 data set is still the misclassification of ripple type. The Wiberg and Harris (1994) classification scheme misclassified 40% of the ripples in the SIS95 data set and 3% in the SIS96 data set. This gives a total misclassification of 22% for both data sets. Most of the problem was in classifying suborbital ripples as orbital ripples. Ripple length was then

based on a proportion of orbital diameter, and ripple steepness was taken as a constant. This then led to the overprediction of both ripple length and height.

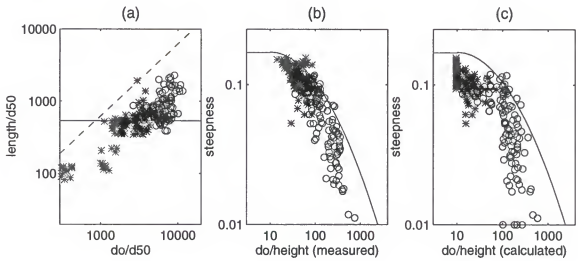

Figure 18. Measured SIS95 (*) and SIS96 (o) ripple data with Wiberg and Harris (1994) model curves, orbital (dashed) and anorbital (solid) for significant near-bottom orbital diameter data. (a) ripple length versus orbital diameter, (b) and (c) steepness versus orbital diameter / ripple height, (b) contains the measured ripple height where as (c) contains the predicted ripple height.

The Nielsen (1981) ripple height and length models produced larger errors when significant bottom conditions were used than when H_{mo} derived conditions were used. This was mainly due to the higher mobility numbers associated with the significant bottom velocities than those derived from H_{mo} and peak period. These larger mobility numbers produced even larger errors in predicting ripple height and length at mobility numbers greater than 100. The tendency of underprediction at high mobility numbers can be seen in figure 17.

The Wiberg and Harris (1994) ripple models produced greater errors in predicting ripple geometry when the near-bottom significant orbital diameter and velocity were used than when H_{mo} and peak period were used to determine orbital diameter and velocity. This was because for most of the SIS95 data set the significant orbital diameter was larger

than the calculated orbital diameter from H_{mo}. Since many of the ripples were misclassified, ripple lengths and heights were based on proportions of orbital diameter. For most of the SIS95 data this led to even higher overpredictions. For the SIS96 data, both the significant method and the H_{no} method performed similarly. The relative errors associated with the predicted ripple geometries when significant near-bottom conditions are used are shown in Table 3.

Table 3. Relative error between measured and predicted ripple geometries when significant near-bottom conditions are used as input.

	Nielsen (1981) field	Wiberg and Harris (1994)
ripple height	3.48	2.98
ripple length	2.14	2.12
ripple steepness	1.84	1.94

New Model Development

As shown in the previous figures, the Wiberg and Harris (1994) and Nielsen (1981) ripple models did not correctly capture all of the trends in the SIS95 and SIS96 data. For this reason, we are motivated to develop new ripple prediction formulae. The new formulae are based solely on mobility number and orbital semi-excursion, which are found by using the near-bottom significant values described previously.

Non-dimensional ripple height (η/A) is described as a function of mobility number (ψ) as follows:

$$\frac{\eta}{A} = 0.09 \qquad \text{for } (\psi \leq 10) \qquad \text{equation 4.11}$$

$$\frac{\eta}{A} = 0.9\psi^{-1} \qquad \text{for } (\psi > 10) \qquad \text{equation 4.12}$$

A plot of (η/A) versus mobility number for the SIS95 and SIS96 data with this curve is shown in figure 19a. The relative error in predicting ripple height with this model is 1.53.

Ripple steepness was also found to be a function of mobility number. The SIS95 and SIS96 data were best described by

$$\frac{\eta}{\lambda} = -0.006\psi^{0.6} + 0.15 \qquad \text{for } \psi < 190 \qquad \text{equation 4.13}$$

$$\frac{\eta}{\lambda} = 0.01 \qquad \text{for } \psi \geq 190 \qquad \text{equation 4.14}$$

This formula was developed by minimizing the relative error with the SIS experimental data and is shown in figure 19b along with the SIS95 and SIS96 data sets. The relative error between predicted and measured values of ripple steepness for the SIS data sets was 1.52 for this formula. It is noted that for mobility numbers greater than 190 a constant steepness of 0.01 is predicted. Since ripple length can be computed by dividing ripple height by ripple steepness, the lower limit of ripple steepness was taken as 0.01 so as to provide reasonable estimates for ripple lengths at high mobility numbers.

The three data points that fall well below the model curves at very low mobility numbers are for sediment with a median diameter of 1.66 mm. The sediment from the inner trough region where these measurements were made had a bimodal distribution, with one mode located around 1.6 mm and the other around 0.2 mm. Diver observations from this region indicate that the larger sediment was located at the ripple crests and the smaller sediment at the ripple troughs. Since the median value for sediment size is used in this analysis, the smaller sediment present in this particular distribution is not represented in the calculation of mobility number.

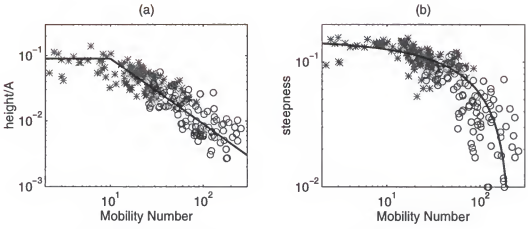

Figure 19. Measured (a)Nondimensional ripple height (η/A) and (b) ripple steepness for SIS95 (*) and SIS96 (o) data with the new model curves. Mobility Number and semi-excursion are calculated from the significant near-bottom orbital velocity and significant orbital diameter.

Ripple length can be determined by dividing ripple height by ripple steepness. The relative error in predicting ripple length for the SIS95 and SIS96 data sets was 1.55. Nielsen (1981) observed different trends in ripple steepness versus mobility number for sediments of different densities. It is noted that all of the field data used to construct this model is from areas where the sediment was composed primarily of quartz sand.

Comparison of new model with previous field ripple measurements

The relationship between the SIS95 and SIS96 data sets and previous field ripple measurements is shown in figure 20. Only small scale field ripple data with ripple lengths of less than 40 cm were included. This was to reduce the chance of representing megaripple data in this small scale ripple analysis. There was a total of 70 measurements that met these criteria. In the determination of relative errors, flatbed conditions were not considered because artificial errors would be induced when height, length, and steepness values were assigned to these conditions. The flatbed conditions are included in figure 20b, and are plotted as a steepness of 0.01.

It is noted that only the Dingler (1974) data was recorded with ultrasonic instrumentation, and that the other field data sets were recorded through diver observations. It is the authors' experience that the measurement of ripple height while diving is subject to large uncertainties. Some of the variation in observed trends between diver collected data and the data that was recorded with ultrasonic instrumentation could be due to diver measurement errors. The new method agrees well with the Dingler (1974) data, however both ripple height and ripple steepness are underpredicted for the Inman (1957) data at low Mobility Numbers and for some of the Nielsen (1984) data. Some of the Nielsen (1984) and Inman (1957) runs contain data with lengths between 30 and 40 cm. Thus some of the disagreement between the curves and the outlying data points may be due to the inclusion of larger scale bedform data even though a cutoff of 40 cm on ripple length was applied to the data.

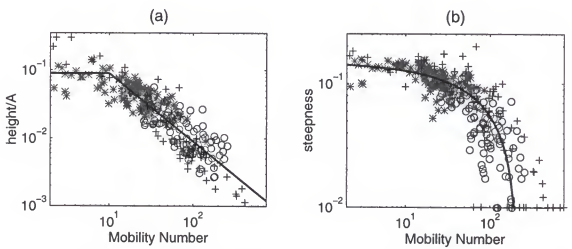

Figure 20. Nondimensional ripple height/ orbital semi-excursion (a) and ripple steepness (b) versus Mobility Number with new model curves and all available field ripple data. Included are previous field measurements from Inman (1957), Dingler (1974), and Nielsen (1984) (+), SIS95 (*) and SIS96 (o).

Table 4. Relative error between measured and predicted ripple geometries for all previous small scale field data.

	New Model	Wiberg and Harris (1994)	Nielsen field (1981)
ripple height	1.82	1.65	2.12
ripple steepness	1.62	1.46	1.68
ripple length	2.04	1.30	1.50

In table four the relative error between measured and predicted ripple geometries are shown for the new model, the Wiberg and Harris (1994) model, and the Nielsen (1981) field model. All available small scale field ripple data measured previous to the SIS95 and SIS96 experiments were used in the calculation of these relative errors. These include the field measurements of Inman (1957), Dingler (1974) and Nielsen (1984). It is shown that the new model performed similarly to the other models in predicting ripple height, and that the Wiberg and Harris (1994) model gave the best predictions. All of the models performed similarly in predicting ripple steepness however the Wiberg and Harris (1994) model did slightly better than the other two. Ripple length was better predicted by the Wiberg and Harris (1994) and Nielsen (1981) than it was with the new model for these data sets. It should be noted that the Wiberg and Harris (1994) model was constructed with the data shown, and that the Nielsen (1981) was constructed with the data shown that was collected prior to 1981. Also, only a single wave-height and wave period were given for each of the measured data points in the previous data sets. Thus significant near-bottom conditions could not be determined for these data sets.

Table 5. Relative error between measured and predicted ripple geometries for all available small scale field data; including the SIS95 and SIS96 data sets.

	New Model	Wiberg and Harris (1994)	Nielsen field (1981)
ripple height	1.60	2.42	2.33
ripple steepness	1.54	1.84	1.70
ripple length	1.68	1.96	2.01

Relative errors between measured and predicted ripple dimensions were calculated for the complete field data set. This data set includes the SIS95, SIS96, and the previously collected data sets discussed above. Table five contains these relative error values. The new model did much better at predicting ripple height than did the other two models. The average error was 60% for the new model whereas errors of 142% and 133% were calculated for the Wiberg and Harris (1994) and the Nielsen (1981) models, respectively. The new model also had better agreement than either of the other two models at predicting ripple steepness and length.

Conclusions

A multiple transducer array was used to remotely measure bedforms during the SIS95 and SIS96 experiments in Duck, North Carolina. Existing methods for predicting small-scale ripple geometry did not capture all of the trends found in this new data set. A new method for predicting ripple geometry is described. This method does not require the calculation of bed shear stress or the classification of ripple regimes as previous models did. This new method relates ripple height and steepness to near bottom mobility number by a few simple relations.

All available field data were used to test the new model and the Nielsen (1981) and Wiberg and Harris (1994) models. The new model did substantially better at predicting ripple height, with average errors of 60% compared to 142% and 133% for the Wiberg and Harris (1994) and the Nielsen (1981) models respectively. The new model also gave better estimates of ripple steepness and length. When only the new SIS95 and SIS96 data sets were used, average errors of approximately 50% were observed in predicting ripple height, steepness, and length with the new ripple prediction method.

CHAPTER 5
OBSERVATIONS OF BEDFORM DYNAMICS

Introduction

Small scale vortex ripples and larger scale megaripples populate much of the near-shore coastal environment. The geometry of these bedforms is important to sediment transport processes. Bedforms directly affect the bottom roughness and thus influence the bottom shear stress, the profile of turbulence, and the rate of sediment transport for given wave and current conditions (Vongvissessomjai, 1984).

The dynamics of bedforms are also important in predicting sediment transport. Ripple migration can account for a significant part of the transported sediment under certain wave conditions, (Osbourne and Vincent, 1993, Hay and Bowen, 1993). Ripple flattening and reformation is also important in the prediction of sediment transport. If ripple destruction under wave groups is not accounted for, the predicted sediment transport rate could differ substantially from the actual transport rate. Observations have shown that under many flow conditions the ripples constantly change to match the flow. These changes can occur on time scales as short as a single wave period (Dingler and Inman, 1976).

The purpose of this chapter is to present observations of small scale ripples and megaripples from a field experiment. Ripple migration, flattening, and reformation is demonstrated for a quartz sand seabed in the near-shore environment. Comparisons of ripple behavior to the hydrodynamic forcing are also presented along with a brief description of the instrumentation.

Experimental Setup

A field experiment investigating sediment transport processes was conducted at the U. S. Army Corps of Engineers Field Research Facility in Duck, North Carolina from October 30 to November 2, 1996. The Sensor Insertion System (SIS) on the research pier was used for instrument deployment. The SIS is a movable system that allows measurements to be made at a multitude of cross-shore locations. The measurements presented herein span a variety of water depths, wave heights, and sediment conditions, as summarized in Appendix A. A cross-shore profile measured during this experiment is shown in Figure 5.

Many instruments were deployed during this experiment. To measure bedforms, a SeaTek multiple transducer array (MTA), a rotating scanning fan beam sonar (RSS), and an underwater video camera were deployed. Two acoustic backscatter sensors and an optical backscatter sensor were deployed to measure suspended sediment and turbidity. An acoustic doppler velocimeter and a strain type pressure sensor were used to record hydrodynamic data. All of these instruments, except for the RSS, were controlled via a data logger located in an underwater package. Once the data was recorded by the data logger, the data was downloaded to a shore-based system and archived.

The SeaTek multiple transducer array (MTA) used in this experiment consists of three sections. The center section is 0.5 meter in length and composed of a 32 element linear array of 5 MHz transducers. The center to center spacing of these transducers is 1.5 cm. The acoustic footprint at 0.5 meter range is approximately 2.5 cm. The system is capable of 1 millimeter vertical resolution under ideal conditions. The center array is flanked on both sides by 1.0 meter arrays. These longer arrays operate at 2 MHz and contain 16 transducers with 6 cm spacing. The acoustic footprint at a range of 0.5 meter is approximately 4.5 cm for these arrays. All three sections were attached together to form a continuous 64 element array with a length of 2.5 meters. This 2.5 meter array is capable of

measuring large scale megaripples, with all 64 transducers, and small scale vortex ripples with the center, 32 element, section. Figure 3 is a schematic of the SeaTek MTA used in this experiment.

Each MTA has its own pressure housing that contains a data logger and the electronics necessary to run the transducers. Each of the MTAs log an entire run of data and then offload this data at the end of the run to the main data logger in the under water package. The data from all of the instruments is then stored in a single file and offloaded to shore.

Several MTA parameters can be changed remotely from a shore-based computer. These include the receiver threshold, blanking period, scan rate, and number of scans to record during each run. The MTAs only record a single range measurement for each transducer per scan. The return signal is run through a comparitor. When the return signal voltage meets a certain prescribed threshold, the time delay from transmit is recorded. This time for the reflected ultrasonic signal to return back to the transducer is then used to determine the distance to the bed. Blanking is used to reduce the number of false returns. Blanking is the time delay, after the transmit pulse is sent, before the comparitor starts to monitor the return signal for a bottom return. The maximum scan rate of the MTA was one profile every two seconds. The MTAs are equipped with time varying gain (TVG). Time varying gain is used to compensate for spherical spreading and water attenuation losses in the acoustic signal.

During periods of high sediment suspension some false returns were recorded with the MTA. For this reason, some of the data presented herein is from profiles representing 20 seconds of data. There are also examples of raw data presented so that time scales on the order of wave periods can be studied.

A rotating scanning sonar equipped with a fan beam transducer was also deployed. The sonar operated at 2.25 MHz and was mounted on a stepper motor with 0.225 degree increments. The width of the fan beam in the far field is nominally 0.9 degrees in the

horizontal and 30 degrees in the vertical. Planform images of the seabed within a radius of 5 meters from the sonar were recorded on video tape. The instrument was able to detect large and medium scale bedforms in regions where the transmitted signal propagated nearly perpendicular to the ripple crests. Large scale ripple orientation and rough estimates of migration rate are possible with such a system (Hay and Wilson, 1994).

A monochrome low light underwater video camera was also mounted next to the MTA. The primary purpose of this camera was to document small scale ripple orientation. During many of the runs, visibility permitted video recording of small scale ripples and visual observation of sediment processes near the bed.

An acoustic doppler velocimeter (ADV) and a pressure transducer were used to measure the current and wave conditions. For most of the data presented herein the near-bottom orbital velocity and orbital excursion time-series were derived from the ADV time series. A fast Fourier transform (FFT) was first performed on the cross-shore velocity time series. This velocity spectrum was then transposed to a bottom velocity spectrum using the linear theory correction factor, k_c.

$$k_c = \frac{\cosh k(h+z)}{\sinh kh} \qquad \text{equation 6.1}$$

An inverse fast Fourier transform (IFFT) was then performed, resulting in the depth corrected bottom time series for orbital velocity. This time series was then integrated to determine a near-bottom orbital excursion time series.

A time series of mobility number, defined as

$$\psi(t) = \frac{u(t)|u(t)|}{(s-1)gd_{50}} \qquad \text{equation 6.2}$$

can then be found from the time series of cross-shore near-bottom orbital velocity, $u(t)$. Mobility number has been shown by several authors to be an important parameter in bedform dynamics (Dingler and Inman, 1976, Nielsen 1981).

Ripple Flattening and Reformation

For several of the SIS96 runs, small scale ripple flattening and reformation were observed. Megaripples exhibit length scales on the order of one meter and do not have regular vortex formation every half-wave cycle (Nielsen, 1992). Megaripple crests are generally more rounded than vortex ripple crests, and can sometimes be superimposed with vortex ripples (Nielsen, 1992). Megaripples are referred to herein as large scale ripples.

Observations of bedform dynamics from the SIS96 experiment indicate that ripple flattening and reformation is related to mobility number. During periods of high peak mobility numbers, ripples tend to be flattened. The reformation of these ripples occurs within a range of mobility numbers that are large enough to move sediment but not so large as to cause flattening.

Figure 21a is a plot of the mobility number time-series and figure 21b is a time-series plot of ripple height for run 2. In this case the ripple heights were determined from the spatial standard deviation time-series for the detrended ripple profiles. The ripple heights were calculated by multiplying the standard deviation by 2.83, which is the multiplier used to obtain height from standard deviation for sinusoidal curves. Figure 22 shows the bedform profile time-series from the center 5 MHz MTA for run 2. Mobility numbers reached values greater than 200 near the 3 minute point of the run. During this period the small scale ripples were flattened, which is shown by the decrease in ripple height during this period in figure 21b. This is also shown in figure 22 and was observed on the underwater video. Once the wave energy decreased, the ripples reformed during minute 4. The ripple profile remained relatively constant during minutes 5 through 8, with no significant migration or growth. During the event between minutes 8 and 9 when peak mobility numbers briefly reached values greater than 150, some decrease in ripple height was observed. The large mobility numbers during minutes 11 and 12 flattened most of the

ripples shown in figure 22. This flattening is also shown in figure 21b by the decrease in ripple height from 0.6 to 0.35 cm. Peak mobility numbers reached values of over 200 during this one minute event. The ripples reformed during the minute following the event. Even though mobility numbers reached values of nearly 200 during the remainder of this run, the ripples were not flattened. This is most likely due to the duration of the event. Only one or two waves created mobility numbers near 200 on this occasion. It appears several waves with mobility numbers larger than 150 are required for significant flattening of small scale ripples.

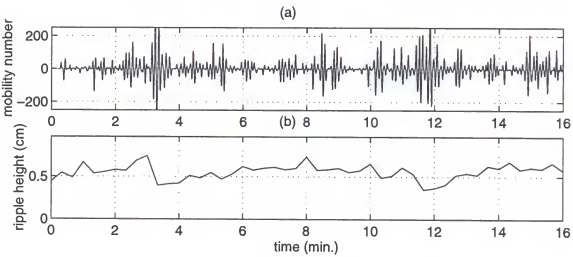

Figure 21. Time series of mobility number (a) and ripple height (b) for run 2.

Figure 22b is a plot of the raw MTA data for minutes 8 through 15 of run 2. The time between profiles is 2 seconds. Light shades correspond to higher bed elevations than do darker shades. False returns from suspended sediment can be seen as light areas during periods of significant sediment suspension. Such events occurred at minutes 9, 10 and 11.5. The ripples were flattened during the event near minute 12. When the ripples were flattened, the seabed was located very close to the mean elevation of the previously rippled bed. It should be noted that during some periods of high suspended sediment concentrations, the MTA recorded false returns from the suspended sediment. Most likely

the true bottom returns, shown after the suspension events, were measured after a significant portion of the suspended sediment settled out of suspension.

For this run, complete ripple reformation occurred during the minute after the ripples were flattened. The peak mobility numbers during minute 13 were near 100. Such mobility numbers seem to be conducive for fast recovery of flattened bedforms. Such flows are strong enough to readily move sediment, however they are not too strong so as to impede ripple formation or cause flattening.

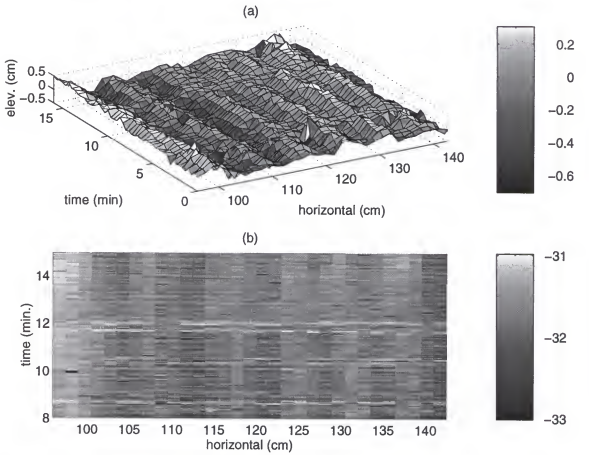

Figure 22. Small scale bedform profiles for run 2. Mesh plot of bedform profiles (a) with time on the y-axis and elevation in centimeters as indicated by the colorbar. Raw MTA bedform profiles for minutes 8 through 15 (b). The time between scans is 2 seconds. Range to the seabed is in centimeters as indicated by the colorbar. Time is plotted on the y-axis and horizontal distance is plotted on the x-axis.

The time-series for mobility number and ripple height are shown in figures 23a and 23b for run number 14. Bedform profiles are shown in figure 24. It is shown in figure

23b that for the first 1.5 minutes the ripples increased in height from 0.5 to 0.75 cm. During the second minute peak mobility numbers briefly reached values over 200. This resulted in a reduction of ripple height to 0.4 cm that quickly recovered to 0.62 cm over the next minute. The ripple profile remained relatively constant until minute 8. During minute 8, the peak mobility numbers reached values of over 200 on several occasions, and remained above 150 for a large portion of the minute. The bedforms were almost completely flattened by this episode. The ripple height, as determined from the spatial standard deviation, for this period was 0.2 cm. The heights of the small scale bedforms remained very small during the period of low mobility numbers through minutes 10 and 11. The peak mobility numbers of near 100 around minutes 12 through 14 resulted in growth of the ripples. Another wave group with a peak mobility number of 200 during minute 15 resulted in a decrease in ripple height. It is noteworthy that the data from the MTA and the video data indicate a nearly flat bed during minutes 9 through 11, and that the ripples begin to reform at their previous locations during minute 12.

Figure 24b is a plot of the raw MTA data for minutes 10 through 15 of run 14. Rapid reformation of the previously flattened ripples is shown in this figure at minute 13. This corresponds to the end of the wave group seen in the mobility number plot between minutes 11 and 13. Reformation of the ripples occurred within 20 seconds after the passing of the wave group. Continual growth in ripple height was observed from minutes 12 through 14 for the ripples with heights of 0.5 cm and lengths of 11 cm. It is noted that the bedslope has not been removed from the data plotted in figure 24b. The elevation of the bed is increasing in the onshore, positive 'x', direction.

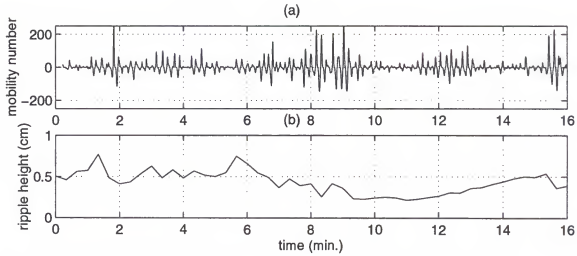

Figure 23. Time series of mobility number (a) and ripple height (b) for run 14

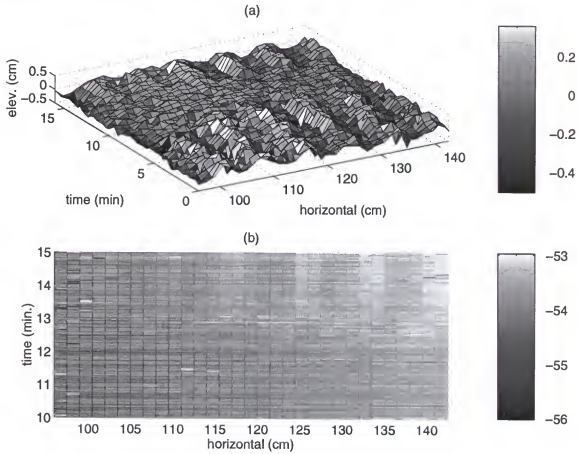

Figure 24. Small scale bedform profiles for run 14. Mesh plot of bedform profiles (a) with time on the y-axis and elevation as indicated by the colorbar in centimeters. Raw MTA bedform profiles for minutes 10 through 15 (b). The time between scans is 2 seconds. Range to the seabed is in centimeters as indicated by the colorbar. Time is plotted on the y-axis and horizontal distance is plotted on the x-axis.

Ripple flattening and reformation were observed during run 20 both with the MTA and under-water video. For most of the other runs, when conditions were energetic enough for ripple flattening, visibility was not sufficient for under-water video viewing of the bedforms. The mobility number time-series for run 20 is plotted in figure 25a and ripple height as determined from the standard deviation is plotted in figure 25b. For several periods during this run the mobility number exceeded values of 200. The small scale bedforms recorded with the 5 MHz MTA are shown in figure 26. It is noted that the small scale ripples shown are superimposed on a migrating megaripple that will be addressed later. Because of this, the ripple heights determined by the standard deviation contain some of the variance due to this larger megaripple and do not accurately depict the heights of only the small scale ripples.

Ripple flattening was observed during the wave groups at minutes 4 and 8. At around the 4.5 minute mark the peak mobility number exceeded 200 during several waves, and ripple flattening was recorded with both the video and MTA. At the 5 minute mark in figure 26b, it can be seen that the measured profile is approximately flat. Again, the white areas in this figure are false returns from suspended sediment. Figure 27 is a compilation of several images from the under-water video recordings during this run. Figure 27a is an image recorded just after most of the suspended sediment settled out of suspension at minute 5:00. This image indicates that the seabed is essentially flat since shadows from ripples are not seen. Figure 27b is an image recorded 35 seconds later. Ripples can be seen in this image. Figure 27c was recorded 1 minute and 10 seconds after the first image. Again, small scale ripples can be clearly seen in this image. The MTA profiles were recorded on a transect parallel with the horizontal axis in figure 27.

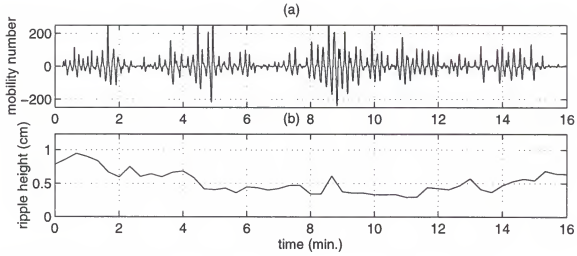

Figure 25. Time series of mobility number (a) and ripple height (b) for run 20.

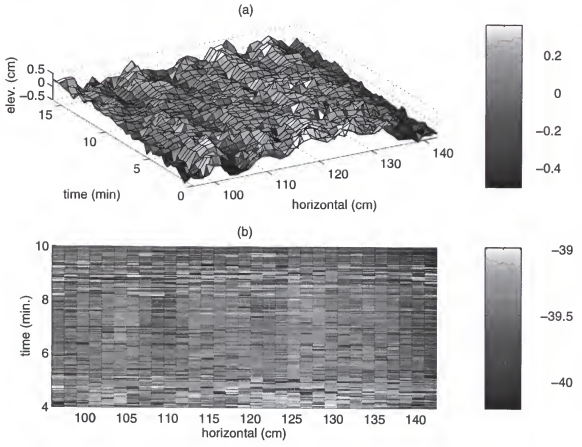

Figure 26. Small scale bedform profiles for run 20. Mesh plot of bedform profiles (a) with time on the y-axis, and elevation in centimeters as indicated by the colorbar. Raw MTA bedform profiles for minutes 4 through 10 (b). The time between scans is 2 seconds. Range to the seabed is in centimeters as indicated by the colorbar. Time is plotted on the y-axis and horizontal distance is plotted on the x-axis.

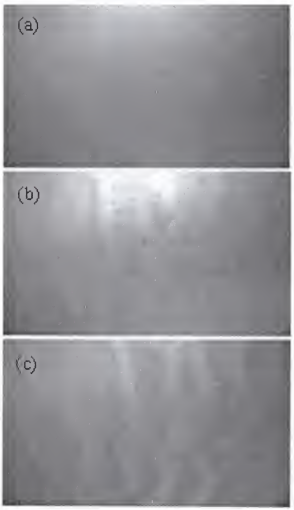

Figure 27. Under-water video images from Run 20 for time 5:00 (a), 5:35 (b), and 6:10 (c). Ripple reformation over the course of one minute is shown.

The flattening of small scale vortex ripples appears to be a function of mobility number. Peak mobility numbers greater than approximately 150 can potentially flatten ripples. Dingler and Inman (1976) suggested that a single wave with a mobility number of over 240 can flatten a rippled bed. The SIS96 bedform observations support this finding. For mobility numbers less than approximately 240 and greater than approximately 150, several waves are required to completely flatten the ripples. Higher mobility numbers require fewer waves to flatten ripples than do lower mobility numbers.

Ripple reformation can occur within a minute after flattening, and in certain conditions within a couple of wave periods. Once the peak mobility numbers decrease to values below approximately 150, the ripples tend to reform. If the peak mobility numbers are too low, the ripples will not reform until appropriate mobility numbers are reached. For most of the data presented, it appears that if the peak mobility numbers remain below approximately 50, ripple reformation is slow. Once mobility numbers of greater than 50 and less than 150 are reached and maintained, the ripples appear to reform rapidly, often within one minute.

Most of the ripple destruction and reformation observed show ripple reformation in roughly the same position as the previous ripple. For many runs slight ripple remnants were observed. This would logically lead to reformation in the same location. However, for other runs an apparently smooth bed was observed with MTA profiles and underwater video recordings. Even during some of these cases the ripples reformed in the same locations. This possibly could be due to some remnant ripples outside of the measurement area or ripple remnants of less than 2 or 3 mm leading to ripple repopulation in the same locations. Since the vertical resolution of the MTA is decreased during periods of high suspended concentration, remnants of less than 2 or 3 mm would not be seen under such flows.

Ripple migration

Large Scale Migration

Migration of large scale ripples, or megaripples, was observed with the complete 64 element MTA. These bedforms had lengths of greater than 40 cm, and heights of 3 to 10 cm. During runs 19 through 21, megaripple migration was observed. Runs 19, 20, and 21 were recorded over an 85 minute period. The profiles from these runs are plotted in figure 29. Run 19, shown by the lowest group of curves, spans minutes 1 to 16. Run 20

is shown in the center group of curves and spans minutes 50 to 66. Run 21 is shown at the top of figure 29 and spans minutes 69 to 85. During these runs the megaripple crest in the center of the profiles migrated approximately 50 cm. This corresponds to an average migration rate of 0.59 cm/min. The height of this bedform ranged from 4 to 6 cm and the length, as measured from a cross-shore transect, ranged from 100 to 130 cm during the course of these runs.

The mobility number time series for runs 19, 20 and 21 are shown in figure 28. During run 20 the wave energy increased, and the mobility number reached values of over 300. The steepness of the megaripple crest decreased during this period. Run 21 had several waves that resulted in mobility numbers of approximately 200. The megaripple in figure 29 remained similar in shape during runs 20 and 21. The forward face of the megaripple migrated approximately 18 cm shoreward during run 20. This compares to 10 cm for run 19 and 8 cm for run 21, when the waves were less energetic.

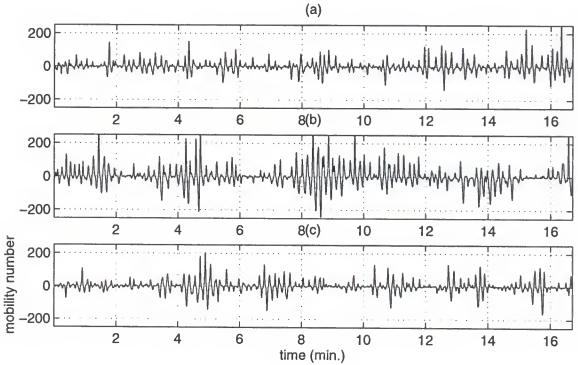

Figure 28. Time series of mobility number for runs 19 (a), 20 (b), and 21 (c).

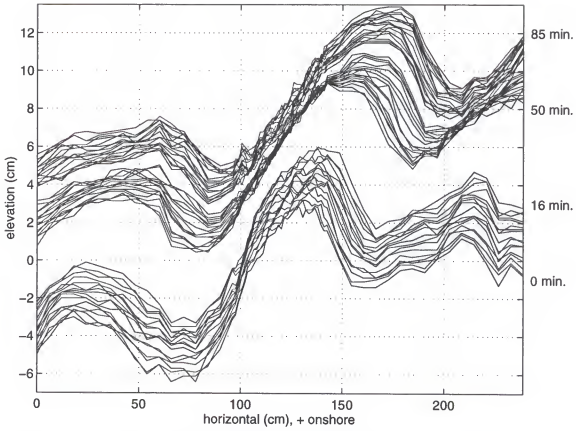

Figure 29. Bedform profiles for runs 19, 20, and 21. One minute separation between profiles, each profile is offset by +2 mm. Time for the profiles is recorded on the right vertical axis.

The megarripples measured with the MTA during runs 19, 20, and 21 were uniform and long crested. Planform images of these megaripples were recorded with the rotating scanning sonar (RSS). An image recorded at the beginning of run 19 is shown in figure 30. The returns from the instrument frame and MTA are outlined in white boxes. The returns from the upslope of the megaripples are shown as white lines extending from the upper right to the lower left of the figure.

Figure 30. Rotating scanning sonar (RSS) image from the beginning of run 19. The white boxes enclose returns from the MTA (top) and instrument mounting arms (lower). Light patches running from upper right to lower left correspond to returns from ripple crests of large scale bedforms. Concentric circles indicate range in one meter increments. The onshore direction is towards the right in the figure.

Ripple migration may account for a significant portion of the total sediment transport for certain wave and current conditions. The migration of the megaripple shown in the center of figure 29 represents a cross-shore transport rate per unit length of beach of 144.7 g cm^{-1} hr^{-1}. This transport rate was calculated by first finding the area under the ripple crest, A_r, for the starting and ending profile of runs 19 and 21, respectively. The center of mass for both of these areas was then found. The cross-shore velocity of the ripple, c, was determined by the horizontal displacement of the center of mass divided by the time between profiles. The length of the ripple, λ, was measured as the cross-shore

distance between troughs. The porosity of the sediment, ϕ, was taken as 0.35 for medium sand. The transport rate associated with the migration of the megripple per unit length of beach was then calculated as

$$Q_s = \frac{(1-\phi)A_r c}{\lambda} \qquad \text{equation 6.3}$$

with $A_r = 357\ cm^2$, c=23.1 cm/hr, and λ=100 cm.

To estimate bedload transport, a Meyer-Peter (1948) type formula was used with a slope modification as suggested by Fresdsøe (1978). This type of bedload formula was designed for unidirectional flows. However an adapted instantaneous version can be used as an indicator for bedload transport under oscillatory flows (Nielsen, 1992). The time-series of mobility number and Swart's (1974) friction factor were used to determine the time series of the grain roughness Shields parameter, $\theta_{2.5}(t)$. The nondimensional bedload transport, $\Phi(t)$, is expressed as:

$$\Phi(t) = 8\left(\theta_{2.5}(t) - 0.05 - 0.1\frac{\partial h}{\partial x}\frac{\theta_{2.5}(t)}{|\theta_{2.5}(t)|}\right)^{3/2}\frac{\theta_{2.5}(t)}{|\theta_{2.5}(t)|} \qquad \text{equation 6.4}$$

for

$$|\theta_{2.5}(t)| > 0.05 + 0.1\frac{\partial h}{\partial x}\frac{\theta_{2.5}(t)}{|\theta_{2.5}(t)|} \qquad \text{equation 6.5}$$

and

$$\Phi(t) = 0 \qquad \text{for} \quad |\theta_{2.5}(t)| \le 0.05 + 0.1\frac{\partial h}{\partial x}\frac{\theta_{2.5}(t)}{|\theta_{2.5}(t)|} \qquad \text{equation 6.6}$$

where the bedload transport rate, $Q_b(t)$, is expressed as

$$Q_b(t) = \Phi(t) d_{50}\sqrt{(s-1)g d_{50}} \qquad \text{equation 6.7}$$

A positive $\theta_{2.5}(t)$ represents a flow in the on-shore (positive x) direction. A positive bottom slope (dh/dx) corresponds to an increase in bed elevation in the on-shore direction.

The average value of the predicted bedload transport rate, $Q_b(t)$, was then calculated for runs 19, 20, and 21 to be 47, 68, and 10 g cm^{-1} hr^{-1} respectively. These compare to a transport rate of 144.7 g cm^{-1} hr^{-1} calculated from the megaripple migration over the course of these runs. It is seen that the sediment transport due to the migration of this megaripple exceeds estimates of bedload transport. Previous authors have suggested that the cross-shore bedload transport can be accounted for in the migration of meter-scale bedforms (Hay and Bowen, 1993). These calculations are consistent with this statement. The bedload transport calculations presented herein are an estimate of the bedload transport rate. Generally such calculations are only used as an order of magnitude estimate of transport.

Megaripple migration was also observed in run 9. The time series for mobility number is shown in figure 31a, and the bedform profiles are plotted in figure 31b. The peak mobility numbers were frequently over 150 and on several occasions during the 16 minute run the mobility numbers were near 250. These measurements were made very near the breakpoint. Because of the highly energetic conditions, no small scale bedforms were present. Two megaripple crests were recorded with the MTA for this run. The heights of the megaripples were approximately 4.5 to 5.5 cm and the cross-shore lengths were approximately 1 meter. The megaripples shown in figure 14b migrated approximately 7 cm during the 16 minute run. This corresponds to a migration rate of 0.44 cm/min.

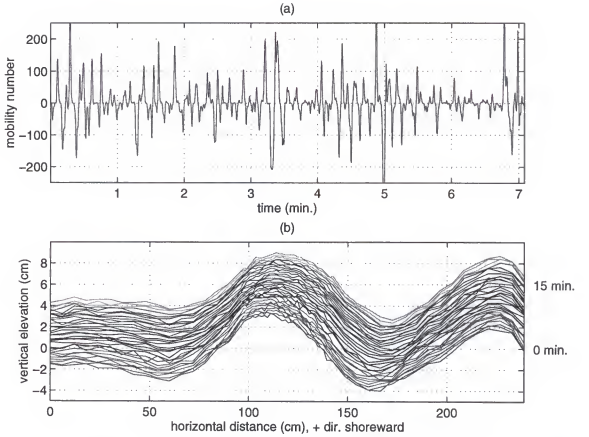

Figure 31. Mobility number time-series for run 9, (a), and bedform time-series (b) showing megaripple migration. Time between profiles is 30 seconds, and each profile is offset by +2 mm. Time is on the right vertical axis.

The megaripple migration of the center crest in run 9 represents a sediment transport rate of 137 g cm^{-1} hr^{-1}. This was calculated using the method described above with an average area of the ripple crest cross-section of 330 cm^2 and a shoreward horizontal translation of the center of mass of this area of 6.7 cm over a 16.7 minute period. The cross-shore length of the ripple was taken as 100 cm. Using equations 6.4, 6.5, and 6.6, the estimated bedload transport rate for this run was 53 g cm^{-1} hr^{-1}. Sediment transport due to megaripple migration during run 9 was approximately 2.5 times larger than the bedload transport estimate for this run. Again, the estimation of bedload transport presented should not be taken as the exact value of bedload transport but only as an order of magnitude estimate.

Small Scale Migration

During several of the runs small scale, or vortex, ripple migration was observed with the 5 MHz MTA. The best indicator for ripple migration found for this data set was the estimated bedload transport rate as predicted by equation 6.6. Equation 6.6 is not only a function of the flow intensity near the bed, but also of flow asymmetry. Ripple migration was generally observed during relatively high mobility number flows with asymmetry between the shoreward and seaward flows. For all instances of migration during this experiment the migration was in the shoreward direction, which was the direction of predicted bedload transport as predicted by equation 6.6.

Figure 32 contains the mobility number time-series and the ripple height time series for run 15. Figure 33 is the corresponding bedform profile time-series for run 15. The average ripple height was 0.4 cm and the average ripple length was 12 cm for this run. Ripple migration was observed over the first 8.5 minutes of run 15. The ripples migrated approximately 4.5 cm during this period which results in an average migration rate of 0.53 cm/min. The calculated average rate of bedload transport was 30.4 g cm^{-1} hr^{-1} for this period. From minutes 8.5 to 13 the average rate of bedload transport was calculated as 3.0 g cm^{-1} hr^{-1}. During this period no significant migration was observed and the ripples gradually increased in height from 0.4 to 0.55 cm. A wave group producing a peak mobility number of over 300 resulted in ripple flattening at minute 14.

Figure 33a is a three-dimensional depiction of the two-dimensional bedform profiles over time. Time is plotted on the y-axis with horizontal distance and elevation on the x and y axis. Figure 33b is a surface plot of the same data. The ripple crests are the light areas and the troughs are the darker areas. Elevations are defined by the color bar to the right of the plot in centimeters. Ripple migration and flattening are observed in this plot.

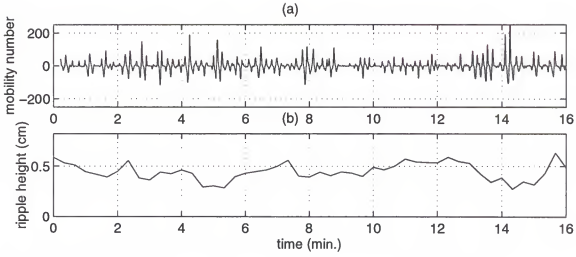

Figure 32. Time series of mobility number (a) and ripple height (b) for run 15.

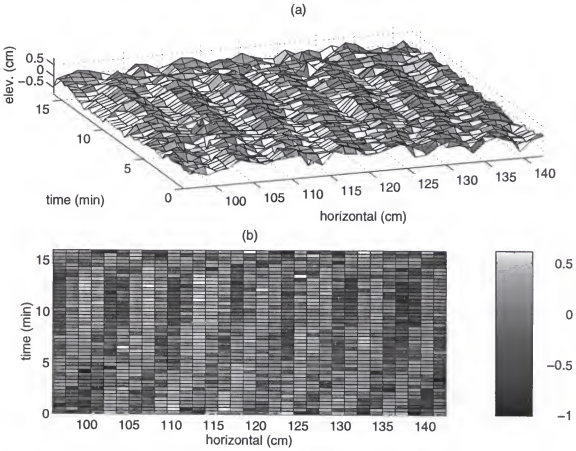

Figure 33. Small scale bedform profiles for run 15. Mesh plot of bedform profiles (a) with time on the y-axis. Surface plot of bedform profiles (b) with time on the y-axis, horizontal distance on the x-axis, and vertical elevation as indicated by the colorbar in centimeters.

Figure 34 contains the mobility number and ripple height time-series for run 16. Figure 35 shows the bedform profile time-series for this same run. The ripples shown migrated an average of 6 cm during the first 8 minutes of run 16. This corresponds to an average migration rate of 0.75 cm/min. Most of this migration occurred during the first 4.5 minutes of the run when the estimated average bedload transport rate was 21.3 g cm^{-1} hr^{-1}. During minutes 4.5 to 7, when the average bedload transport was calculated as 9.7 g cm^{-1} hr^{-1}, little migration occurred. The ripples present during this period had average heights of 0.6 cm and lengths of 9 cm. Ripple height continued to build for the first 7.5 minutes of this run from 0.4 to 0.7 cm. The ripples were then flattened by a group of waves at the 7.5 minute mark. The maximum mobility number during this wave group was 216.

Ripple reformation was not observed until minute 12.5. This probably is due to the destructive effects of the intermittent waves between minutes 9 and 12 that resulted in mobility numbers of near 150. The ripples reformed within a minute during the calmer conditions between minutes 12.5 and 13. No significant ripple migration was observed during minutes 13 to 16. During this period the calculated average bedload transport rate was 19 g cm^{-1} hr^{-1}.

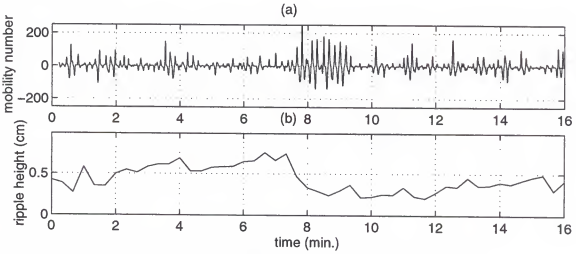

Figure 34. Time series of mobility number (a) and ripple height (b) for run 16.

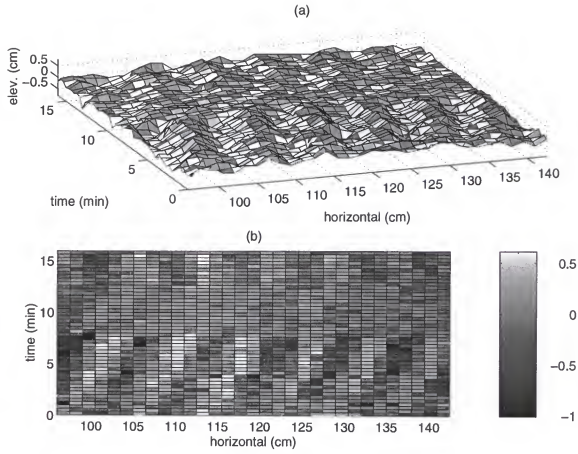

Figure 35. Small scale bedform profiles for run 16. Mesh plot of bedform profiles (a) with time on the y-axis. Surface plot of bedform profiles (b) with time on the y-axis, horizontal distance on the x-axis, and vertical elevation as indicated by the colorbar in centimeters.

During a few of the runs, no ripple migration was seen even during high mobility number flows. An example of this is run 3, which is shown in figures 36 and 37. Single events with mobility numbers of over 150 caused some flattening throughout the run, however no significant migration was observed. The estimated average bedload transport rate, from equation 6.6, for this run was 5.2 g cm^{-1} hr^{-1}. Even during the relatively energetic first four minutes of the run the estimated bedload transport rate was 7 g cm^{-1} hr^{-1}. This low value indicates little asymmetry in the near-bottom orbital flows. This is also the case for run 2, which is plotted in figures 21 and 22. Both of these runs were in depths of over 5 meters, thus the orbital velocities were more symmetric than those measured in more shallow water.

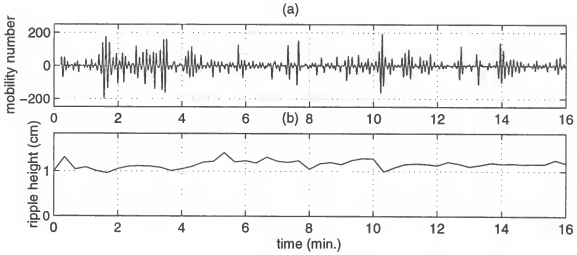

Figure 36. Time series of mobility number (a) and ripple height (b) for run 3.

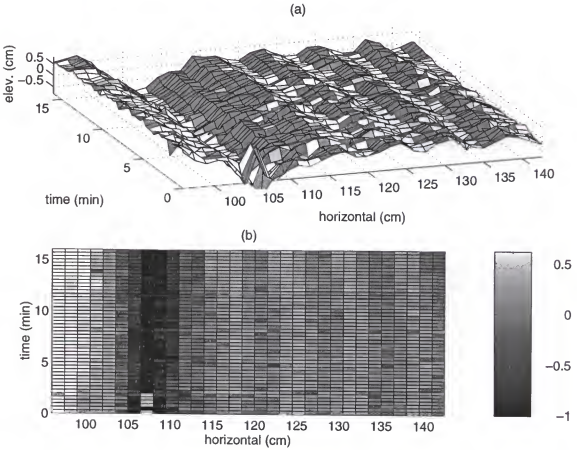

Figure 37. Small scale bedform profiles for run 3. Mesh plot of bedform profiles (a) with time on the y-axis. Surface plot of bedform profiles (b) with time on the y-axis, horizontal distance on the x-axis, and vertical elevation as indicated by the colorbar in centimeters.

Figure 38 is a time series of bedform profiles from run 19. It should be noted that the small scale bedforms in figure 38 are superimposed on the crest of a larger bedform that is migrating shoreward. This larger scale migration was discussed in the previous section and is shown in figure 29. The mobility number time-series for run 19 is plotted in figure 28a.

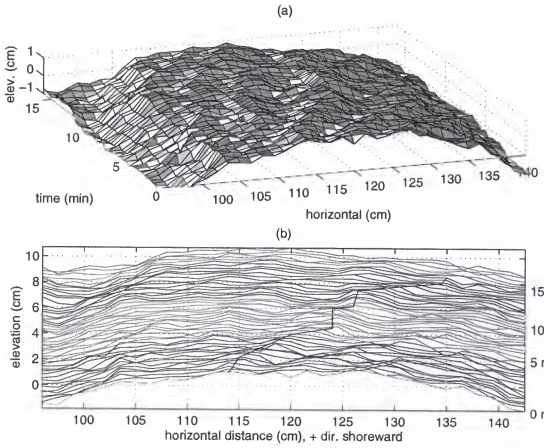

Figure 38. Small scale bedform profiles for run 19. Mesh plot of bedform profiles (a) with time on the yaxis. Bedform profiles offset to show development (b). The first profile of the run is plotted as the lower curve, subsequent profiles are offset by +0.2 cm. The time separation between profiles is 20 seconds. The right vertical axis indicates time in minutes for the profiles.

Run 19 was chosen because an apparent change in ripple migration rate was observed during this run. The solid line intersecting the profiles in figure 38b roughly corresponds to the crest location of a single ripple as it migrates shoreward. The elapsed time in minutes from the beginning of the run is shown on the right vertical axis next to the appropriate profiles. This time corresponds to the time shown in figure 28 of the mobility number time series.

Figure 39 is an image of the seabed from the under water video taken at the beginning of run 19. Under water video recorded during this run indicate a brick-pattern ripple formation with many bifurcations in the ripple crests. The 5 MHz MTA was oriented so that profiles were recorded along a line parallel to the horizontal axis in figure 39. When wave groups were present large suspension events would result. The sediment would then settle out of suspension between wave groups. On video, the ripples appear to become flat after these suspension events and then rebuild between wave groups, such as those shown for run 20 in figure 27. The average small scale ripple height and length during this run were 0.7 cm and 12 cm, respectively.

Figure 39. Underwater video image from the beginning of run 19 showing brick-pattern ripples.

It is shown by the line following a single ripple crest in figure 38b that the ripple migration rate varied over the course of the run. The estimated rate of bedload transport, from equation 6.6, was 39 g cm^{-1} hr^{-1} for minutes 1.5 to 6. The ripple crest marked in figure 38 migrated 10 cm during this 4.5 minute period. This corresponds to an average migration rate of 2.2 cm/min.

During minutes 6 to 8.5, the estimated bedload transport rate was 13.2 g cm^{-1} hr^{-1} and no significant migration was observed. A single wave group resulted in mobility numbers of over 100 for minutes 8.5 to 9. This flattened the ripples and caused an apparent shoreward shift of 2 cm in the ripple crests over this 30 second period. Such a shift would correspond to a 4 cm/min migration, however the bedform profile time series does not indicate a coherent ripple migration during this period, but rather a flattening and reformation.

No significant migration was observed during minutes 9 to 11.5. The estimated bedload transport rate for this period was 16 g cm^{-1} hr^{-1}. During minutes 12 to 13.5 significant ripple migration was observed, and the estimated rate of bedload transport was 110 g cm^{-1} hr^{-1}. The marked ripple in figure 11 migrated approximately 8 cm during this 1.5 minute period. This corresponds to a migration rate of 5.3 cm/min. From minutes 13.5 to 14.5 no significant ripple migration was observed. During this period the estimated average rate of bedload transport was 17 g cm^{-1} hr^{-1}. Peak mobility numbers were relatively high, between 150 and 200, for the remainder of the run. During this period, minutes 14.5 to 17, the bedforms were flattened. Shoreward migration appears to be the case, however it is difficult to determine a migration rate for this energetic period.

Since these ripples are superimposed on the crest of a megaripple, contraction of flow might have resulted in lower mobility number flows producing a larger than expected impact on the small scale ripples. Ripple flattening was not observed for mobility numbers of near 100 in the any of the other runs. Also, migration rates of over 5 cm/min were not observed during any other runs. Such high migration rates could in part be due to the

migration of the underlying megaripple. The mechanics of ripple migration, especially when the ripple is superimposed on a migrating megaripple, are not well understood.

Previous authors have suggested that mean bottom currents can result in ripple migration (Dingler and Inman, 1976). It is noted that the average distance from the seabed to the velocity meter was over 1.8 m for this experiment. The maximum measured mean cross-shore current for the SIS96 experiment was 0.03 m/s. Since the actual near-bottom velocities were not measured, it is difficult to compare ripple migration with mean bottom currents. No correlation was seen between measured mean currents, measured over one meter off of the seabed, and ripple migration for this experiment.

The small scale ripple migration observed during the SIS96 experiment supports the use of the estimated bedload transport, by equation 6.6, as an indicator for small scale ripple migration. For the SIS96 experiment, ripple migration was observed when the estimated rate of bedload transport exceeded a value of approximately 20 g cm^{-1} hr^{-1}. The dimensional bedload transport rate in equation 6.6 had better agreement with observations of ripple migration than did the non-dimensional bedload transport rate shown in equations 6.4 and 6.5. A distinct threshold for the existence of ripple migration could not be found for the SIS96 data when the non-dimensional bedload transport rate was used as an indicator. The dimensional bedload transport rate contains an additional d_{50} to the 1.5 power term. It appears, at least for this data set, that this term has importance in determining ripple migration.

Model Comparisons

Model comparisons of the small scale ripple measurements from the SIS96 experiment were presented in chapter 5. Megaripple measurements made with the whole MTA are presented in this chapter. For some of the runs, the megaripple crests were not normal to the MTA. For these runs the RSS was used to measure the angle between the

MTA and the megaripple crests. This angle was then used to correct the ripple lengths measured with the MTA.

Observations of megaripples indicate that the spacing between megaripple crests, ripple length, is proportional to orbital diameter. Ripples with lengths proportional to orbital diameter have previously been referred to as orbital ripples (Clifton, 1976). Wiberg and Harris (1994) proposed that orbital ripple length, λ_{orb}, is proportional to orbital diameter, d_o, by the relation

$$\lambda_{orb}=0.62\ d_o \qquad \text{equation 6.8}$$

and that orbital ripple steepness is equal to a constant value of 0.17. This follows from Miller and Komar (1980) who proposed a multiplier of 0.65 instead of 0.62.

Wiberg and Harris (1994) adopt the approximate criteria proposed by Clifton and Dingler (1984) that orbital ripples occur when the ratio of orbital diameter to grain diameter, d_o/ d_{50}, is less than 2000. During the SIS96 experiment ripples with length scales proportional to orbital diameter were observed in conditions too energetic for the existence of vortex ripples, such as in run 9 shown in figure 14. Megaripples with length scales proportional to orbital diameter were measured even when significant mobility numbers of over 200 and d_o/d_{50} values of over 10000 were observed.

Megaripple measurements are shown in figure 40 as '+'s and small scale ripples are shown as 'o's with the Wiberg and Harris (1994) orbital ripple model curves plotted as the solid lines. Measurements of megaripple lengths agree well with the Wiberg and Harris (1994) orbital ripple length formula. However, measured megaripple steepnesses were generally below their predicted value of 0.17 for orbital ripples. The dashed line in figure 40c is at a constant steepness of 0.065. This was the average value of megaripple steepness for the SIS96 data set. It should be noted that megaripples were considered present if the steepness of the bedforms from the whole 2.5 meter MTA were larger than

0.03. In figure 40a nondimensional ripple lengths are plotted versus nondimensional orbital diameter. The solid curve is the Wiberg and Harris (1994) orbital ripple curve. The dashed line was calculated using equation 6.7 for orbital ripple length and a constant steepness value of 0.065.

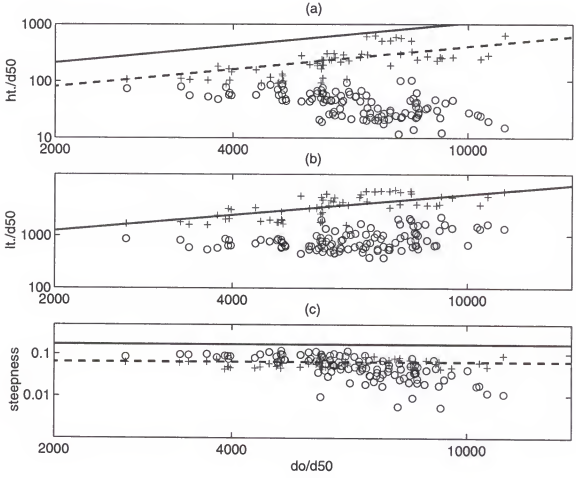

Figure 40. Measured SIS96 small scale (o) and large scale (+) ripple data versus nondimensional orbital diameter for nondimensional ripple height (a), length (b), and steepness (c). The Wiberg and Harris (1994) orbital ripple curves are shown as solid lines, new suggested curves are shown as dashed lines.

It is shown in figure 40 that the coexistence of both small scale vortex ripples and large scale megaripples is possible at many values of d_o/ d_{50}. It appears that at low values of d_o/ d_{50} length and height scales of the small and large scale bedforms begin to merge. The region where small scale bedforms begin to scale with the near bottom orbital diameter has generally been referred to as the orbital ripple range. These measurements show that orbital ripples can exist at both large and small values of d_o/ d_{50}.

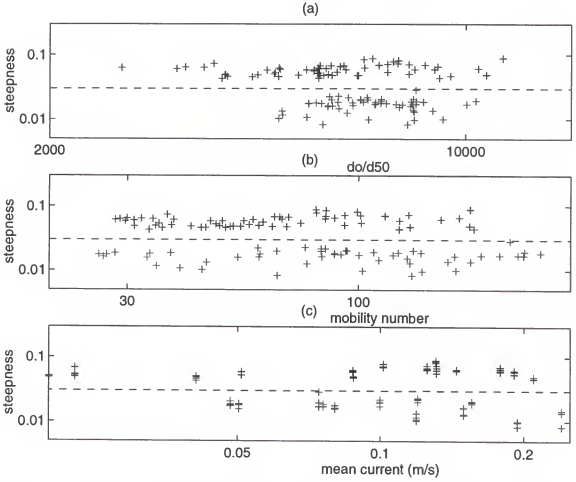

Figure 41. Megaripple steepness versus nondimensional orbital diameter, d_o/ d_{50}, (a), mobility number (b), and mean net current measured 1.5 meters above the bed (c) for the SIS96 data set.

As shown in figure 41, megaripples were observed at the full range of orbital diameters, mobility numbers, and mean current values encountered during the SIS96 data set. For many of the runs megaripples were not present. For these runs the steepness of the bedforms measured with the whole MTA were generally less than 0.03. When the bedform steepness was less than 0.03, megaripples were said not to exist. The dashed lines in figure 41 represent a steepness of 0.03. The data below this line is said to not contain megaripples and was not included in the previous analysis of megaripple dimensions.

It should be noted that the steepnesses determined from the whole MTA are always greater than zero, even when no large scale bedforms were present. This is mainly due to the aliasing of small scale ripples in the 2 MHz MTA profiles. Since transducer spacing on the 2 MHz MTA is 6 cm, it is possible to alias small bedforms with lengths less than 12 cm into the 2 MHz MTA profile.

No significant correlations between flow and sediment parameters were found for the existence of megaripples. Mean cross-shore and long-shore currents, median sediment diameter, local bedslope, orbital diameter, mobility number, grain roughness Shields parameter, and bedload transport rates were all compared to the data and did not result in any relation for the existence of megaripples.

Conclusions

A 64 element multiple transducer array (MTA) is capable of high-resolution measurements of small and large scale bedform profiles. Temporal scales on the order of wave periods can be measured as well as the migration, flattening, and rebuilding of small-scale bedforms with heights of less than 1 cm.

Observations from the SIS96 experiment indicate that the flattening of small-scale vortex ripples is a function of mobility number. Groups of waves with peak mobility

numbers of over approximately 150 can potentially flatten ripples. Single waves with peak mobility numbers of larger than approximately 240, which also was suggested by Dingler and Inman (1976), can flatten a rippled bed. Ripple reformation can occur within a minute after flattening, and in certain conditions within a couple of wave periods. Rapid ripple reformation appears to occur when peak mobility numbers are between 50 and 150. Ripple reformation is slow when peak mobility numbers remain less than approximately 50. When mobility numbers reach values of over approximately 150 during a rebuilding period, ripple flattening can occur. Thus mobility numbers larger than 150 can impede the reformation process.

It was observed that a significant part of the total cross-shore sediment transport may be accounted for in the migration of megaripples. Small scale ripple migration was observed when the estimated bedload transport rate was greater than approximately 20 g cm^{-1} hr^{-1} as predicted by equation 6.6. Ripples appear to migrate in the same direction as indicated by the direction of the predicted bedload transport. Since a net transport predicted by equation 6.6 represents skewness in near bottom velocities, it appears that small scale ripple migration is a function of the asymmetry in near-bed orbital flows.

Megaripple lengths measured during the SIS96 experiment were roughly proportional to near-bottom orbital diameter by the relation proposed by Wiberg and Harris (1994) for orbital ripples. It has previously been proposed that these orbital ripples exist when d_o/d_{50} <2000 (Clifton and Dingler, 1984). However, megaripples with lengths proportional to orbital diameter were observed at the full range of d_o/d_{50}, even at values of over 10000. Measured megaripple steepness was found to be approximately 0.065.

Ripples were observed in every run during the SIS96 field experiment. Seabed measurements were made at several cross-shore locations and under many different wave conditions. Many of the measurements contained both small and large scale ripples, while others contained only small or only large scale ripples. Even in some conditions when plane-bed conditions were anticipated, small scale ripples were observed to form in the

periods between wave groups. These measurements indicate that in order to properly model sediment transport processes, ripple dynamics such as ripple migration, flattening, and reformation should be considered.

CHAPTER 6
DISCUSSION AND CONCLUSIONS

A newly developed instrument, the multiple transducer array (MTA), proved capable of measuring small and large scale bedform profiles with a resolution that was previously unobtainable. Field experiments show that under energetic flows with peak mobility numbers of over 240, bedform profiles can be recorded with an MTA. The MTA has several advantages over previous systems used to measure bedforms, these include: (1) no moving parts, which have caused vibration and fouling in previous systems; (2) the ability to measure a complete profile in under 2 seconds, whereas even rotating systems require 20 seconds; (3) remote operation, no diver assistance is required as in previous tracking systems; (4) a physically small system, previous profilers were substantially larger, this system is thus easier to deploy and creates a lesser impact on flow patterns; (5) a maximum vertical resolution of 1 mm and horizontal resolution of 2 cm.

The MTA in it's present state has several limitations. The most significant limitation is that only two-dimensional bedform profiles are measured with the device. It has been shown previously, and in this research, that many types of bedforms can be highly three-dimensional. Describing the seabed from only a single transect is subject to errors due to the three-dimensionality of many bedforms. When water clarity permitted, under-water video observations were used to classify the three-dimensionality of small scale bedforms and record their orientation. A rotating scanning sonar was used to measure the orientation of megaripples and their three-dimensionality.

The MTA is capable of 1 mm vertical resolution under ideal conditions. The vertical resolution of the MTA is limited by the transducer footprint and the bedslope over the footprint, as well as the amount of acoustic scatterers suspended above the seabed. Since

ideal conditions are rarely encountered in the field, the resolution of the MTA can be substantially less than 1 mm. During periods of intense flow, such as during the flattening of bedforms, the MTA can completely lose the bottom. An example of this can be seen in figures 22b and 24b. During periods of high sediment suspension, the MTA recorded echoes from the suspended sediment. These are evident by the white areas in the figures. For this reason, representative profiles from 20 seconds of data were used in much of the analysis.

A multiple transducer array was used to measure bedforms during the SIS95 and SIS96 experiment in Duck, NC. Existing methods for predicting small-scale ripple geometry did not capture all of the trends found in this new data set. A new method for predicting ripple geometry is developed. This method does not require the calculation of bed shear stress or the classification of ripple regimes as previous models did. This new method relates ripple height and steepness to near bottom mobility number by a few simple relations.

All available field data were used to test the new model and the Nielsen (1981) and Wiberg and Harris (1994) models. The new model did substantially better at predicting ripple height, with average errors of 60% compared to 142% and 133% for the Wiberg and Harris (1994) and the Nielsen (1981) models respectively. The new model also gave better estimates of ripple steepness and length. When only the new SIS95 and SIS96 data sets were used, average errors of approximately 50% were observed in predicting ripple height, steepness, and length with the new ripple prediction method.

As mentioned, the new model had average errors of approximately 50% in predicting ripple geometry, even for the data that it was formulated from. This is significantly less than the errors calculated from previous prediction techniques. However, with ever increasing field measurements, ripple prediction methods should continue to improve.

Observations from the SIS96 experiment indicate that the flattening of small-scale vortex ripples is a function of mobility number. Groups of waves with peak mobility

numbers of over approximately 150 can potentially flatten ripples. Single waves with peak mobility numbers of larger than approximately 240, which also was suggested by Dingler and Inman (1976), can flatten a rippled bed. Ripple reformation can occur within a minute after flattening, and under certain conditions within a couple of wave periods. Rapid ripple reformation appears to occur when peak mobility numbers are between 50 and 150. Ripple reformation is slow when peak mobility numbers remain less than approximately 50. Mobility numbers larger than 150 can impede the reformation process by flattening ripple crests.

Megaripple migration was observed to account for a significant part of the cross-shore sediment transport under near breaking wave conditions. Small scale ripple migration appears to be a function of the asymmetry in near-bed orbital flows. Ripple migration was observed when the estimated bedload transport rate was greater than approximately 20 g cm^{-1} hr^{-1} as predicted by equation 6.6. Ripples appear to migrate in the same direction as indicated by the direction of the predicted bedload transport.

It should be noted that significant small scale ripple migration was only observed during 4 of the 58 runs. Thus the trends observed during these few runs might not hold in the general sense. Also, only two incidences of megaripple migration were observed during these two experiments. Because of this, conclusions about megaripple migration cannot be made with any certainty.

Measured megaripple lengths could be approximated as a proportion of the near-bottom orbital diameter by the relation proposed by Wiberg and Harris (1994) for orbital ripples. Megaripples with lengths proportional to orbital diameter were observed at the full range of d_o/d_{50}, even at values of over 10000. Megaripple steepnesses were approximately equal to 0.065.

All of the data presented herein was collected at the Army Corps of Engineers Field Research Facility in Duck, North Carolina. The instruments were deployed by the sensor insertion system located on the research pier. Since all measurements were made at the

same location, during similar times of the year, and very near a substantial structure, the data presented might not represent the sediment dynamics observed at other sites during similar conditions. Without these structures, however, such a data set could not have been collected.

Ripples were observed in every run during the SIS95 and SIS96 field experiments. Seabed measurements were made at several cross-shore locations and under many different wave conditions. Many of the measurements contained both small and large scale ripples, while others contained only small or only large scale ripples. Even in some conditions when plane-bed conditions were anticipated, small scale ripples were observed to form in the periods between wave groups. These measurements indicate that in order to properly model sediment transport processes, ripple dynamics such as ripple migration, flattening, and reformation should be considered.

APPENDIX A
SIS95 AND SIS96 DATA AND PLOTS

Key to terms in appendix A.

D50	(mm)	- median sediment diameter
depth	(m)	- local water depth
Do (sig)	(m)	- significant near-bottom orbital diameter, each run divided into 4 sections
Hmo	(m)	- wave height from surface elevation spectrum
Loc	(m)	- cross-shore location of measurements as shown in pier profiles
Tp	(s)	- peak period from surface elevation spectrum
Uo (sig)	(m/s)	- significant near-bottom orbital velocity
η	(cm)	- small scale ripple height from 0.5 meter array
λ	(cm)	- small scale ripple length from 0.5 meter array
η large	(cm)	- ripple height from whole 2.5 meter array
λ large	(cm)	- ripple length from whole 2.5 meter array
U mean	(m/s)	- mean cross-shore current (positive onshore)
V mean	(m/s)	- mean long-shore current

Table A1. SIS96 Hydrodynamic data

Run	Loc	depth	Hmo	Tp	D50	Do (sig) 1	Do (sig)2	Do (sig) 3	Do (sig) 4	Uo (sig) 1	Uo (sig) 2	Uo (sig) 3	Uo (sig) 4	U mean	V mean
		(m)	(m)	(s)	(mm)	(m)	(m)	(m)	(m)	(m/s)	(m/s)	(m/s)	(m/s)	(m/s)	(m/s)
1	494	5.8	1.21	6.40	0.121	0.98	0.74	1.06	0.69	0.56	0.47	0.59	0.36	-0.01	0.24
2	494	5.7	0.99	6.40	0.121	0.99	0.83	1.10	0.96	0.52	0.45	0.57	0.51	-0.02	0.19
3	494	5.7	0.90	6.40	0.121	0.99	0.76	0.78	0.72	0.51	0.39	0.40	0.34	-0.05	0.14
4	494	5.7	0.61	5.82	0.121	0.58	0.59	0.65	0.59	0.29	0.30	0.28	0.26	-0.20	0.12
5	243	3.9	0.48	10.67	0.190	0.83	0.75	0.76	0.92	0.33	0.33	0.37	0.39	-0.02	-0.21
7	225	3.1	0.52	10.67	0.196	0.74	1.12	1.11	1.09	0.34	0.46	0.46	0.44	-0.03	-0.13
8	225	2.9	0.40	4.00	0.202	0.73	0.68	0.53	0.66	0.32	0.31	0.33	0.30	-0.01	-0.14
9	201	1.6	0.32	9.85	0.185	2.00	1.74	1.67	1.05	0.73	0.63	0.74	0.61	----	----
10	201	1.4	0.32	9.85	0.185	1.53	1.92	1.45	1.86	0.81	0.84	0.70	0.79	0.02	-0.07
11	207	1.4	0.59	12.80	0.208	1.46	1.69	1.76	1.71	0.80	0.89	0.93	0.88	0.03	-0.07
12	207	2.4	0.36	7.11	0.184	0.82	0.88	0.72	0.89	0.38	0.34	0.32	0.37	0.01	-0.04
13	207	2.5	0.39	10.67	0.186	1.16	0.73	0.89	1.05	0.46	0.31	0.33	0.41	-0.01	0.02
14	207	2.7	0.60	10.67	0.208	1.46	1.61	1.68	1.50	0.55	0.66	0.64	0.54	-0.02	-0.05
15	207	2.6	0.55	10.67	0.208	1.53	1.46	1.16	1.70	0.55	0.58	0.45	0.67	-0.01	-0.05
16	207	2.5	0.55	10.67	0.208	1.38	1.50	1.59	1.32	0.56	0.60	0.63	0.53	-0.01	-0.10
17	207	2.5	0.48	8.00	0.208	1.23	1.27	1.24	1.42	0.45	0.50	0.47	0.53	0.03	-0.12
18	207	2.4	0.51	9.85	0.208	1.50	1.42	1.38	1.71	0.56	0.56	0.53	0.68	0.03	-0.15
19	225	2.8	0.55	10.67	0.202	1.20	1.37	1.25	1.56	0.46	0.53	0.54	0.65	-0.02	-0.12
20	225	2.6	0.69	10.67	0.202	1.73	1.82	2.12	1.66	0.61	0.74	0.71	0.64	-0.03	-0.18
21	225	2.6	0.59	10.67	0.202	1.18	1.79	1.23	1.50	0.43	0.64	0.49	0.58	-0.02	-0.19
22	225	2.9	0.54	9.14	0.192	1.48	1.30	2.22	1.34	0.56	0.51	0.75	0.50	-0.01	-0.13
23	225	3.1	0.55	11.64	0.192	1.45	1.37	1.54	1.42	0.50	0.51	0.56	0.54	-0.02	-0.10
25	225	3.2	0.37	11.64	0.180	0.88	1.02	0.83	0.87	0.30	0.33	0.29	0.29	-0.00	-0.09
26	238	3.7	0.48	10.67	0.190	0.99	1.13	1.08	1.12	0.36	0.41	0.40	0.43	-0.01	-0.09
27	238	3.6	0.47	10.67	0.190	1.08	1.03	1.06	1.20	0.38	0.38	0.39	0.41	-0.02	-0.05
28	527	7	0.46	10.67	0.121	0.69	0.71	0.71	0.97	0.23	0.25	0.23	0.32	0.01	-0.08
29	527	7	1.11	3.12	0.121	0.66	0.78	0.73	0.81	0.22	0.26	0.23	0.27	0.01	-0.05
30	232	2.8	0.48	10.67	0.179	1.44	1.18	1.03	1.18	0.52	0.43	0.39	0.45	0.02	-0.00

Table A2. SIS96 Ripple Data

Run	η 1	η 2	η 3	η 4	λ 1	λ 2	λ 3	λ 4	η 1 large	η 2 large	η 3 large	η 4 large	λ 1 large	λ 2 large	λ 3 large	λ 4 large
	(cm)	(cm)	(cm)	(cm)	(cm)	(cm)	(cm)	(cm)	(cm)	(cm)	(cm)	(cm)	(cm)	(cm)	(cm)	(cm)
1	0.4	0.5	0.6	0.7	10	10	8	17	0.9	0.8	1.1	0.9	65	57	79	107
2	0.5	0.5	0.5	0.6	14	17	20	26	0.7	0.8	0.8	0.7	76	78	79	84
3	0.8	0.7	0.7	0.8	13	16	13	15	0.9	1.4	1.1	1.2	72	110	69	71
4	0.6	0.6	0.5	0.5	7	8	8	7	1.1	0.8	1.0	1.1	103	61	90	90
5	1.1	1.1	1.1	1.1	14	12	12	11	3.0	3.1	2.7	2.5	80	77	73	67
7	0.9	1.2	1.4	1.3	11	14	18	20	3.6	3.7	3.2	3.7	53	61	57	72
8	1.1	1.1	1.5	1.6	11	12	18	17	2.1	2.1	2.2	2.2	32	33	34	37
9	0.4	0.9	0.2	0.4	31	26	42	37	5.2	4.8	4.7	4.4	105	101	106	101
10	0.6	0.5	0.5	0.5	29	28	19	12	3.6	3.3	3.2	2.4	127	171	190	139
11	0.7	0.9	0.7	0.5	23	24	35	21	2.5	2.6	2.5	2.7	148	154	135	159
12	1.5	1.3	1.4	1.5	15	15	16	15	1.7	1.7	1.6	1.7	45	43	49	49
13	1.7	1.1	1.1	0.9	19	15	16	15	2.0	1.9	1.8	1.7	36	48	40	41
14	0.5	0.5	0.3	0.4	11	11	33	21	2.9	2.5	2.4	3.0	156	158	129	166
15	0.4	0.4	0.4	0.5	11	12	12	14	2.6	3.4	2.3	2.8	148	196	130	138
16	0.4	0.6	0.2	0.4	10	8	43	22	3.6	3.1	3.3	3.3	176	159	194	150
17	0.6	0.5	0.5	0.6	15	12	10	8	3.3	3.1	3.3	3.2	145	134	165	147
18	0.4	0.5	0.6	0.6	13	15	12	12	3.7	3.5	3.4	3.3	179	175	171	174
19	0.6	0.7	0.9	2.1	11	15	17	34	6.2	5.9	5.9	6.0	128	130	125	115
20	0.7	0.5	0.5	0.5	17	26	28	13	5.5	5.3	4.9	4.8	110	114	111	114
21	0.5	0.6	0.7	0.6	18	13	10	11	4.8	4.6	4.4	3.8	109	109	114	98
22	0.4	0.4	0.3	0.4	18	21	27	18	10.9	11.7	12.2	12.1	142	146	146	146
23	0.5	0.5	0.5	0.5	14	17	15	12	11.4	9.6	9.8	9.9	150	144	143	142
25	1.3	1.4	1.5	1.6	13	14	14	14	1.8	2.0	2.1	2.2	30	33	36	35
26	0.8	0.9	0.8	0.9	9	9	9	9	5.3	4.9	4.4	4.5	139	129	118	114
27	1.2	1.1	1.2	1.2	12	10	10	11	3.6	3.7	3.9	4.3	99	90	94	104
28	0.6	0.6	0.6	0.6	7	8	8	7	1.6	1.4	1.3	1.3	88	88	77	84
29	0.6	0.6	0.7	0.7	8	7	7	7	1.3	1.4	1.4	1.3	74	75	73	72
30	1.9	1.2	0.8	0.8	35	31	14	12	5.9	5.4	5.4	4.7	117	112	113	98

Table A3. SIS95 Hydrodynamic Data

Run	Loc	depth	Hmo	Tp	D50	Do (sig) 1	Do (sig)2	Do (sig) 3	Do (sig) 4	Uo (sig) 1	Uo (sig)2	Uo (sig) 3	Uo (sig) 4
	(m)	(m)	(m)	(s)	(mm)	(m)	(m)	(m)	(m)	(m/s)	(m/s)	(m/s)	(m/s)
1	347	6.10	0.71	3.76	0.285	0.54	0.44	0.42	0.61	0.28	0.27	0.25	0.25
2	347	6.33	0.65	3.76	0.285	0.48	0.54	0.52	0.54	0.23	0.28	0.28	0.29
3	347	6.42	0.80	4.27	0.285	0.52	0.48	0.47	0.53	0.31	0.31	0.28	0.32
4	347	6.53	0.66	4.27	0.285	0.46	0.58	0.59	0.68	0.25	0.28	0.32	0.29
5	347	6.58	0.73	4.27	0.285	0.57	0.55	0.49	0.48	0.27	0.30	0.28	0.31
6	347	6.69	0.83	4.27	0.285	0.51	0.75	0.49	0.61	0.32	0.32	0.31	0.36
7	347	6.78	0.85	4.57	0.285	0.58	0.54	0.58	0.48	0.38	0.30	0.34	0.31
8	347	6.79	0.92	4.92	0.285	0.55	0.84	0.58	0.49	0.33	0.44	0.32	0.32
9	347	6.82	0.85	4.27	0.285	0.46	0.55	0.63	0.60	0.28	0.29	0.37	0.32
10	347	6.16	0.41	4.92	0.285	0.53	0.43	0.43	0.59	0.18	0.19	0.20	0.20
11	267	1.94	0.31	4.27	0.176	0.59	0.93	1.10	0.81	0.29	0.45	0.41	0.41
12	267	1.90	0.31	4.57	0.176	0.62	0.70	0.67	0.75	0.36	0.39	0.37	0.38
13	267	1.62	0.27	4.57	0.176	0.63	0.66	0.84	0.63	0.33	0.40	0.41	0.32
14	267	1.65	0.38	6.40	0.238	1.09	0.98	1.01	0.94	0.52	0.46	0.57	0.43
15	226	1.63	0.21	4.27	0.207	0.59	0.53	0.44	0.65	0.26	0.26	0.28	0.31
16	226	1.76	0.22	4.57	0.207	0.60	0.54	0.57	0.63	0.26	0.30	0.28	0.31
17	226	1.82	0.23	4.57	0.207	0.76	0.42	0.66	0.61	0.31	0.23	0.29	0.30
18	226	1.91	0.24	4.27	0.207	0.61	0.67	0.63	0.66	0.29	0.28	0.31	0.33
19	226	1.99	0.26	16.00	0.207	0.73	0.70	0.70	0.56	0.30	0.31	0.30	0.32
20	226	2.14	0.25	5.33	0.207	0.55	0.62	0.65	0.67	0.30	0.30	0.28	0.31
21	226	2.25	0.27	7.11	0.207	0.62	0.77	0.62	0.60	0.28	0.33	0.29	0.29
22	198	4.19	0.37	7.11	0.397	0.68	0.73	0.62	0.55	0.31	0.30	0.26	0.23
23	198	4.21	0.31	7.11	0.397	0.59	0.44	0.56	0.56	0.23	0.20	0.22	0.24
24	186	3.90	0.44	6.40	0.641	0.89	0.66	1.00	1.04	0.38	0.29	0.39	0.35
25	186	3.86	0.63	8.00	1.124	1.23	1.21	1.30	1.28	0.54	0.42	0.55	0.54
26	186	3.80	0.69	7.11	1.124	1.32	1.12	1.19	1.45	0.55	0.52	0.51	0.59
27	171	2.80	0.28	7.11	1.662	0.68	0.57	0.55	0.52	0.29	0.28	0.23	0.24
28	165	2.72	0.29	7.11	0.175	0.67	0.62	0.52	0.55	0.31	0.29	0.24	0.22
29	155	2.25	0.22	7.11	1.466	0.54	0.49	0.63	0.46	0.29	0.24	0.27	0.26
30	155	2.20	0.24	6.40	1.466	0.62	0.63	0.48	0.52	0.34	0.33	0.31	0.37

Table A4. SIS95 Ripple Data

Run	η 1 (cm)	η 2 (cm)	η 3 (cm)	η 4 (cm)	λ 1 (cm)	λ 2 (cm)	λ 3 (cm)	λ 4 (cm)
1	1.6	1.5	1.6	1.6	13	13	13	13
2	1.3	1.4	1.5	1.2	10	12	11	10
3	1.4	1.3	1.5	1.6	12	10	13	15
4	1.7	1.8	1.8	1.9	16	16	15	15
5	1.8	1.8	1.7	1.9	15	15	15	15
6	1.7	1.6	1.6	1.6	15	15	15	15
7	1.4	1.4	1.6	1.4	14	14	15	14
8	1.5	1.4	1.4	1.4	13	14	15	15
9	1.4	1.5	1.5	1.6	14	15	13	15
10	1.4	1.4	1.4	1.4	10	10	10	10
11	1.2	1.0	1.1	1.1	14	11	13	12
12	1.1	1.4	1.2	1.2	13	13	12	12
13	1.4	1.4	1.3	1.2	12	11	12	11
14	1.2	0.9	1.0	0.7	16	10	11	9
15	1.1	1.2	1.3	1.2	13	13	13	14
16	1.3	1.4	1.4	1.5	10	11	11	12
17	1.2	1.2	1.1	1.2	11	9	9	12
18	0.7	1.0	0.9	1.0	12	13	12	14
19	0.8	0.8	0.8	0.9	7	7	8	9
20	0.8	0.8	0.8	0.9	7	7	8	9
21	0.8	0.8	1.0	1.1	9	8	9	10
22	3.0	2.8	3.3	2.9	22	19	23	21
23	2.4	3.1	2.3	2.7	17	21	16	18
24	2.0	1.8	1.8	1.9	14	13	13	14
25	1.8	1.9	2.1	2.1	13	14	14	15
26	2.0	2.2	2.3	1.7	14	15	15	12
27	1.4	1.4	1.6	1.4	14	14	17	15
28	1.6	1.1	1.8	1.3	24	18	34	17
29	2.2	2.8	2.7	2.4	16	18	17	17
30	2.4	2.5	2.3	2.2	18	18	17	17

APPENDIX B
SIS95 AND SIS96 PROGRAMS AND DATA FILE DESCIPTIONS

Description of files

Below is an explanation of some of the data files and matlab m-files used to analyze the SIS95 and SIS96 data

Data files:

cond96.mat - D50, depth, Hmo, Tp, fname, bottom slope, location and side of pier for all 30 runs. Used by allmod.m to determine predicted ripple dimensions. Spectrums are from both current T.S. and Pressure T.S. hmocur and Tpcur are from the current. Hm02 has 2 sec. cutoff, Hmo has 3 sec. (from pres) Tp2 has 2 sec. cutoff, Tp has 3 sec. (from pres) Bottom orbital diameter spectrum also calculated. Tpdcur - peak period of bottom diameter spect. from curr. dmocur - 4.01*the area under the bottom orbital diam. spectr. Tpd & Dmo - from pressure T.S., same as above in derivation

rip96.mat - measured ripple dimensions. Output of reval596.m and revalw96.m

s(file #)(day)m.mat - data for each run, contains ripple data (prof, prof15, profx, as well as slow instr., location, time, raw mta data, rms of acoustics. prof contains representative ripple profiles for every 20 sec (10 profiles), prof15 is over 30 sec,(15 prof.) The length of the profiles is 67. 1 to 64 are distances to the bed in mm, 65 is sec. passed midnight at beginning of profile, 66 is the day, and 67 is the number of seconds per representative profile.

Program files:

allmod.m - Calculates predicted ripple dimensions using Hmo derived values. Wiberg/Harris (1994), Nielsen(1981), Wikramanayake (1994), Grant/Madsen (1982) ripple models are used. Program calls fwik.m to calculate friction factor for GM and W models using kelvin function. Uses Cond96.mat as input for measured variables

calibd.m - The same as Eric's calibrat.m except that it calls the despikf.m function to 'despike' the pressure data, and the elevation and orientation of the adv is correct for run

10 and 11 (when it was directed downward) Calibrates all slow instruments, determines directional statistics for waves.

despike.m - removes spikes from the SIS96 pressure time series. Takes derivative of time series and sets threhold for the maximum change in pressure per dt. If threshold is exceeded, it takes the mean of the surrounding two points. Recalulates derivative until threshold criterion is met. Saves new pressure time series as prescor.

despikf.m - function version of previous program

hist96.m - a function used to determine the bottom location by a histogram approach. Called by prof96.m

hmo96.m - takes despiked prescor, and current T.S. to determine Hmo and Tp from each. Also calculates the botom orbital diameter spectrum from both press. and curr. and finds Dmo and Tpd. Save output as waves96.mat.

mesh96.m - plots MTA data as 3-D plot over time. Uses profx, and prof15 variables

modsig96.m - calculates predicted ripple dimensions using Jetté and Hanes (1997), Wiberg and Harris (1994), and Nielsen (1981) models. Uses significant bottom conditions to perform calculations

prof96.m - determines representative bottom profiles calls hist96.m, saves results

reval596.m - Takes prof15 and profx and determines ripple heights, lengths, and steepness for 5 MHz (0.5m) array

revalw96.m - same as above except that it determines ripple dimensions for the whole 2.5 meter array

pier96.m - plots the survey data (contained in m-file) for the SIS96 experiment

plot96.m - plots bottom profiles for total array and 5 MHz portion. Finds bottom slopes for each. Uses profx and prof15 variable

timser.m - plots current or pressure sensor time series with bedforms (surface plot) and bedforms profiles with offset

Listing of programs

```
%%%%%%%%%%%%%%%%%%%%%%%%% ailmod95.m %%%%%%%%%%%%%%%%%%%%%%%%%%%%%%%%%%%%
%%%%% COMPUTES RIPPLE TYPE AND GEOMETRIES USING WIBERG,NIELSEN %%%%%
%%%%%  and Wikramanayake, and Grant-Madsen  Models          %%%%%
%%%%%  INPUT DEPTH, GRAIN SIZE, WAVE HEIGHT, WAVE PERIOD      %%%%%
%%%%%  WRITTEN BY CHRIS JETTE' last update 5-19-97 %%%%%
%%%%% automatically runs thru complete set of wave data for Duck 95
load d:\chris\sis95\stats95

%%%%%  g = gravity(m/s^2), Depth = water depth(m), Tp = wave period(s)
%%%%%  Hmo = wave height(m),l= wave length, lt = ripple wave length,D50(mm)
%%%%%  ho, ha, hs = ripple height(m), do = wave orbital diameter, d =grain size
%%%%%  tp = ripple type
    typ=zeros(30,3);
g=9.81;
nu=1.4e-06;  %%% kinematic viscosity of sea-water (m^2/s)
for i=1:length(Hmo),
 t=Tp(i); wh=Hmo(i);  h=Depth(i); r=(i);
 c = (g*h)^.5;                    %%shallow water wave celerity
 l = c*t;                        %% wave length (shallow water)
 sig = 2*3.141/t;                  %% angular wave frequency
 d = (D50(i))/1000;                  %% D50 = sediment diameter (mm)


%%%%%%%%%%%%%%%%%%%%%%%%%%%% WIBERG METHOD
%%%%%%%%%%%%%%%%%%%%%%%%%%%%%%%%%%%%%%%%

   la = 535*d;
   %%%%%%%%%%%%%%%%%%%%%%%%%%%%%%%%%%%%
flag=0;
  ik=1;
  while(flag==0)
    if (ik*h)>10
      nk=(sig^2)/9.81;
    end
    if (ik*h)<0.3142
      nk=sig/sqrt(9.81*h);
    end
        if ((ik*h)<=10) & ((ik*h)>=0.3142)
      nk=((sig)^2)/(9.81*tanh(ik*h));
    end
    if abs(nk-ik)<0.001
      flag=1;
    else
      ik=nk;
    end
  end
  k=nk;
  flag=0;
clear flag ii ik nk


   do = wh/sinh(k*h);
   d1=wh*g*k/((sig^2)*cosh(k*h));
%%%% ITTERATE TO FIND ANORBITAL RIPPLE HEIGHT (ha), hai= initial value

hai=.05;
flag=0;
while flag==0
  % ha = la*exp(-0.095*(log(do/hai))^2+0.442*log(do/hai)-2.28);
   ha=la*exp(-0.095*(log(do/hai))^2 + 0.442*log(do/hai)-2.28);
```

```
  if abs(ha-hai)<.001 , flag=1;
  else
   hai = (hai + ha)/2;
  end
end


%%%%% CLASSIFY TYPE OF RIPPLES ORBITAL(rt=0) ANORBITAL(rt=1) SUBORBITAL(rt=2)

if (do/ha)<20,
  rt = 0;     %orbital ripple
elseif (do/ha)>100,
  rt = 1;     %anorbital ripple
else,
  rt = 2;     %suborbital ripple
end

if rt == 0,
 ltw=0.62*do;
 sw=0.17;
 htw=sw*ltw;
 tp=['Orb'];

elseif rt == 1,
 sw=ha/la;
 htw=ha;
 ltw=la;
 tp=['Ano'];

elseif rt == 2,
 lo=0.62*do;
 ltw=exp((log(do/ha)-log(100))/(log(20)-log(100)))*(log(lo)-log(la))+log(la));
 %% iterate to find suborb ripple height and steepness
 flag=0;
 while flag==0
  hs = ltw*exp(-0.095*(log(do/ha))^2+0.442*log(do/ha)-2.28);
  if abs(hs-ha)<.001 , flag=1; htw=hs;
  else
   ha = (hs + ha)/2;
  end
 end
 sw=htw/ltw;
 tp=['Sub'];

end

%%%%%%%%%%%%%%%%%%%%%%%%%%%%%%%%%% NIELSEN METHOD
%%%%%%%%%%%%%%%%%%%%%%%%%%%%%%%%%%


  s=2.65;                    %% s= specific gravity

  a=do/2;     %% a= water semi-excursion

  mn = (a*sig)^2/((s-1)*g*d);          %% mn= mobility number


fw=exp((5.213*(2.5*d/a)^.194) - 5.977);  %% fw= wave friction factor
theta= .5*fw*mn;                    %% theta= Sheild's parameter


if mn<156
  htr=a*(.275 - .022*mn^.5);
else
  htr=0;  % no ripple if above 156
end

  ltr=a*(2.2 - .345*mn^(0.34));

  sr=.182 -.24*theta^1.5;
```

```
  if mn>10
    hti=a*21*mn^(-1.85);
  else
    hti=a*(.275 - .022*mn^.5);
  end

  lti=a*exp((693-.37*(log(mn))^8)/(1000+ .75*(log(mn))^7));
  si=.342-.34*theta^.25;
%%%%%%%%%%%%%%%%%%%%%%%%%%%% Nalin's Method %%%%%%%%%%%%%%%%%%%%%%%%%%%%
  fwi=fwik(a,sig,d);  %%% Call routine to solve Kelvin itteration for
                %% friction factor from Grant and Madsen (1982)

   %fwik=exp(5.213*((2.5*d/a)^.194) - 5.977); %% fw= wave friction factor

   mnwik = (a*sig)^2/((s-1)*g*d);          %% mn= mobility number

   thetawik= .5*fwi*mnwik;                 %% theta= Sheild's parameter

   S=(d/(4*nu))*((s-1)*g*d)^0.5;

   % S= (d*g*(s-1)/(4*nu))*(d)^0.5;    % wrong eqn. for S
    Z=thetawik/S;

   if Z<=0.012
    htwik=a*0.018*(Z^(-0.5));
   else
    htwik=a*0.0007*(Z^(-1.23));
   end

   if Z<=0.016
    stwik=0.15*(Z^(-0.009));
   else
    stwik=0.010*(Z^(-0.65));
   end

   ltwik=htwik/stwik;
%%%%%%%%%%%%%%%%%%%%%%%% Madsen and Grant (1982) %%%%%%%%%%%%%%%%%%%%%%%%

  brk=1.8*(S)^0.6;   %% breakoff pt.
  thetac=0.05;  %% Critical Shield's parameter (from Nielsen book)
  if (theta./thetac) <brk
    htgm=a*0.22*(thetawik./thetac)^(-0.16);
    stgm=0.16*(thetawik./thetac)^(-0.04)  ;
  else
    htgm=(0.48*a.*S^(0.8))*(thetawik./thetac)^(-1.5)
    stgm=(0.28*S^(0.6))*(thetawik./thetac)^(-1.0)
    thetawik./thetac
  end
  ltgm=htgm/stgm;

%%%%%%%%%%%%%%%%%%%%%% change results from meters to centimeters%%%%%%%%%
  lti=lti*100; hti=hti*100; si=si; ltr=ltr*100; htr=htr*100; sr=sr;
  htw=htw*100; ltw=ltw*100; sw=sw; htwik=htwik*100; ltwik=htwik/stwik;
  ltgm=ltgm*100; htgm=htgm*100;
%%%%%   RECORD RESULTS  %%%%%
  clc
  d1s(i,1)=d1;
  dos(i,1)=do;
  lengthi(i,1)=lti;
  heighti(i,1)=hti;
  steepi(i,1)=si;
  lengthr(i,1)=ltr;
  heightr(i,1)=htr;
  steepr(i,1)=sr;
  ts(i,1)=t;
  tps(i,1)=rt;
  type(i,:)=tp;
  heightw(i,1)=htw;
  lengthw(i,1)=ltw;
  steepw(i,1)=sw;
  thetas(i,1)=theta;
```

```
mns(i,1)=mn;
as(i,1)=a;
f(i,1)=fw;
run(i,1)=r;
ds(i,1)=do;
Zs(i,1)=Z;
fwik(i,1)=fwi;  % Grant-Madsen Friction factor
thetawik(i,1)=thetawik;  %Grant-Madsen Shield parameter
Ss(i,1)=S;      % Nalin's 'S'
heightwik(i,1)=htwik;
lengthwik(i,1)=ltwik;
steepwik(i,1)=stwik;
heightgm(i,1)=htgm;
lengthgm(i,1)=ltgm;
steepgm(i,1)=stgm;

end
%give short names to variables
lti95=lengthi; hti95=heighti; sti95=steepi; ltr95=lengthr; htr95=heightr; str95=steepr;
type95=tps; htw95=heightw; ltw95=lengthw; stw95=steepw; theta95=thetas; mn95=mns; a95=as;
fw95=f; do95=dos; t95=ts; do95=ds; d195=d1s; Z95=Zs; htwik95=heightwik; ltwik95=lengthwik;
stwik95=steepwik; htgm95=heightgm; ltgm95=lengthgm; stgm95=steepgm; S95=Ss;
Depth95=Depth;  Hmo95=Hmo; Tp95=Tp; D5095=D50;
y=input('enter y to save results    ','s');
if y=='y'
 save allmod95 lti95 hti95 sti95 ltr95 htr95 str95 stw95 do95 d1s95 ltw95 htw95 theta95 mn95 a95 fw95 Depth95 D5095...
      t95 type95 do95  Z95 S95 htwik95 ltwik95 stwik95 htgm95 ltgm95 stgm95 fwik95 thetawik95 Hmo95 Tp95
end


% calibd.m
% 11/23/96                Eric Thosteson
% Program to calibrate pressure, OBS, and ADV data from the DUCK96 SIS experiment.
% The following values are determined:  pressure time series, concentration times series
% from OBS, u and v flow time series, water depth, height of pressure, ADV, and OBS from
% bed, mean magnitude and direction of longshore current, surface elevation time series,
% directional spectrum using maximum entropy method for direction, peak wave frequency
% and its corresponding direction.

% Modifications

% 2/13/97  Eric Thosteson , 2/14/97 Chris Jette'
% Note:  Runs 10 & 11 had the current meter oriented downward instead of upward.
% calls despikd.m to 'despike' the pressure data.
% Note: Runs 9,10,11,and 29 are irrepairable

% Load appropriate file
index =10;  %starting file number
while index<31
if index<=4, fname=['s2900',num2str(index),'m'];
 elseif index<=9, fname=['s3000',num2str(index),'m'];
 elseif index<=11, fname=['s300',num2str(index),'m'];
 elseif index<=21, fname=['s310',num2str(index),'m'];
 elseif index>21,  fname=['s010',num2str(index),'m'];
end
eval(['load d:\chris\sis96\',fname])

% Set plotflag=1 for plotted results, savflag=1 for saved plots

 plotflag=1;
 savflag=0;

 disp(['Calibrating...' 10 10])

% Clear out data not used in this analysis and close figure windows

 clear fnames path f2rms f5rms dummy mtar1 mtar2
%  close all

% Determine sample frequency base on start and end times of file
```

```
begsecs=times(4,1)*3600+times(5,1)*60+times(6,1);
endsecs=times(4,2)*3600+times(5,2)*60+times(6,2);
ttlsecs=endsecs-begsecs;
sampfreq=round(length(spmen(1,:))/ttlsecs);

% Calibrate pressure and determine depths - runs 10 & 11 are corrected
% for flipped ADV.

pres=spmen(3,:)*0.00835-6.768;
prescor=despikf(pres,index); %  Call despike to 'despike' pressure
pbar=mean(prescor);
h_mta=mean(mean(mtar3(4:19,:)))/1000;
h_pres=h_mta+0.81;

h_obs=h_mta-0.07;
h=h_pres+pbar;

% Calibrate velocities and determine longshore current magnitude and direction

u=spmen(4,:)*1.187e-3-2.457;
ubar=mean(u);
v=spmen(5,:)*1.203e-3-2.492;
vbar=mean(v);
ls_mag=sqrt(ubar^2+vbar^2);
if (index~=10) & (index~=11)
  h_adv=h_mta+1.55;
else
  h_adv=h_mta-0.15;
  v=-v;   % u vel is same, v vel is opposite when downward
  vbar=-vbar;
end


% Correct directions based on pierside.

% Resulting orientation - x-axis positive onshore, right-hand rule

if (side=='N')
        v=-v;
        vbar=-vbar;
else
        u=-u;
        ubar=-ubar;
end

% Direction is computed with 0 degrees to the left when
% facing offshore

ls_dir=270-atan2(vbar,ubar)*180/pi;
if ls_dir>360
        ls_dir=ls_dir-360;
end

% Determine surface elevation spectrum - no direction

[Sxx,Sxxc,freqs,eta]=psurf(prescor,h_pres,h,sampfreq,128);

% Frequency limit utilized in determination of Hm0.  Note that freqlim is an index.
% Set to appropriate value.

freqlim=length(freqs)/sampfreq;  % Cutoff at 0.5 hz (2 second wave)
Hm0=4*sqrt(trapz(freqs(1:freqlim),Sxx(1:freqlim)));
[peakval peakidx]=max(Sxx(1:freqlim));
Tpeak=1/freqs(peakidx);

% Directional surface elevation spectrum - directional portion by maximum entropy method
% maxent.m returns direction with 0 degrees offshore - this is rotated by 90 degrees and
% corrected so angle is in clockwise sense.  This is in agreement with the long shore
% current calculation.

[Sxx,freqs,A0,A1,B1,A2,B2]=datafcs(prescor,u,v,h,h_pres,h_adv,sampfreq,128);
```

```
[freqs,phi,E]=maxent(Sxx,freqs,A0,A1,B1,A2,B2);
phi_deg=90-phi.*180./pi;
[dirval diridx]=max(E(:,peakidx));
Tdir=phi_deg(diridx);

% Calibrate OBS & get statistics

obs_conc=sprmen(1,:).*1.409e-3-0.164;
obs_max=max(obs_conc);
obs_min=min(obs_conc);
obs_bar=mean(obs_conc);

% Plot results (if flag is set)

if plotflag
 figure(1)
 plot(freqs(1:freqlim),[Sxxc(1:freqlim) (2*Sxx(1:freqlim)-Sxxc(1:freqlim))], ...
        '-b',freqs(1:freqlim),Sxx(1:freqlim),'-g')
 title('Surface elevation spectrum')
 xlabel('Frequency (hz)')
 ylabel('Spectral density (m^2)*s')
 if savflag
        savefile=sprintf('peps sespec%02d',index);
  eval(savefile);
      end

 figure(2)
 plot(1:length(eta),[eta' (prescor-mean(prescor))'])
 title('Pressure and surface elevation time series')
 xlabel('Elapsed time (s)')
 ylabel('Meters of salt water')
 if savflag
        savefile=sprintf('peps setmsr%02d',index);
  eval(savefile);
      end

 figure(3)
 res=200;
 xi = linspace(freqs(1),freqs(freqlim),res);
 mint = min(phi_deg);
 maxt = max(phi_deg);
 yi = linspace(mint,maxt,res)';
 zi = interp2(freqs(1:freqlim),phi_deg,E(:,1:freqlim),xi,yi,'cubic');
 S=[180,45];                % Light direction
 surfl(xi,yi,zi,S)
 axis([0 freqs(freqlim) min(phi_deg) max(phi_deg) 0 max(max(E(:,1:freqlim)))]);
 set(gca,'ydir','reverse')
 shading flat
 colormap bone
 xlabel('Frequency (hz)')
 ylabel('Direction (degrees)')
 zlabel('Spectral density (m^2)*s/radian')
 if savflag
        savefile=sprintf('peps dspec%02d',index);
  eval(savefile);
      end

 figure(4)
 contour(freqs(1:freqlim),phi_deg,E(:,1:freqlim),25)
 set(gca,'ydir','reverse')
 xlabel('Frequency (hz)')
 ylabel('Direction (degrees)')
 zlabel('Spectral density (m^2)*s/radian')
 if savflag
        savefile=sprintf('peps dcont%02d',index);
  eval(savefile);
      end

end
% Save results, increment index and restart
```

```
 savefile=sprintf('save stats%02d ',index);
 savestat=[savefile 'times sampfreq side pres prescor eta u v ls_mag ls_dir h h_mta ' ...
           'h_pres h_obs h_adv Sxx Sxxc freqs E phi_deg Hm0 Tpeak Tdir obs_conc ' ...
    'obs_max obs_min obs_bar loc prof15 prof profx'];
 eval(savestat)

 index=index+1;
 save index index
 clear
 load index
end
```

```
%%% despike.m
%% de-spikes pressure data from SIS96 experiment
%% takes the derivative of the press. signal w.r.t time
%% if dp/dt is above maxd, the value at this point is taken
%% as the mean of the two adjacent points, loop is continued
%% until the threshold is no longer exceeded
%% Runs 9,10,11,4,29 are too 'spiky' to repair.
%% Runs 3,7,13,22,23,26,27,28,30 are the runs which need repair
%% and can be reasonably repaired, all other runs appear fine
for index=[1:8,12:28,30]
 if index<10
  eval(['load stats0',num2str(index)])
 else
  eval(['load stats',num2str(index)])
 end
figure(1)
flg=1; n=0; m=0;
 maxd=0.2;
if index==13
 maxd=0.08;
elseif index==22
 maxd=0.14;
end
len=length(pres);
prescor=pres;
while flg==1;
m=m+1;
d=abs(diff(prescor));  % takes the derivative of pres
[mx ind]=max(d);  %finds the maximum derivative
 if mx>=maxd & m<200
  for i=2:length(d)-1
   if d(i)>maxd
    prescor(i+1)=[prescor(i)+prescor(i+2)]/2;
     if m==1, n=n+1;, end % count number of orig. bad pts.
   end
  end
 else
  flg=0;
 end
end
x=1:len;
n
subplot(4,1,1)
plot(x(1:len/4),pres(1:len/4),'w')
hold on
plot(x(1:len/4),prescor(1:len/4),'r')
title(['Run ',num2str(index),'   thresh: dp/dt=',num2str(maxd)])
hold off
subplot(4,1,2)
plot(x(len/4:len/2),pres(len/4:len/2),'w')
hold on
plot(x(len/4:len/2),prescor(len/4:len/2),'r')
hold off
subplot(4,1,3)
```

```
plot(x(len/2:3*len/4),pres(len/2:3*len/4),'w')
hold on
plot(x(len/2:3*len/4),prescor(len/2:3*len/4),'r')
hold off
subplot(4,1,4)
plot(x(3*len/4:len),pres(3*len/4:len),'w')
hold on
plot(x(3*len/4:len),prescor(3*len/4:len),'r')
hold off
figure(1)
pause
end



function [prescor]=despikf(pres,index)
%%% despikf.m   - function to despike pressure
%% de-spikes pressure data from SIS96 experiment
%% takes the derivative of the press. signal w.r.t time
%% if dp/dt is above maxd, the value at this point is taken
%% as the mean of the two adjacent points, loop is continued
%% until the threshold is no longer exceeded
%% Runs 9,10,11,29 are too 'spiky' to repair.
%% Runs 3,7,13,22,23,26,27,28,30 are the runs which need repair
%% and can be reasonably repaired, all other runs appear fine

flg=1; n=0; m=0;
 maxd=0.2;
if index==13
 maxd=0.08;
elseif index==22
 maxd=0.14;
end
len=length(pres);
prescor=pres;
while flg==1;
m=m+1;
d=abs(diff(prescor));  % takes the derivative of pres
[mx ind]=max(d);  %finds the maximum derivative
 if mx>=maxd & m<200
  for i=2:length(d)-1
   if d(i)>maxd
    prescor(i+1)=[prescor(i)+prescor(i+2)]/2;
     if m==1, n=n+1;, end % count number of orig. bad pts.
   end
  end
 else
  flg=0;
 end
end
x=1:len;
figure(1)
subplot(4,1,1)
plot(x(1:len/4),pres(1:len/4),'w')
hold on
plot(x(1:len/4),prescor(1:len/4),'r')
title(['Run ',num2str(index),'   thresh: dp/dt=',num2str(maxd)])
hold off
subplot(4,1,2)
plot(x(len/4:len/2),pres(len/4:len/2),'w')
hold on
plot(x(len/4:len/2),prescor(len/4:len/2),'r')
hold off
subplot(4,1,3)
plot(x(len/2:3*len/4),pres(len/2:3*len/4),'w')
hold on
plot(x(len/2:3*len/4),prescor(len/2:3*len/4),'r')
hold off
subplot(4,1,4)
plot(x(3*len/4:len),pres(3*len/4:len),'w')
```

```
hold on
plot(x(3*len/4:len),prescor(3*len/4:len),'r')
hold off
figure(1)
end



function ripple=hist96(mta96,p)
% 11-12-96  Chris Jette' hist96.m
% Given matrix mta96(len(1),len(2)), where mta96(1:2,:) are time/day
% and mta96(len(1),:) is # sec to take profile ($hould be zero)
% this function determines a
% representative ripple profile for each consecutive
% 'p' scans( 1:p,p+1:2*p,etc.) using a histogram
% to determine the mode elevation for each of the elements(transducers)
% during the 10 scan group. It returns a (# trans +3,n) matrix, the times
% for the beginning of each group are stored in the 1st and 2nd locations,
% and the time in sec for which the profile represents (ex. 20) is stored
% in the last location, n is the number of profiles calculated
% "a"= file number used to set mn (minumum) value of elev

len=size(mta96);



numb=floor(len(2)/p);            % number of profiles to calculate
ripple=zeros(len(1),numb); nu=0; oc=zeros(37,1);
for scan=[1:p:numb*p]
 nu=nu+1;
 for element=[3:len(1)-1]  % the index of actual range data
  med=floor(median(mta96(element,scan:scan+p))); % find median bottom loc. for all ranges
  lin=linspace(med-99,(med+100),200);  % x axis for histogram (distances) 1mm per bin
  [n,elev]=hist(mta96(element,scan:(scan+10)),lin); % histogram n=# occur., elev=distances
  n=fliplr(n); elev=fliplr(elev); %flip matrices so that max routine will look at
                    % the number of occurance of larger elev's 1st
  [occur,ind]=max(n(2:199)); % find index for max # occurances skip 1st bin
                  % because all returns less than med-100 in 1st bin same for high bin
  if occur>=4
   dist=elev(ind)-1; % use index to find corresponding distance
  elseif occur<4
   lin=linspace(med-98,(med+100),100); % 2mm per bin
   [n,elev]=hist(mta96(element,scan:(scan+p)),lin); % histogram n=# occur., elev=distances
   n=fliplr(n); elev=fliplr(elev); %flip matrices so that max routine will look at
                    % the number of occurance of larger elev's 1st
   [occur,ind]=max(n(2:99)); % find index for max # occurances skip 1st bin and last
   dist=elev(ind)-1; %use index to find distance subtract one due to bin size of 2mm
   if occur<4 %       rem( dist<(max(elev)-10) %requirements)
     lin=linspace(med-97,(med+110),70); % 3mm per bin
     [n,elev]=hist(mta96(element,scan:(scan+p)),lin);
     n=fliplr(n); elev=fliplr(elev);
     [occur,ind]=max(n(2:69)); % find index for max # occurances skip 1st bin and last
     dist=elev(ind)-2; %use index to find distance subtract two due to bin size of 3mm
   end
  end

  ripple(1:2,nu)=mta96(1:2,scan);
  ripple(element,nu)=dist;
  ripple(len(1),nu)=2*p; %time over which the profile represents, sec.

end
end


%hmo96.m  determine hmo and amo - along with peak periods for data
% Uses 'stats' data as input for elev. pres., prescor, sampfreq
% Also finds Hmo using the current information (h_adv, u, v)

for ind=[1:30]
if ind<10
 eval(['load d:\chris\sis96\stats\stats0',num2str(ind)])
```

```
else
 eval(['load d:\chris\sis96\stats\stats',num2str(ind)])
end

nFFT=256;                          %  number of points for FFT
nfreqf=(nFFT/2);                   % Size of full freq. band
fcuth=0.333;                       % High cut off freq.
fcutl=0.05;                        % Low cut off freq.
Sp=zeros(nfreqf,1);                % pressure spectrum
Su=zeros(nfreqf,1);                % u current spectrum
Sv=zeros(nfreqf,1);                % v current spectrum
delt=1/sampfreq;                   % dt between samples
depth=mean(prescor)+h_pres;

npr=length(prescor);
if npr>=512
 nprc=(2^fix(log2(npr)));   % Cut Pressure data up to power 2

  Presc=(prescor(1:nprc))';
  uc=(u(1:nprc))';
  vc=(v(1:nprc))';
  %
  freq=1/delt;
  dfreq=freq/nFFT;                 % Frequency increment
  fband=(0:nfreqf-1)*dfreq;        % The full frequency band
  ncuth=fix(fcuth/dfreq); ncutl=ceil(fcutl/dfreq);
  fbandc=fband(ncutl:ncuth);       % Cutted Fr. Band
  fbandi=fband(ncutl-1:ncuth+1);
  sigma=2*pi*fbandc;
  %
  %% Getting Wave spectrum
  %
  Sp=spect(Presc,nFFT,delt);       % One-side spectrum for Press
  Su=spect(uc,nFFT,delt);                  % U current
  Sv=spect(vc,nFFT,delt);                  % V current
  Ps=Sp(ncutl:ncuth);              % H/L-freq. filter
  Us=Su(ncutl:ncuth);
  Vs=Sv(ncutl:ncuth);

   Kw=sitfork(depth,fbandc);
   Kp=cosh(Kw*h_pres)./cosh(Kw*depth);
   Ku=sigma.*cosh(Kw*h_adv)./sinh(Kw*depth);  % current correction
   Dp=1./sinh(Kw*depth);
   %Dp=9.81*Kw./(((fbandc*2*pi).^2).*cosh(Kw*depth));  %Bottom Do multiplier
   Wspect=Ps./(Kp.^2);
   Dspect=Wspect.*(Dp.^2); % Aspect = bottom orbital diameter spectrum
   Uspect=Us./(Ku.^2);
   Vspect=Vs./(Ku.^2);
   Dspectu=Uspect.*(Dp.^2); % bottom orbital from current
   Dspectv=Vspect.*(Dp.^2);

  hmocur(ind)=4.01*sqrt(trapz(fbandi,[0 Uspect 0])...
    +trapz(fbandi,[0 Vspect 0]));  % sum spectrums from u and v
  [mcur,fcur]=max(Uspect + Vspect);
  Tpcur(ind)=1/fbandc(fcur);

  dmocur(ind)=4.01*sqrt(trapz(fbandi,[0 Dspectu 0])...
    +trapz(fbandi,[0 Dspectv 0]));%same as above but for semi-exc.
  [mam,fdcur]=max(Dspectv +Dspectu);
  Tpdcur(ind)=1/fbandc(fdcur);

  hmo=4.01*sqrt(trapz(fbandi,[0 Wspect 0]));  % from pressure
  dmo=4.01*sqrt(trapz(fbandi,[0 Dspect 0]));  % from pressure

   Hmo(ind)=hmo;
   [wsm,fmi]=max(Wspect);
   Tp(ind)=1/fbandc(fmi);          % Peak period
   Dmo(ind)=dmo;
   [dsm,dfmi]=max(Dspect);
   Tpd(ind)=1/fbandc(dfmi);        % Peak period from orbital dia.
```

```
    figure(1)
     ipspect=ifft(Ps);
      subplot(4,1,1)
     plot(fbandc,Wspect,'b')
     hold on
     plot(fbandc,Uspect+Vspect,'r')
     hold off
     v=axis;
     title(['Surf. Elev. Hmo=',num2str(hmo),'  ',num2str(hmocur(ind)),...
          'm  Tp=',num2str(Tp(ind))])
     ylabel('m^2-sec')

     subplot(4,1,2)
     plot(fbandc,Uspect,'r')
     hold on
     plot(fbandc,Vspect,'b')
     hold off
     title([num2str(ind),'U(r) and V(b) Depth=',num2str(depth),'m elev.= ',num2str(h_adv),'m'])
     ylabel('m^2-sec')
     %axis(v);
      subplot(4,1,3)

     plot(fbandc,Dspect)
     hold on
     plot(fbandc,Dspectu+Dspectv,'r')
     title(['Dmo= ',num2str(dmo),'m Tp= ',num2str(Tpd(ind))])
     ylabel('m^2-sec')
     xlabel('Frequency in Hz')
     hold off
      subplot(4,1,4)
     Kpb=1./cosh(Kw*depth);
     Bspect=Wspect.*(Kpb.^2);
     plot(fbandc,Bspect)
     %axis(v)
     title('Corrected Bottom Pressure Spectrum')
     ylabel('m^2-sec')
  pause %%%%%%%%%%%%%%%%%%%%%%%%%%%%%%%%%%%%%%%%%%%
else
  Hmo(ind)=0, Tpa(ind)=0; Dmo(ind)=0; Tp(ind)=0;
end
  Hm02(ind)=Hm0; Tp2(ind)=Tpeak; % with 0.5 hz. cut off
end
% save waves96 Hmo Dmo Hm02 Tp Tpd Tp2 hmocur Tpcur dmocur Tpdcur


%% mesh96.m
%% plots a mesh plot with ripple data from 64 element array
%% plots entire array and the 5MHz center region separately
clf,clear
l=zeros(30,1); s=zeros(30,1);, fn=zeros(30,7);
for index=[1:30]
if index<=9, fname=['stats0',num2str(index)];
 elseif index>9, fname=['stats',num2str(index)];
end
eval(['load ',fname])
num=floor(length(prof15)/30)-1;

x5=linspace(96,96+46.5,32);
 med=median(prof15(:,1:64)); len=size(prof15,1);
 men=mean(med); % mean of median profile (mm)
for i=1:len
 nprof(i,:)=men/10-prof15(i,1:64)/10; %orient profile for plot (cm)
end
prof5=nprof(:,17:17+31);

 time=(0:size(nprof,1)-1)*prof15(1,67); % time axis for plot
figure(1)
if side=='S'
 x5=fliplr(x5);
 profx=fliplr(profx);
```

```
end
subplot(2,1,1)

mesh(profx,time,nprof)
hold on
n=axis; zmin=n(5); zmax=n(6);
zm=zmax;
if zm>20
 med=median(nprof(:,:)); %find median prof to set axis
 med5=median(prof5(:,:));
 maxz=3*max(med); minz=3*min(med);
 maxz5=1+max(med5);

 if min(med5)>min(median(prof5(:,:)));
  minz5=-1+min(median(prof5(:,:))); %account for sinking of frame during run
 else
  minz5=-1+min(med5);
 end
zmax=maxz; zmin=minz;%zmax=10; zmin=-10; %%%%%%%%%%%%%%
end
axis([0 max(profx) 1 max(time) zmin zmax])


plot3([x5(1),x5(1)],[0,0],[prof5(1,1),zmin])
plot3([x5(32),x5(32)],[0,0],[prof5(1,32),zmin])
plot3([x5(32),x5(32)],[0,max(time)],[zmin,zmin])
plot3([x5(1),x5(1)],[0,max(time)],[zmin,zmin])
plot3([x5(1),x5(32)],[0,0],[zmin,zmin])
hold off

title(['Plot of MTA SIS96 data -',fname,' ', ...
 num2str(loc),side,' each profile represents ',num2str(prof15(1,67)),' sec.'])


xlabel('distance (cm) : onshore is + dir.')
ylabel('time - sec')
zlabel('vetical (cm)')
subplot(2,1,2)
mesh(x5,time,prof5)
xlabel('centimeters')
title('MTA1 - middle section of above plot')
zlabel('vertical (cm)')
xlabel('horizontal (cm)')
ylabel('time - sec')
n=axis; zmin=n(5); zmax=n(6);

if zm>20
 zmax=maxz5; zmin=minz5;%zmax=2;,zmin=-6; %%%%%%%%%%%%%%%%
end
axis([96 96+46.5 1 max(time) zmin zmax])
hold on
plot3([x5(1),x5(1)],[0,0],[prof5(1,1),zmin])
plot3([x5(32),x5(32)],[0,0],[prof5(1,32),zmin])
plot3([x5(1),x5(32)],[0,0],[zmin,zmin])
plot3([x5(32),x5(32)],[0,max(time)],[zmin,zmin])

hold off
pause
clear prof x prof15 profx m1 m2 m3 men profm nprof
clear x5 prof5 nprof  miny maxy miny5 maxy5 mn maxz5 minz5
clear maxz minz %med
end
hold off



%%%%%%%%%%%%%%%%%%%%%%% modsig96.m%%%%%%%%
%%%%%%%%%%%%%%%%%%%%%%%%%%%%%%%%%%%%%%%%%%%%%%%%%%%%%%%%
%%%% COMPUTES RIPPLE TYPE AND GEOMETRIES USING WIBERG,NIELSEN, AND JETTE  %%%%  MODELS%%%%
%%%% Uses significant excursion and bottom velocities        %%%%
%%%%  INPUT DEPTH, GRAIN SIZE, sigexc, sigcur       %%%%
```

```
%%%%  WRITTEN BY CHRIS JETTE' last update 5-31-97 %%%%
%%%%  automatically runs thru complete set of wave data for Duck 96
load d:\chris\sis96\stats96

%%%%  g = gravity(m/s^2), Depth = water depth(m), Tp = wave period(s)
%%%%  Hmo = wave height(m),lt= wave length, lt = ripple wave length,D50(mm)
%%%%  ho, ha, ha = ripple height(m), do = wave orbital diameter, d =grain size
%%%%  tp = ripple type
 zeromat=zeros(30,4);
 zeromat(6,:)=[NaN NaN NaN NaN];
 zeromat(24,:)=[NaN NaN NaN NaN];
 typ95s=zeromat; % for runs 6 and 24 of SIS96 data insert NaN
 sti96s=zeromat; hti96s=zeromat; lti96s=zeromat;
 str96s=zeromat; htr96s=zeromat; ltr96s=zeromat;
 stw96s=zeromat; htw96s=zeromat; ltw96s=zeromat;
 stj96s=zeromat; htj96s=zeromat; ltj96s=zeromat;
 rnn96s=zeromat;  shield96s=zeromat; f96s=zeromat;
g=9.81;
nu=1.4e-06;  %%% kinematic viscosity of sea-water (m^2/s)
for i=[1:5,7:23,25:30]
 for j=1:4
 h=Depth(i); r=(i);
 d = (D50(i))./1000;     %% D50 = sediment diameter (mm)
 do= sigexc(i,j);
 u=sigvel(i,j);

%%%%%%%%%%%%%%%%%%%%%%%%%%%%%% WIBERG METHOD
%%%%%%%%%%%%%%%%%%%%%%%%%%%%%%

   la = 535*d;

 %%%% ITTERATE TO FIND ANORBITAL RIPPLE HEIGHT (ha), hai= initial value

hai=.05;
flag=0;
while flag==0
  % ha = la*exp(-0.095*(log(do/hai))^2+0.442*log(do/hai)-2.28);
   ha=la*exp(-0.095*(log(do/hai))^2 + 0.442*log(do/hai)-2.28);

    if abs(ha-hai)<.0001 , flag=1;
    else
     hai = (hai + ha)/2;
    end
end


 %%%%% CLASSIFY TYPE OF RIPPLES ORBITAL(rt=0) ANORBITAL(rt=1) SUBORBITAL(rt=2)

if (do/ha)<20,
   rt = 0;      %orbital ripple
elseif (do/ha)>100,
   rt = 1;      %anorbital ripple
else,
   rt = 2;      %suborbital ripple
end

if rt == 0,
  ltw=0.62*do;
  sw=0.17;
  htw=sw*ltw;
  tp=['O'];

elseif rt == 1,
  sw=ha/la;
  htw=ha;
  ltw=la;
  tp=['A'];

elseif rt == 2,
  lo=0.62*do;
  ltw=exp(((log(do/ha)-log(100))/(log(20)-log(100)))*(log(lo)-log(la))+log(la));
```

```
 %% itterate to find suborb ripple height and steepness
 flag=0;
 while flag==0
  hs = ltw*exp(-0.095*(log(do/ha))^2+0.442*log(do/ha)-2.28);
  if  abs(hs-ha)<.001 , flag=1; htw=hs;
  else
    ha = (hs + ha)/2;
  end
 end
  sw=htw/ltw;
  tp=['S'];

end

%%%%%%%%%%%%%%%%%%%%%%%%%%%%%% NIELSEN METHOD
%%%%%%%%%%%%%%%%%%%%%%%%%%%%%%

   s=2.65;                          %% s= specific gravity

   a=do./2;       %% a= water semi-excursion

   mn = (u)^2/((s-1)*g*d);          %% mn= mobility number


 fw=exp((5.213*(2.5*d/a)^.194) - 5.977);  %% fw= wave friction factor
 theta= .5*fw*mn;                         %% theta= Sheild's parameter

 if mn<156
   htr=a*(.275 - .022*mn^.5);
 else
   htr=0;  % no ripple if above 156
 end

   ltr=a*(2.2 - .345*mn^(0.34));
   sr=.182 - .24*theta^1.5;

   if mn>10
     hti=a*21*mn^(-1.85);
   else
     hti=a*(.275 - .022*mn^.5);
   end

   lti=a*exp((693-.37*(log(mn))^8)/(1000+ .75*(log(mn))^7));
   si=.342-.34*theta^.25;
%%%%%%%%%%%%%%%%%%%%%%%%%%%%%%
%  jette and hanes (1997) method
if mn>10
 htj=a*0.9*mn^(-1);
else
  htj=a*0.09;
end

if mn<190
 stj=-0.006*mn^0.6) + 0.15;
else
 stj=0.01;
end

ltj=htj/stj;

%%%%%%%%%%%%%%%%%%%%%%% change results from meters to centimeters%%%%%%%%%
 hti=hti*100; hti=hti*100; si=si; ltr=ltr*100; htr=htr*100; sr=sr;
 htw=htw*100; ltw=ltw*100; sw=sw; ltj=ltj*100; htj=htj*100; stj=stj;
%%%%%   RECORD RESULTS  %%%%%
sti96s(i,j)=si; hti96s(i,j)=hti; lti96s(i,j)=lti;
str96s(i,j)=sr; htr96s(i,j)=htr; ltr96s(i,j)=ltr;
stj96s(i,j)=stj; htj96s(i,j)=htj; ltj96s(i,j)=ltj;
 stw96s(i,j)=sw; htw96s(i,j)=htw; ltw96s(i,j)=ltw;
 mn96s(i,j)=mn;  shield96s(i,j)=theta; f96s(i,j)=fw;
typ96s(i,j)=tp;
```

```
end
end

save mod96sig lti96s ltj96s htj96s hti96s sti96s ltr96s htr96s str96s stj96s stw96s ltw96s htw96s shield96s mn96s f96s typ96s



%%%%%%%%%%%%% prof96.m %%%%%%%%%%%%%%%%%%
  % Used to calculate representative
  % profiles for SIS96 MTA data for every p*2 sec,
  % p scans of data. Final profiles (prof), have
  % a length of 67 (prof(:,65:66) is the time stamp)
  % prof(:,67) is the number of seconds for which
  % the profile covers (p*2 sec). All ranges are in
  % millimeters. MTAR1 began sampling before MTAR2,
  % which began sampling before MTAR3. Thus first the
  % time when MTAR3 began sampling is found, then the
  % time that MTAR1 stopped sampling is found. The
  % difference is the time for which profiles are com-
  % puted. profx is the corresponding horizontal scale
  % to plot prof(:,1:64) with.

for index=[5:30]
 if index<=4, fname=['s2900',num2str(index),'m'];
  elseif index<=9, fname=['s3000',num2str(index),'m'];
  elseif index<=11, fname=['s300',num2str(index),'m'];
  elseif index<=21, fname=['s310',num2str(index),'m'];
  elseif index>21,  fname=['s010',num2str(index),'m'];
 end
 eval(['load ',fname])

 % find start of MTAR3, end of MTAR1, corr. MTAR2 index
 start=mtar3(2,2);s3=2;
 stop=mtar1(2,length(mtar1));
 s1=1;
 while mtar1(2,s1)<mtar3(2,s3)
  s1=s1+1;
 end
  s2=1;
 while mtar2(2,s2)<mtar3(2,s3)
  s2=s2+1;
 end

 totlen=length(mtar1)-s1; % total length of synced profiles
 mta1=mtar1(2:size(mtar1,1),s1:s1+totlen);% remove 1st zero
 for i=1:totlen
  mta1(21,i)=mean([mta1(20,i),mta1(22,i)]); % x-ducer 19 down
 end
 mta2=mtar2(2:size(mtar2,1),s2:s2+totlen);
 mta3=mtar3(2:size(mtar3,1),s3:s3+totlen);

 p=15; %number of scans to use per representative prof.

 %%% call hist96.m function to determine bottom
 % location using histogram approach
 prof1=hist96(mta1,p);
 prof2=hist96(mta2,p);
 prof3=hist96(mta3,p);

 % prof is the composite profile w/ day and time
 %  and the number of seconds the profile represents


for i=1:size(prof3,2)
 time=prof1(1:2,i);
 avg=prof1(size(prof1,1),i);
 p1(i,:)=fliplr(prof1(3:size(prof1,1)-1,i)');
 p2(i,:)=fliplr(prof2(3:size(prof2,1)-1,i)');
 p3(i,:)=prof3(3:size(prof3,1)-1,i)';
 p=[p3(i,:),p1(i,:),p2(i,:),time(1),time(2),avg];
```

```
  prof15(i,:)=p;
end

  profx=[linspace(0,90,16),linspace(96,96+46.5,32),...
    linspace(148.5,238.5,16)];
  figure(1)
  plot(profx,prof15(:,1:64))
  xlabel('Horizontal Distance -cm')
  ylabel('Vertical Distance - mm')
  title(['Plot of MTA data ',fname,' ',num2str(loc),side,' representative profiles for every ',num2str(p*2),' sec.'])
%%%%%%%%%% remove % infront of below statement to save
  %eval(['save ',fname,' prof prof15 profx f2 f5 loc mtar1 mtar2 mtar3 side spmen times'])
  clear prof profx f2 f5 loc mtar1 mtar2 mtar3 side spmen times prof15

end



%%  Reval596.m 11-25-96  Calculate ripple dimensions for SIS96 5 MHz
%% Duck SIS96 Ripple profile analysis
%% follows ripple profile recording each local maximum and local min.
%% Output variables, fname, ht5,lt5 ( splits run up into 4 sections)
%% determines ripple dimensions for each profile then averages over
%% each of the four sections to get representative dimensions
%% averages elevation differences between local max. and local min.
%% averages horizontal differences between local max. and min.
%% input values are prof15 and profx - SIS96 data
%% prof15 - range measurements, profx - corresponding horiz. coord.
%% recalculates ripple dimensions with a threshold of .5*aht

clg, hold off, check=0;
ht5=zeros(4,30); lt5=zeros(4,30);  %output variable
fn=zeros(30,7);
for index=[1:30]
if index<=4, fname=['s2900',num2str(index),'m'];
 elseif index<=9, fname=['s3000',num2str(index),'m'];
 elseif index<=11, fname=['s300',num2str(index),'m'];
 elseif index<=21, fname=['s310',num2str(index),'m'];
 elseif index>21,  fname=['s010',num2str(index),'m'];
end
eval(['load ',fname])

numprof=size(prof15,1);% number of rep. profiles in file
ahtt=zeros(1,numprof); altt=zeros(1,numprof); ahta=zeros(1,numprof);
alta=zeros(1,numprof); stime=zeros(1,numprof);


prof5=prof15(:,17:48);   % 32 element 5MHz array analysis
 x5=profx(:,17:48);   % x axis for 32 element array (cm)
 % profiles with linear trend subtracted, mm to cm, rectified
 detrend5=(detrend(prof5')/(-10))';

for pr=1:numprof  % step through profiles
  z=ceil(pr/(numprof/4)); %break up profiles into four sections (1:4)
  xi=x5;
  yi=detrend5(pr,:);
  j=length(yi);
  k=1; min=0; t=3; max=0;
 %% t=type of slope 1=upslope , 2=downslope, 0=no slope

 while k+1<j,
  k=k+1;
  s=yi(1,k);
  e=yi(1,k+1);
  el=xi(k);

% if up slope

  if s<e;
   if t == 2,
     min=min+1;
```

```
    hmin(min)=s;
    lmin(min)=el;
    t= 1;
   elseif t == 0,
    min=min+1;
    hmin(min)=s;
    lmin(min)=el;
    t=1;
   else
   t=1;
   end

 % if down slope

  elseif s>e,
   if t == 1,
    max=max+1;
    hmax(max)=s;
    lmax(max)=el;
    t= 2;
   elseif t == 0,
    max=max+1;
    hmax(max)=s;
    lmax(max)=el;
    t=2;
   else
    t=2;
   end

 % if no slope

  elseif s==e,
   t=0;
  end
 end

 %determine average ripple height and length

 if min<max,
  n=min;
 else ,
  n=max;
 end

 for i=1:n,
  ht=0; lt=0;
  h(i)=hmax(i)-hmin(i);
  ht=sum(h);
 end
 if min>1,
  for j=1:min-1
   l(j)=lmin(j+1)-lmin(j);
   lt=sum(l);
   nl=min-1;
  end
 else
  for j=1:max-1
   l(j)=lmax(j+1)-lmax(j);
   lt=sum(l);
   nl=max-1;
  end
 end
 aht=ht/n;
 alt=lt/nl;

 %%%%%%%%%%%%%%%%%%%%%%%%%%%%%Threshold%%%%%%%%%%%%%%%%%%%%%%%%%%%%
 %%%%%%%%%%%%%%%%%%%%%%%%%%%%%% new method %%%%%%%%%%%%%%%%%%%%
 p=min+max;
 if lmin(1,1)<lmax(1,1),
  hall(1:2:p)=hmin; % make array of max and min hts
  hall(2:2:p)=hmax;
```

```
  lall(1:2:p)=lmin; % make array of max and min lts
  lall(2:2:p)=lmax;

  m=1;
else,
  hall(1:2:p)=hmax;
  hall(2:2:p)=hmin;
  lall(1:2:p)=lmax;
  lall(2:2:p)=lmin;

  m=0;
end

%% Threshold set to 3mm in ht.
thresh1=0.3;
c=1;  ct=c+1;  n=1;
while ct<=length(hall),

 if abs(hall(c)-hall(ct))>=thresh1,
  halla(n)=hall(c);
  lalla(n)=lall(c);
  c=ct; ct=c+1; n=n+1;

 else,
  if ct+1<=length(hall),
   if hall(c)>hall(c+1)  %looking for min
     if hall(ct+1)>hall(c)
       c=ct+1;
     end
   elseif hall(c+1)>hall(c)  %looking for max
     if hall(ct+1)<hall(c)
       c=ct+1;
     end
   end
  end
  ct=ct+2;
 end
end
halla(n)=hall(c);
lalla(n)=lall(c);
if length(halla)<2;
  check=1;  % if no ripples found set check=1

elseif halla(1)<halla(2),
   hmina=halla(1:2:length(halla));
   lmina=lalla(1:2:length(lalla));
   hmaxa=halla(2:2:length(halla));
   lmaxa=lalla(2:2:length(lalla));
else,
   hmina=halla(2:2:length(halla));
   lmina=lalla(2:2:length(lalla));
   hmaxa=halla(1:2:length(halla));
   lmaxa=lalla(1:2:length(lalla));
end


%% determine average riple height, length, and steepness
%%% average riple height= average distance between each max and min
if check~=1  % if there were ripples present, else skip to end
for i=1:length(halla)-1
 ht(i)=abs(halla(i)-halla(i+1));
end
ahta(pr)=sum(ht)/length(ht);

for i=1:length(lalla)-1
 lt(i)=lalla(i+1)-lalla(i);
end
alta(pr)=2*(sum(lt)/length(lt));
%%%%%%%%%%%%%%%%%%%%%%%%%%%%%%%%%%%%%%%%%%%%%%%%%%%%%%%%%%%%%%%%%%%%%%
%%%%%% Threshold set to fraction of above ripple height %%%%%
c=1;  ct=c+1;  n=1;
```

```
if length(ht)>=5  % if more than five ripples found, reset threshold
 if 0.5*ahta(pr)>thresh1
  thresh2=0.5*ahta(pr);
 else thresh2=thresh1;
 end
else thresh2=thresh1;
end

while ct<=length(hall),

 if abs(hall(c)-hall(ct))>=thresh2,
  hallt(n)=hall(c);
  lallt(n)=lall(c);
  c=ct; ct=c+1; n=n+1;

 else,
  if ct+1<=length(hall),
   if hall(c)>hall(c+1)  %looking for min
    if hall(ct+1)>hall(c)
     c=ct+1;
    end
   elseif hall(c+1)>hall(c)  %looking for max
    if hall(ct+1)<hall(c)
     c=ct+1;
    end
   end
  end
  ct=ct+2;
 end
end

hallt(n)=hall(c);
lallt(n)=lall(c);
if length(hallt)<2;
  check=1;  % no ripples present
elseif hallt(1)<hallt(2),
  hmint=hallt(1:2:length(hallt));
  lmint=lallt(1:2:length(lallt));
  hmaxt=hallt(2:2:length(hallt));
  lmaxt=lallt(2:2:length(lallt));
else,
  hmint=hallt(2:2:length(hallt));
  lmint=lallt(2:2:length(lallt));
  hmaxt=hallt(1:2:length(hallt));
  lmaxt=lallt(1:2:length(lallt));
end


%% determine average ripple height, length, and steepness
%%% average riple height= average distance between each max and min
 elseif check==1 % if statement from 1st threshold method if no ripples
 end  % end for above elseif
if check==1
 ahtt(pr)=0;, altt(pr)=50; % if no ripples present
else
 for i=1:length(hallt)-1
  ht(i)=abs(hallt(i)-hallt(i+1));
 end
 ahtt(pr)=sum(ht)/length(ht);

 for i=1:length(lallt)-1
  lt(i)=lallt(i+1)-lallt(i);
 end
 altt(pr)=2*(sum(lt)/length(lt));
end

if check~=1,
subplot(4,1,z)
plot(xi,yi,'w')
axis([96 142.5 -3 3])
hold on
```

```
plot(x5,detrend5(pr,:),'b')
%plot(lmina,hmina,'*')
%plot(lmaxa,hmaxa,'*')
%plot(lmint,hmint,'ro')
plot(lmint,hmint,'rx')
%plot(lmaxt,hmaxt,'ro')
plot(lmaxt,hmaxt,'rx')
elseif check==1;%%%% if check==1
  subplot(4,1,z)
  text(115,2.2,'*')
  plot(x5,detrend5(pr,:),'b')
  axis([96 142.5 -3 3])
end
check=0;  % set check back to zero

figure(1)

clear lmint lmaxt lmin lmax hmint hmaxt hmax hmin  xi yi n nl
clear  e el h ht i j k l lt max min hall hallt lall lallt c ct m nrs
clear p t s lmina lmaxa hmina hmaxa  halla lalla
hold on
end % for individual profile loop

ln=floor(length(ahtt)/4);
for z=1:4   % plot text on graphs
 ht5(z,index)=mean(ahtt((z-1)*ln+1:z*ln)); %output variable
 lt5(z,index)=mean(altt((z-1)*ln+1:z*ln)); %output variable
 fn(index,:)=fname;
 subplot(4,1,z)
 set(get(gcf,'children'),'Fontsize',10)
 text(98,2.2,['Ripple Ht.= ',num2str(round(mean(ahtt((z-1)*ln+1:z*ln))*10)/10),' cm'])
 text(120,2.2,['Ripple Lt.= ',num2str(round(mean(altt((z-1)*ln+1:z*ln))*10)/10),' cm'])

 if z==2|3
  ylabel('Vertical - cm','Fontsize',10)
 end
 hr=floor(prof15((z-1)*ln+1,65)/3600);
 mn=floor((prof15((z-1)*ln+1,65)-hr*3600)/60);
 sec=floor(prof15((z-1)*ln+1,65)-hr*3600-mn*60);
 if z==1,
   title(['Detrended SIS96 5MHz Ripple Pattern   ',fname,'  ',num2str(loc),side,'  ',num2str(hr),':',num2str(mn),':',num2str(sec)],'Fontsize',10)
 else,
   title([num2str(hr),':',num2str(mn),'          '],'Fontsize',10)
 end
 if z==4
  xlabel('Horizontal Distance in cm','Fontsize',10)
 end
end
 hold off, clg
end  % for file loop T loop



%%  Revalw96.m 11-25-96  Calculate ripple dimensions for SIS96
%%  Whole array analysis
%% Output variables, fname, ht5,lt5 ( splits run up into 4 sections)
%% determines ripple dimensions for each profile then averages over
%% each of the four sections to get representative dimensions
%% averages elevation differences between local max. and local min.
%% averages horizontal differences between local max. and min.
%% input values are prof15 and profx - SIS96 data
%% prof15 - range measurements, profx - corresponding horiz. coord.
%% recalculates ripple dimensions with a threshold of .5*aht

clg, hold off, check=0;
htw=zeros(4,30); ltw=zeros(4,30);  %output variable
fn=zeros(30,7);
for index=[1:30]
if index<=4, fname=['s2900',num2str(index),'m'];
 elseif index<=9, fname=['s3000',num2str(index),'m'];
```

```
 elseif index<=11, fname=['s300',num2str(index),'m'];
 elseif index<=21, fname=['s310',num2str(index),'m'];
 elseif index>21,  fname=['s010',num2str(index),'m'];
end
eval(['load ',fname])

numprof=size(prof15,1);% number of rep. profiles in file
ahtt=zeros(1,numprof); altt=zeros(1,numprof); ahta=zeros(1,numprof);
alta=zeros(1,numprof); stime=zeros(1,numprof);


%%%%% Smooth Ripple Profile with Spline function, detrend, and rectify %%%%%
%nrs=37; smrip=zeros(4,109); mrip=zeros(1,4);
%x=linspace(1,nrs,nrs);
%xi=linspace(1,nrs,3*nrs-2);
%smlen=xi*12;
%for z=1:4
% smrip(z,:)=spline(x,ripple(3:39,(z-1)*4+1),xi);
% mrip(z)=round(mean(ripple(3:39,((z-1)*4+1))));
% smrip(z,:)=smrip(z)-smrip(z,:);
% ripple(3:39,z)=detrend(mrip(z)-ripple(3:39,((z-1)*4+1)));
% stime(z)=ripple(1,((z-1)*4+1));
%end

profw=prof15(:,1:64);  % whole array
profx;   % x axis for array (cm)
 % profiles with linear trend subtracted, mm to cm, rectified
 detrend5=(detrend(profw')/(-10))';

for pr=1:numprof  % step through profiles
  z=ceil(pr/(numprof/4)); %break up profiles into four sections (1:4)
  xi=profx;
  yi=detrend5(pr,:);
  j=length(yi);
  k=1; min1=0; t=3; max1=0;
  %% t=type of slope 1=upslope , 2=downslope, 0=no slope

  while k+1<j,
   k=k+1;
   s=yi(1,k);
   e=yi(1,k+1);
   el=xi(k);

% if up slope

  if s<e;
   if t == 2,
     min1=min1+1;
     hmin(min1)=s;
     lmin(min1)=el;
     t= 1;
   elseif t == 0,
     min1=min1+1;
     hmin(min1)=s;
     lmin(min1)=el;
     t=1;
   else
   t=1;
   end

% if down slope

  elseif s>e,
   if t == 1,
     max1=max1+1;
     hmax(max1)=s;
     lmax(max1)=el;
     t= 2;
   elseif t == 0,
     max1=max1+1;
     hmax(max1)=s;
```

```
    lmax(max1)=e1;
    t=2;
   else
    t=2;
   end

% if no slope

  elseif s==e,
   t=0;
  end
end

%determine average ripple height and length

if min1<max1,
  n=min1;
else ,
  n=max1;
end

for i=1:n,
  ht=0; lt=0;
  h(i)=hmax(i)-hmin(i);
  ht=sum(h);
end
if min1>1,
 for j=1:min1-1
  l(j)=lmin(j+1)-lmin(j);
  lt=sum(l);
  nl=min1-1;
 end
else
 for j=1:max1-1
  l(j)=lmax(j+1)-lmax(j);
  lt=sum(l);
  nl=max1-1;
 end
end
aht=ht/n;
alt=lt/nl;

%%%%%%%%%%%%%%%%%%%%%%%%%%%%%%%%Threshold%%%%%%%%%%%%%%%%%%%%%%%%%%%%%%%%
%%%%%%%%%%%%%%%%%%%%%%%%%%%%%%%% new method %%%%%%%%%%%%%%%%%%%%%%%%%%%%
p=min1+max1;
if lmin(1,1)<lmax(1,1),
  hall(1:2:p)=hmin; % make array of max and min hts
  hall(2:2:p)=hmax;
  lall(1:2:p)=lmin; % make array of max and min lts
  lall(2:2:p)=lmax;

  m=1;
else,
  hall(1:2:p)=hmax;
  hall(2:2:p)=hmin;
  lall(1:2:p)=lmax;
  lall(2:2:p)=lmin;

  m=0;
end

%% Threshold set to 5mm in ht.
thresh1=0.5;
c=1; ct=c+1; n=1;
while ct<=length(hall),

 if abs(hall(c)-hall(ct))>=thresh1,
  halla(n)=hall(c);
  lalla(n)=lall(c);
  c=ct; ct=c+1; n=n+1;
```

```
 else,
  if ct+1<=length(hall),
   if hall(c)>hall(c+1)  %looking for min
     if hall(ct+1)>hall(c)
       c=ct+1;
     end
   elseif hall(c+1)>hall(c)  %looking for max
     if hall(ct+1)<hall(c)
       c=ct+1;
     end
   end
  end
  ct=ct+2;
 end
end
halla(n)=hall(c);
lalla(n)=lall(c);
if length(halla)<2;
  check=1;  % if no ripples found set check=1

elseif halla(1)<halla(2),
   hmina=halla(1:2:length(halla));
   lmina=lalla(1:2:length(lalla));
   hmaxa=halla(2:2:length(halla));
   lmaxa=lalla(2:2:length(lalla));
else,
   hmina=halla(2:2:length(halla));
   lmina=lalla(2:2:length(lalla));
   hmaxa=halla(1:2:length(halla));
   lmaxa=lalla(1:2:length(lalla));
end


%% determine average riple height, length, and steepness
%%% average riple height= average distance between each max and min
if check~=1  % if there were ripples present, else skip to end
for i=1:length(halla)-1
 ht(i)=abs(halla(i)-halla(i+1));
end
ahta(pr)=sum(ht)/length(ht);

for i=1:length(lalla)-1
 lt(i)=lalla(i+1)-lalla(i);
end
alta(pr)=2*(sum(lt)/length(lt));
%%%%%%%%%%%%%%%%%%%%%%%%%%%%%%%%%%%%%%%%%%%%%%%%%%%%%%%%%%%%
%%%%%% Threshold set to fraction of above ripple height %%%%%
c=1;  ct=c+1;  n=1;
if length(ht)>=3  % if more than three ripples found, reset threshold
 if 0.7*ahta(pr)>thresh1
  thresh2=0.7*ahta(pr);
 else thresh2=thresh1;
 end
else thresh2=thresh1;
end

while ct<=length(hall),

 if abs(hall(c)-hall(ct))>=thresh2,
  hallt(n)=hall(c);
  lallt(n)=lall(c);
  c=ct; ct=c+1; n=n+1;

 else,
  if ct+1<=length(hall),
   if hall(c)>hall(c+1)  %looking for min
     if hall(ct+1)>hall(c)
       c=ct+1;
     end
   elseif hall(c+1)>hall(c)  %looking for max
     if hall(ct+1)<hall(c)
```

```
    c=ct+1;
   end
  end
 end
 ct=ct+2;
end
end

hallt(n)=hall(c);
lallt(n)=lall(c);
if length(hallt)<2;
  check=1;  % no ripples present
elseif hallt(1)<lhallt(2),
  hmint=hallt(1:2:length(hallt));
  lmint=lallt(1:2:length(lallt));
  hmaxt=hallt(2:2:length(hallt));
  lmaxt=lallt(2:2:length(lallt));
else,
  hmint=hallt(2:2:length(hallt));
  lmint=lallt(2:2:length(lallt));
  hmaxt=hallt(1:2:length(hallt));
  lmaxt=lallt(1:2:length(lallt));
end


%% determine average ripple height, length, and steepness
%%% average riple height= average distance between each max and min
 elseif check==1 % if statement from 1st threshold method if no ripples
 end  % end for above elseif
if check==1
 ahtt(pr)=0;, altt(pr)=50; % if no ripples present
else
 for i=1:length(hallt)-1
  ht(i)=abs(hallt(i)-hallt(i+1));
 end
 ahtt(pr)=sum(ht)/length(ht);

 for i=1:length(lallt)-1
  lt(i)=lallt(i+1)-lallt(i);
 end
 altt(pr)=2*(sum(lt)/length(lt));
end

if check~=1,
subplot(4,1,z)
plot(xi,yi,'w')

hold on
plot(profx,detrend5(pr,:),'b')
%plot(lmina,hmina,'*')
%plot(lmaxa,hmaxa,'*')
%plot(lmint,hmint,'ro')
plot(lmint,hmint,'rx')
%plot(lmaxt,hmaxt,'ro')
plot(lmaxt,hmaxt,'rx')
elseif check==1;%%%% if check==1
  subplot(4,1,z)
  text(115,2.2,'*')
  plot(profx,detrend5(pr,:),'b')

end
check=0;  % set check back to zero

figure(1)

clear lmint lmaxt lmin lmax hmint hmaxt hmax hmin  xi yi n nl
clear  e el h ht i j k l lt max1  min1  hall hallt lall lallt c ct m nrs
clear p t s lmina lmaxa hmina hmaxa  halla lalla
hold on
end % for individual profile loop
```

```
ln=floor(length(ahtt)/4);
mx1=max(detrend5(1,:)); mn1=min(detrend5(1,:)); % set axis
 if mx1<2
   mx1=2;
 end
 if mn1>-2,
  mn1=-2;
 end

for z=1:4   % plot text on graphs
 htw(z,index)=mean(ahtt((z-1)*ln+1:z*ln)); %output variable
 ltw(z,index)=mean(altt((z-1)*ln+1:z*ln)); %output variable
 fn(index,:)=fname;


 subplot(4,1,z)
 axis([0 238.5 mn1-1 mx1+1])
 set(get(gcf,'children'),'Fontsize',10)
 text(10,mx1-0.8,['Height = ',num2str(round(mean(ahtt((z-1)*ln+1:z*ln))*10)/10),' cm'])
 text(150,mx1-0.8,['Length = ',num2str(round(mean(altt((z-1)*ln+1:z*ln))*10)/10),' cm'])

 if z==2|3
  ylabel('Vertical - cm','Fontsize',10)
 end
 hr=floor(prof15((z-1)*ln+1,65)/3600);
 mn=floor((prof15((z-1)*ln+1,65)-hr*3600)/60);
 scc=floor(prof15((z-1)*ln+1,65)-hr*3600-mn*60);
 if z==1,
   title(['Detrended SIS96 Ripple Pattern   ',fname,'  ',num2str(loc),side,'  ',num2str(hr),':',num2str(mn),':',num2str(sec)],'Fontsize',10)
 else,
   title([num2str(hr),':',num2str(mn)],'Fontsize',10)
 end
 if z==4
  xlabel('Horizontal Distance in cm','Fontsize',10)
 end
end
 hold off, clg
end  % for file loop T loop



%% pier96.m
%%% Profile of FRF pier Taken 10-30-96 (Eric/Chris)
%%% Data from lead line to top of rail - 4:30 - 5:30 pm
%%% S is south side, N is north side, all measurements in ft.

S=[11.7 10.3 09.8 06.6 10.2 13.6 18.3 21.5 23.1 24.8 27.8 33.1 32.1 ...
   31.8 31.3 32.0 33.7 35.8 38.7 42.6 43.9 44.9 45.2 45.5 45.8 45.9 ...
   45.7 45.0 44.3 44.2 43.9 43.9 45.0 46.4 48.3 49.6 50.7 51.9 53.0 ...
   53.4 54.5 55.0 55.9 56.5 56.9];

N=[11.7 10.3 09.8 06.6 10.2 13.3 18.3 21.0 23.1 24.1 27.8 32.0 31.7 ...
   31.4 30.9 31.5 33.0 35.0 38.9 43.0 45.2 46.5 47.0 46.7 47.5 47.4 ...
   47.1 46.7 46.1 45.7 45.2 45.1 46.2 47.1 48.3 49.6 50.5 52.0 52.8 ...
   53.4 54.3 54.9 55.2 55.3 55.9];

dis=[120 140 160 180 200 220 260 300 340 380 420 460 500 540 580 620 ...
     660 700 740 780 820 860 900 940 980 1020 1060 1100  1140 1180 ...
     1220 1260 1300 1340 1380 1420 1460 1500 1540 1580 1620 1660 1700 ...
     1740 1780];

wl=30.0; %% waterlevel at 30.0 ft.
x=[660 680 740 760 780 800 1620 1730];
xm=x.*0.3408;
north=30-N;
south=30-S;
dism=dis*0.3408; %change to meters
northm=north*0.3408; % change to meters
southm=south*0.3408; % change to meters
subplot(2,1,1)
plot(dism,northm,'-.',dism,southm)
```

```
hold on
axis([min(dism) max(dism) min(northm) max(northm)])
plot(dism,zeros(size(dism)),'--')
for i=1:length(x)
plot([xm(i) xm(i)],[1 -5])
end
hold off
xlabel('Distance in meters')
ylabel('Elevation in meters')
title('FRF Pier Profile 10:30:96 5:00pm')
text(400,5,'_._=South, __=North')
subplot(2,1,2)
% plot profile in feet
plot(dis,north,'-.',dis,south)
hold on
axis([min(dis) max(dis) min(north) max(north)])
plot(dis,zeros(size(dis)),'--')

for i=1:length(x)
plot([x(i) x(i)],[5 -20])
end
hold off
xlabel('Distance in feet')
ylabel('Elevation in feet')

figure(1)



%% plot96.m
%% plots a 2-D plot with ripple data from 64 element array
%% plots entire array and the 5MHz center region separately
%% if offset==1, each profile will be subtracted from the mean
%% of that profile, else if offset~=1, all profiles will be subtracted
%% from the mean value of all of the profiles.  The latter shows
%% subsidance of the SIS boom during some of the runs
clf,clear
offset=1;  %% change to other than 1 for constant offset
l=zeros(30,1); s=zeros(30,1),, fn=zeros(30,7);
for index=[1:30]
if index<=9, fname=['stats0',num2str(index)];
 elseif index>9, fname=['stats',num2str(index)];
end
eval(['load d:\chris\sis96\sis96c~1\',fname])
num=floor(length(prof15)/30)-1;

x5=linspace(96,96+46.5,32);
 med=median(prof15(:,1:64)); len=size(prof15,1);
 men=mean(med); % mean of median profile (mm)
for i=1:len
 if offset==0;
  nprof(i,:)=median(prof15(i,1:64))/10-prof15(i,1:64)/10; %orient profile for plot (cm)
 else
   nprof(i,:)=men/10-prof15(i,1:64)/10; %orient profile for plot (cm)
 end
end
prof5=nprof(:,17:17+31); % 5MHz center portion

figure(1)
if side=='S'
  x5=fliplr(x5);
  profx=fliplr(profx);
end
%%%%% determine slope (b) of seabed using polyfit function
for i=1:len
 b(i,:)=polyfit(profx,nprof(i,:),1); % entire array
 bx(i,:)=polyfit(x5,prof5(i,:),1); % 5MHz portion
end
bm=median(b);
bmx=median(bx);
subplot(2,1,1)
```

```
plot(profx,nprof(1:len/3,:)','r')
hold on
plot(profx,nprof(len/3 +1:2*len/3,:)','w')
plot(profx,nprof(2*len/3+1:len,:)','b')
plot(profx,profx.*bm(1) + bm(2),'r-.')   %%plot slope
hold off
n=axis; zmin=n(3); zmax=n(4);
zm=zmax;
if zm>20
 med=median(nprof(:,:)); %find median prof to set axis
 med5=median(prof5(:,:));
 maxz=3*max(med); minz=3*min(med);
 maxz5=1+max(med5);

 if min(med5)>min(median(prof5(:,:)));
   minz5=-1+min(median(prof5(:,:))); %account for sinking of frame during run
 else
  minz5=-1+min(med5);
 end
zmax=maxz; zmin=minz;%zmax=10; zmin=-10; %%%%%%%%%%%%%%%
end
axis([0 max(profx) zmin zmax])
hold on
plot([96 96],[zmin zmax],'r-.')
plot([96+46.5 96+46.5],[zmin zmax],'r-.')
hold off
grid on

title(['MTA SIS96 data -',fname,' ', ...
 num2str(loc),side,' profiles represent ',num2str(prof15(1,67)),...
 ' sec. slope=',num2str(bm(1),2)])


xlabel(['                                          ',...
   '       distance (cm) : onshore is + dir.'])
ylabel('vertical (cm)')

subplot(2,1,2)
plot(x5,prof5(1:len/3,:)','r')
hold on
plot(x5,prof5(len/3 +1:2*len/3,:)','w')
plot(x5,prof5(2*len/3+1:len,:)','b')
plot(x5,x5*bmx(1)+bmx(2),'r-.')  %plot slope
xlabel('centimeters')
title(['middle section  slope =',num2str(bmx(1),2),'              ',...
   '                ])
xlabel('horizontal (cm)')
ylabel('vertical (cm)')
n=axis; zmin=n(3); zmax=n(4);
if zm>20
 zmax=maxz5; zmin=minz5;%zmax=2;,zmin=-6; %%%
end
axis([96 96+46.5 zmin zmax])

hold off
pause
slope(index)=bm(1);
slope5(index)=bmx(1);
clear prof x mtar1 mtar2 mtar3 m1 m2 m3 men profm nprof pro b bx
clear x5 prof5 nprof  miny maxy miny5 maxy5 mn maxz5 minz5 bm bmx
clear maxz minz med
%% save slope information
end
hold off


%timser.m
%Chris Jette, 4-2-97
%plot timeseries of press. or current
% plot bedform profile timeseries
load stats96
```

```
g=9.81;
%for index=[2:5,7:23,25:30];
for index=[2];
clg
 if index<10, fname=['stats0',num2str(index)];
 else, fname=['stats',num2str(index)];
 end
eval(['load ',fname])

subplot(3,1,1)
timeaxis=[1:length(botvel)]/(sampfreq*60); % plot in minutes
%plot(timeaxis,botvel)
%plot(timeaxis,u)
mobn=(botvel.^2)./(1.65*g*D50(index)/1000);
plot(timeaxis,mobn)
xlabel('time in minutes')
ylabel('Mobility Number')
%ylabel('cross-shore vel. (m/s)')
%title(['SIS96 Near-bottom cross-shore velocity time-series for run',num2str(index)])
title(['SIS96 Mobility Number time-series for run',num2str(index)])
%axis([min(timeaxis) max(timeaxis) min(botvel) max(botvel)])
axis([min(timeaxis) max(timeaxis) min(mobn) max(mobn)])
grid on
%% remove
  prof15=prof;
%%%%%
x5=linspace(96,96+46.5,32);
 med=median(prof15(:,1:64)); len=size(prof15,1);
 men=mean(med); % mean of median profile (mm)
for i=1:len
 nprof(i,:)=men/10-prof15(i,1:64)/10; %orient profile for plot (cm)
end
prof=nprof(:,17:17+31);
time=prof15(:,65);

if side=='S'
  x5=fliplr(x5);
  profx=fliplr(profx);
end

nan=ones(32,1)*NaN;

%%% plot

prof5f=[prof'];
time=(([time])-time(1))/60;
detrend5=detrend(prof5f)';
if time(length(time))>20
  detrend5=detrend5(1:2:length(prof5f),:);
  time=time(1:2:length(time));
end
figure(1)
subplot(3,1,2)
% plots mesh or contour plot
% surfl(x5,time,detrend5,[40 10],[0 0.9 0.2 1])
surf(x5,time,detrend5)
%waterfall(x5,time,detrend5)
%mesh(x5,time,detrend5)
%contour(x5,time,detrend5)
xlabel('horizontal (cm)')
ylabel('time (min)')
zlabel('elev. (cm)')
title('SIS96 MTA1')
axis([96.96+46.5 min(time) max(time) -0.8 0.8]) % use for meshplot
%set(view([340,70]))
set(view([360,90]))
caxis([-1 0.6])
colormap(bone)
colorbar
caxis([-0.5 0.35])
hold off
```

```
figure(1)
subplot(3,1,3)
% plots mesh or contour plot
 surf1(x5,time,detrend5,[40 10],[0 0.9 0.2 1])
%surf(x5,time,detrend5)
%waterfall(x5,time,detrend5)
%mesh(x5,time,detrend5)
%contour(x5,time,detrend5)
xlabel('horizontal (cm)')
ylabel('time (min)')
zlabel('elev. (cm)')
title('S1S96 MTA1')
axis([96 96+46.5 min(time) max(time) -0.8 0.8]) % use for meshplot
set(view([340,70]))

caxis([-1 0.6])
colormap(bone)
grid on
caxis([-0.5 0.35])
hold off
figure(2)
subplot(2,1,1)
for i=1:length(detrend5)
  detrend5(i,:)=detrend5(i,:)+i*0.2;
end
plot(x5,detrend5(1:10,:),'r')
hold on
plot(x5,detrend5(11:20,:),'g')
plot(x5,detrend5(21:30,:),'b')
plot(x5,detrend5(31:length(detrend5(:,1))',:),'r')
xlabel('Horizontal Distance (cm), + dir. shoreward')
ylabel('elevation (cm)')
title(['MTA1 Profiles, ',num2str(time(2)-time(1)),'  min between profiles, 2 mm offset'])
axis([96 96+46.5 min(detrend5(1,:)) max(detrend5(length(detrend5),:))])
orient tall
hold off
grid on
pause
clear prof x mtar1 mtar2 mtar3 m1 m2 m3 men profm nprof
clear nprof  miny maxy miny5 maxy5 mn maxz5 minz5 sampfreq
clear maxz minz med detrend5 u v pres fname timeaxis botvel len
%pause
end
```

REFERENCES

Bagnold, R. A., Motion of waves in shallow water: Interaction between waves and sand bottoms, Proc. R. Soc. London Ser. A, 187, 1-15, 1946.

Boyd, R., D. L. Forbes, and D. E. Heffler, Time-sequence observations of wave-formed sand ripples on an ocean shore face, Sedimentology, 35, 449-464, 1988.

Carstens, M. R., R. M. Neilson, and H. D. Altinbilek, Bedforms generated in the laboratory under oscillatory flow: Analytical and experimental study, Tech. Memo. 28, U.S. Corps of Eng., Coastal Eng. Res. Center, June 1969.

Clifton, H. E., Wave-formed sedimentary structures: A conceptual model in beach and near-shore sedimentation, edited by R. A. Davis, Jr. and R. L. Ethington, SEPM Spec. Publ., 24, 126-148, 1976.

Clifton, H, E., and J. R. Dingler, Wave-formed structures and paleoenvironmental reconstruction, Mar. Geo., 60, 165-198, 1984.

Coates, R. F. W., Underwater acoustic systems, New York, J. Wiley, 1989.

Dingler, J. R., Wave formed ripples in near-shore sands, Ph. D. thesis, Univ. of Calif. San Diego, 1974.

Dingler, J. R., and D. L. Inman, Wave-formed ripples in near-shore sands, Proc. Fifteenth Conf. Coastal Engng., Amer. Soc. Civil Eng., 1976.

Fresdsøe J., Sedimentation of river navigation channels, Journal of the Hydraulics Division (ASCE), Vol. 104, No. HY2, pp.223-236, 1978.

Grant, W. D., and O. S. Madsen, Movable bed roughness in unsteady oscillatory flow, J. Geophys. Res., 87, 469-481, 1982.

Greenwood, B., R. G. Richards, and R. W. Brander, Acoustic imaging of sea-bed geometry: A high resolution remote tracking sonar (HRRTS II), Marine Geo., 112, 207-218, 1993.

Hay, A. E. and A. J. Bowen, Spatially correlated depth changes in the nearshore zone during autumn storms, J. Geophys. Res., 98: 12,387-12,404, 1993.

Hay, A. E., R. Craig, and D. Wilson, Nearshore bedform evolution during waning storms: megaripple migration and scale collapse, (submitted manuscript), 1996.

Hay, A. E., and D. J. Wilson, Rotary sidescan images of nearshore bedform evolution during a storm, Marine Geo., 119, 57-65, 1994.

Inman, D.L., Wave generated ripples in near-shore sans, Tech. Memo. 100, 66 pp., U.S. Army Corps of Eng., Beach Erosion Board, Washington, D.C., 1957.

Jetté, C. D., and D. M. Hanes, High-resolution sea-bed imaging: an acoustic multiple transducer array, Meas. Sci. Technol. 8 , 787-792, IOP Publ., 1997.

Jetté, C. D., and D. M. Hanes, Measurements of Wave Generated Bedforms, Proc. Twenty-fifth Coastal Eng. Conf., Orlando, FL, 3129-3142, Amer. Soc. Civil Eng., New York, 1996.

Krauss, N.C., and J. M. Smith, SUPERTANK laboratory data collection project, Technical report CERC-94-3, 1994.

Kawata, Y., T. Shirai, and Y. Tshuchiya, Field observation of sand ripples under rough sea state, Coastal Engn., 2164-2175, 1992.

Meyer-Peter, E. and R. Muller, Formulas for bed-load transport, Proc Int Ass Hydr Struct Res, Stockholm, 1948.

Miller, M. C., and P. D. Komar, Oscillation sand ripples generated by laboratory apparatus, J. Sediment. Petrol., 50, 173-182, 1980a.

Miller, M. C., and P. D. Komar, A field investigation of the relationship between oscillating ripple spacing and the near bottom water orbital motions, J. Sediment. Petrol., 50, 183-191, 1980b.

Mogridge, G. R., and J. W. Kamphius, Experiments on bedform generation by wave action, Proc. of the 13th Coastal Eng. Conf., 1123-1142, Am. Soc. Civil Eng., 1972.

Nielsen, P., Coastal bottom boundary layers and sediment transport, Advanced Series on Ocean Engineering - Vol. 4, pp.129-142. World Scientific, New Jersey, 1992.

Nielsen, P., Field measurements of the time-averaged suspended sediment concentration under waves, Coastal Engn., 8,51-72, 1984.

Nielsen, P., Dynamics and geometry of wave-generated ripples, J. Geophys. Res., 86, 6467-6472, 1981.

Osbourne, P. D. and C. E. Vincent, Dynamics of large and small scale bedforms on a macrotidal shoreface under shoaling and breaking waves, Marine Geo., 115, 207-226, Elsevier Publ., Amsterdam, 1993.

Ribberink, J. S., A. Al-Salem, Sediment transport, sediment concentrations and bedforms in simulated asymmetric wave conditions, Report H 840 Part V, Delft Hydraulics, Delft, the Netherlands, 1992.

Sato, S., K. Horikawa, Sand ripple geometry and sand transport mechanism due to irregular oscillatory flows, Proc. of the 21st Coastal Eng. Conf., 1748-1762, 1988.

Sleath, J. F. A., Sea Bed Mechanics, Wiley Interscience, 1984.

Swart, D. H., Offshore sediment transport and equilibrium beach profiles, Delft. Hydr. Lab. Publ. No. 131, 1974.

Tunsdall, E. B., and D. L. Inman, Vortex generation by oscillatory low over rippled surfaces, J. Geophys. Res., 80, 3475-3485, 1975.

Urick, R. J., Principles of Under Water Sound, McGraw Hill, 1983.

Vincent, C. E., D. M. Hanes, and A. J. Bowen, Acoustic measurements of suspended sand on the shoreface and the control of concentration by bed roughness, Marine Geo., 96, 1-18, Elsevier Science Publ., Amsterdam, 1991.

Vincent C. E. & P. D. Osbourne, Bedform dimensions and migration rates under shoaling and breaking waves, Continental Shelf Research, 13, 1267-1280, 1993.

Vongvissessomjai, S., Oscillatory ripple geometry, Fournal of Hydraulic Engrg., ASCE, Vol. 110, No. 3, 1984.

Wiberg, P.L., and C. K. Harris, Ripple geometry in wave dominated environments, J. Geophys. Res., 99, 775-789, 1994.

Wikramanayake, P. N., Velocity profiles and suspended sediment transport in wave-current flows, Ph.D. Thesis, Dept. of Civil Engineering, Mass. Inst. of Tech., Cambridge, Mass., 1993.

Wolf , P.R., Elements of Photogrammetry, 2nd Edition, McGraw Hill, New York, 1983.

BIOGRAPHICAL SKETCH

The author was born on July sixteenth of 1969 in the town of Vero Beach, Florida. While living in Vero Beach he discovered his love for the ocean. He was open water scuba certified at the age of twelve. At that time he realized that his profession would some how involve the ocean. He went to high school in Morganton, North Carolina, and spent every summer back in Vero Beach. While land-locked in Morganton his interests turned to physical fitness and music.

Upon graduation from high-school he moved back to Vero Beach and attended college at the Florida Institute of Technology. During these school years he was introduced to surfing, and has had a passion for it ever since. In August of 1991 he received his B.S. in Ocean Engineering with honors from F.I.T.. The following December he moved to Gainesville, and began graduate work in the field of Coastal Engineering under Dr. Daniel M. Hanes. He received his M. E. degree in Coastal Engineering in August, 1994, and continued graduate work under Dr. Hanes. He married his lovely wife, Monica, in May of 1995.

He founded SeaTek Instrumentation and Engineering in July of 1995. Future plans include continued instrumentation development with SeaTek Instrumentation.

I certify that I have read this study and that in my opinion it conforms to acceptable standards of scholarly presentation and is fully adequate, in scope and quality, as a dissertation for the degree of Doctor of Philosophy.

Daniel M. Hanes, Chairman
Associate Professor of Coastal and
Oceanographic Engineering

I certify that I have read this study and that in my opinion it conforms to acceptable standards of scholarly presentation and is fully adequate, in scope and quality, as a dissertation for the degree of Doctor of Philosophy.

Robert G. Dean
Graduate Research Professor of Coastal and
Oceanographic Engineering

I certify that I have read this study and that in my opinion it conforms to acceptable standards of scholarly presentation and is fully adequate, in scope and quality, as a dissertation for the degree of Doctor of Philosophy.

D. M. Sheppard
Professor of Coastal and
Oceanographic Engineering

I certify that I have read this study and that in my opinion it conforms to acceptable standards of scholarly presentation and is fully adequate, in scope and quality, as a dissertation for the degree of Doctor of Philosophy.

Robert J. Thieke
Assistant Professor of Coastal and
Oceanographic Engineering

I certify that I have read this study and that in my opinion it conforms to acceptable standards of scholarly presentation and is fully adequate, in scope and quality, as a dissertation for the degree of Doctor of Philosophy.

Joann Mossa
Associate Professor of Geography

This dissertation was submitted to the Graduate Faculty of the College of Engineering and to the Graduate School and was accepted as partial fulfillment of the requirements for the degree of Doctor of Philosophy.

December 1997

Winfred M. Phillips
Dean, College of Engineering

Karen A Holbrook
Dean, Graduate School